Measurements of differential cross-sections in four-lepton events in 13 TeV proton-proton collisions with the ATLAS detector

The ATLAS collaboration

E-mail: atlas.publications@cern.ch

ABSTRACT: Measurements of four-lepton differential and integrated fiducial cross-sections in events with two same-flavour, opposite-charge electron or muon pairs are presented. The data correspond to $139\,\mathrm{fb}^{-1}$ of $\sqrt{s} = 13\,\mathrm{TeV}$ proton-proton collisions, collected by the ATLAS detector during Run 2 of the Large Hadron Collider (2015–2018). The final state has contributions from a number of interesting Standard Model processes that dominate in different four-lepton invariant mass regions, including single Z boson production, Higgs boson production and on-shell ZZ production, with a complex mix of interference terms, and possible contributions from physics beyond the Standard Model. The differential cross-sections include the four-lepton invariant mass inclusively, in slices of other kinematic variables, and in different lepton flavour categories. Also measured are dilepton invariant masses, transverse momenta, and angular correlation variables, in four regions of four-lepton invariant mass, each dominated by different processes. The measurements are corrected for detector effects and are compared with state-of-the-art Standard Model calculations, which are found to be consistent with the data. The $Z \to 4\ell$ branching fraction is extracted, giving a value of $(4.41 \pm 0.30) \times 10^{-6}$. Constraints on effective field theory parameters and a model based on a spontaneously broken $B - L$ gauge symmetry are also evaluated. Further reinterpretations can be performed with the provided information.

Contents

1 Introduction

This paper presents measurements of differential and integrated fiducial cross-sections of four-lepton events, containing two same-flavour, opposite-charge electron or muon pairs. The data used correspond to 139 fb^{-1} of $\sqrt{s} = 13$ TeV proton-proton collisions, collected by the ATLAS detector [1, 2] during Run 2 of the Large Hadron Collider (LHC) [3] between 2015 and 2018.

Several interesting Standard Model (SM) processes contribute to this final state, with the possibility of additional contributions from beyond-the-SM (BSM) physics. The dominant SM contribution is from the quark-induced t-channel $q\bar{q} \to 4\ell$ process, shown in
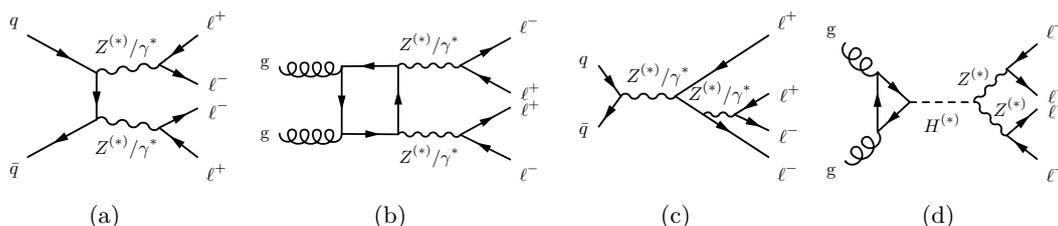
Figure 1. Main contributions to the $pp \to 4\ell(\ell = e, \mu)$ process: (a) t-channel $q\bar{q} \to 4\ell$ production, (b) gluon-induced $gg \to 4\ell$ production via a quark loop, (c) internal conversion in Z boson decays and (d) Higgs-boson-mediated s-channel production (here: gluon-gluon fusion). The superscript $(*)$ refers to a particle that can be either on-shell or off-shell, whereas $*$ indicates that it is always off-shell.

figure 1(a). Gluon-induced $gg \to 4\ell$ production contributes at next-to-next-to-leading order (NNLO) in quantum chromodynamics (QCD), via a quark loop, as shown in figure 1(b). The $Z \to 4\ell$ process, shown in figure 1(c), dominates in the four-lepton invariant mass, $m_{4\ell}$, region close to the Z boson mass, m_Z [4]. The $H \to Z^{(*)}Z^{(*)} \to 4\ell$ process, shown in figure 1(d) for the gluon-gluon production mode, dominates in the $m_{4\ell}$ region close to the Higgs boson mass, m_H [4]. Here the superscript $(*)$ refers to a particle that can be either on-shell or off-shell.

BSM contributions can arise from modifications to the SM couplings of the Higgs boson, the gauge bosons and from possible four-fermion interactions. Contributions are also possible from models producing four leptons either via the decay of Z bosons or of new BSM particles. For example, cascade decays of new particles introduced by the Minimal Supersymmetric SM, with parameters set such that searches based on missing transverse momentum [5] are insensitive, can nevertheless contribute to four-lepton final states [6]. Other examples include generic models with additional gauge boson(s), Z', which may be pair-produced and decay into lepton pairs, or models with additional Higgs bosons which may decay into a pair of Z bosons.

The measurements are corrected for the effects of the detector. Observables are defined in terms of final-state particles, rather than in terms of a particular process. The definition is inclusive of particles in addition to the two lepton pairs, including neutrinos, other leptons, hadrons, photons and any possible BSM particles, although the leptons are required to be isolated from other particles. There are therefore small SM contributions from top-quark pair production in association with a dilepton pair, from triboson processes, where at least two bosons decay leptonically, and from events where τ-leptons decay to muons or electrons. Using this definition results in minimal dependence of the measurement on the modelling of these other SM processes. The dependence on SM modelling is transferred to the theoretical predictions that are used in comparisons with the data.

Cross-sections are measured differentially as a function of various kinematic variables, and integrated fiducial cross-sections are also provided. The primary observable, $m_{4\ell}$, is measured inclusively, sliced in other kinematic variables, and in different lepton flavour categories. Additional differential cross-sections are measured, including dilepton invariant

masses and transverse momenta, and angular correlation variables between leptons, in four regions of $m_{4\ell}$, each dominated by different processes. The $m_{4\ell}$ distributions and a subset of the other variables, measured in a region where $m_{4\ell}$ is above the on-shell ZZ production threshold, have been presented previously at this centre-of-mass energy, using a smaller dataset [7–9] and by the CMS collaboration using a similar dataset [10]. The current result is more inclusive than previous measurements, in particular the previous requirement that the invariant mass of at least one of the dilepton pairs be close to m_Z is removed. This gives sensitivity to BSM processes where there are sources of dilepton pairs other than Z boson decays. The cross-section measurement in the region close to m_Z is used to extract the $Z \rightarrow 4\ell$ branching fraction.

BSM contributions to this final state may lead to discrepancies between the measured cross-sections and the SM predictions. The measurements can therefore be used to set limits on a wide range of BSM models. The methods used to correct the data for the effects of the detector are shown to be robust against the addition of BSM contributions, as is discussed in section 5.4. Since the cross-sections are defined at particle-level, they can be compared with BSM theory predictions or improved SM predictions without the need to simulate the ATLAS detector. The data and the SM predictions are available in HEPData [11], with the analysis included in the Rivet [12] library, allowing straightforward comparison with other predictions.

2 ATLAS detector

The ATLAS detector at the LHC covers nearly the entire solid angle around the collision point, as detailed below for each sub-detector.[1] It consists of an inner tracking detector (ID) surrounded by a thin superconducting solenoid, electromagnetic and hadronic calorimeters, and a muon spectrometer incorporating three large superconducting toroidal magnets.

The ID, immersed in a $2\,\mathrm{T}$ axial magnetic field, provides charged-particle tracking for $|\eta| < 2.5$. It consists of a high-granularity silicon pixel detector covering the vertex region and typically providing four measurements per track. This is followed by the silicon microstrip tracker, which usually provides eight measurements per track. These silicon detectors are complemented by the transition radiation tracker (TRT), which enables radially extended track reconstruction up to $|\eta| = 2.0$. The TRT also provides electron identification information based on the fraction of hits (typically 30 in total) above a higher energy-deposit threshold corresponding to transition radiation.

The calorimeter system covers the pseudorapidity range $|\eta| < 4.9$. Within $|\eta| < 3.2$, electromagnetic calorimetry is provided by barrel and endcap high-granularity lead/liquid-argon (LAr) calorimeters, with an additional thin LAr presampler covering $|\eta| < 1.8$ to cor-

---

[1]ATLAS uses a right-handed coordinate system with its origin at the nominal interaction point (IP) in the centre of the detector and the z-axis along the beam pipe. The x-axis points from the IP to the centre of the LHC ring, and the y-axis points upwards. Cylindrical coordinates (r, ϕ) are used in the transverse plane, ϕ being the azimuthal angle around the z-axis. The rapidity is defined as $y = (1/2) \ln\left[(E + p_z)/(E - p_z)\right]$, where E is the energy of a particle and p_z is the momentum component in the beam direction. The pseudorapidity is defined in terms of the polar angle θ as $\eta = -\ln \tan(\theta/2)$. Angular distance is measured in units of $\Delta R \equiv \sqrt{(\Delta\eta)^2 + (\Delta\phi)^2}$.

rect for energy loss in material upstream of the calorimeters. Hadronic calorimetry is provided by the steel/scintillator-tile calorimeter, segmented into three barrel structures within $|\eta| < 1.7$, and two copper/LAr hadronic endcap calorimeters covering $1.5 < |\eta| < 3.2$. The solid angle coverage is completed with forward copper/LAr and tungsten/LAr calorimeter modules optimised for electromagnetic and hadronic measurements respectively.

The muon spectrometer (MS) comprises separate trigger and high-precision tracking chambers measuring the deflection of muons in a magnetic field generated by the superconducting air-core toroids. A set of precision chambers covers the region $|\eta| < 2.7$ with three layers of monitored drift tubes, complemented by cathode-strip chambers in the forward region, where the background is highest. The muon trigger system covers the region $|\eta| < 2.4$ with resistive-plate chambers in the barrel, and thin-gap chambers in the endcap regions.

Interesting events are selected by the first-level trigger system implemented in custom hardware, followed by algorithms implemented in software in the high-level trigger [13].

3 Fiducial region definition and measured variables

3.1 Fiducial definition

The fiducial phase space is defined according to the kinematic acceptance of the detector, with kinematics that ensure a high efficiency to trigger on the events, and is designed to be as inclusive as possible while keeping backgrounds from non-prompt[2] leptons relatively small. This phase space is defined by a kinematic selection applied at particle-level[3] using final-state, prompt leptons (including those from τ-lepton decays). In order to align the particle-level definition of lepton kinematics as closely as possible to their measurements in the detector, prompt electrons are 'dressed' by adding to their four-momenta the four-momenta of prompt photons within a cone of size $\Delta R = 0.1$ around the electron. This is done because the experimental measurement of electron energies in the calorimeter includes the energy of nearby photons. If the photon is near more than one electron, it is assigned to the nearest. This dressing is not applied to prompt muons because their four-momenta are measured using the ID and the MS, and the four-momenta of nearby photons are not included in the measurement. Prompt leptons are required to be isolated from other particles. Their isolation is tested by forming a scalar sum of the transverse momenta, p_T, of all charged particles within a cone of $\Delta R = 0.3$ around the lepton. The ratio of this sum to the p_T of the lepton is required to be less than 0.16. If another selected lepton is within the cone, the momentum of this lepton is not included in the sum.

Electrons (muons) are required to have $p_T > 7$ (5) GeV and $|\eta| < 2.47$ (2.7). Events are required to contain at least four such leptons that can be grouped into at least two same-flavour, opposite-charge pairs. This results in three possible flavour configurations: $e^+e^-e^+e^-$ (4e), $e^+e^-\mu^+\mu^-$ (2e2μ) and $\mu^+\mu^-\mu^+\mu^-$ (4μ). Additional particles (leptons,

---

[2]'Prompt' refers to leptons and photons that do not originate from hadron decays. This definition of prompt excludes leptons originating from hadronic resonances such as $J/\psi \to \ell^+\ell^-$ and $\Upsilon \to \ell^+\ell^-$ [14].

[3]'Particle-level' refers to a definition based on final-state particles equivalent to the particles produced from a Monte Carlo event-generator simulation, without simulating the effects of the detector. The data are corrected to this level such that they can be compared directly with theoretical predictions.

neutrinos, photons, hadrons and possible BSM particles) are allowed to be present in the event. Events are also required to satisfy the following:

- $p_T > 20$ GeV for the leading lepton (in p_T).

- $p_T > 10$ GeV for the sub-leading lepton (in p_T).

- The invariant mass of any same-flavour, opposite-charge lepton pair that can be formed in the event is required to satisfy $m_{\ell\ell} > 5$ GeV.

- The angular separation between any two leptons in the event is required to satisfy $\Delta R > 0.05$.

These requirements are made to minimise experimental uncertainties and are justified in section 5.1.

3.2 Lepton pairing

Leptons are paired in order to define some of the measured variables. The same-flavour, opposite-charge pair with an invariant mass closest to m_Z is selected as the primary pair in the event. Of the remaining leptons, the same-flavour, opposite-charge pair with an invariant mass closest to m_Z is selected as the secondary pair, completing a quadruplet of leptons. Therefore, only one quadruplet is defined even in events containing more than four leptons. This selection strategy ensures that pairs corresponding to on-shell Z bosons for the dominant ZZ pair production process are formed preferentially.

3.3 Measured variables

The integrated fiducial cross-section is measured over the full fiducial phase space and in four $m_{4\ell}$ regions dominated by: single Z boson production ($60 < m_{4\ell} < 100$ GeV), Higgs boson production ($120 < m_{4\ell} < 130$ GeV), on-shell ZZ production ($180 < m_{4\ell} < 2000$ GeV) and off-shell ZZ production ($20 < m_{4\ell} < 60$ GeV or $100 < m_{4\ell} < 120$ GeV or $130 < m_{4\ell} < 180$ GeV).

A number of differential fiducial cross-sections are also measured, providing kinematic information about the events, which are each varyingly sensitive to the modelling of the SM processes, including QCD and electroweak corrections, and to possible BSM contributions. The $m_{4\ell}$ distribution is measured single-differentially as well as double-differentially with the four-lepton transverse momentum, $p_{T,4\ell}$, and the absolute four-lepton rapidity, $|y_{4\ell}|$. The single-differential $m_{4\ell}$ distribution is also measured in $4e$, 4μ and $2e2\mu$ events separately.

The following variables are measured in the four regions of $m_{4\ell}$ defined above:

- The invariant mass of the primary (secondary) lepton pair: m_{12} (m_{34}).

- The transverse momentum of the primary (secondary) lepton pair: $p_{T,12}$ ($p_{T,34}$).

- A variable sensitive to the polarisation of the decaying particle: $\cos\theta_{12}^*$ ($\cos\theta_{34}^*$) is the cosine of the angle between the negative lepton in the primary (secondary) dilepton rest frame, and the primary (secondary) lepton pair in the laboratory frame.

- The absolute rapidity difference between the primary and secondary lepton pairs, $|\Delta y_{\text{pairs}}|$.

- The difference in the azimuthal angle between the primary and secondary lepton pairs, $|\Delta \phi_{\text{pairs}}|$.

- The difference in the azimuthal angle between the leading lepton and sub-leading lepton (in p_{T}) of the quadruplet, $|\Delta \phi_{\ell\ell}|$.

4 Theoretical predictions and simulation

Simulated events are used to correct the observed events for detector effects, as well as to provide the particle-level predictions with systematic uncertainties for comparisons with the measured data. The various simulated samples and their uncertainties are described in this section.

The $q\bar{q} \to 4\ell$ process, including $Z \to 4\ell$, was simulated with the SHERPA v2.2.2 event generator [15]. Matrix elements were calculated at next-to-leading-order (NLO) accuracy in QCD for up to one additional parton and at leading-order (LO) accuracy for up to three additional parton emissions. The higher-order corrections include initial states with a gluon, but the $q\bar{q} \to 4\ell$ notation is kept for simplicity. The calculations were matched and merged with the SHERPA parton shower based on Catani-Seymour dipole factorisation [16, 17], using the MEPS@NLO prescription [18–21]. The virtual QCD corrections were provided by the OPENLOOPS library [22, 23]. The NNPDF3.0nnlo set of PDFs [24] was used, along with the dedicated set of tuned parton-shower parameters (tune) developed by the SHERPA authors. All SHERPA v2.2.2 samples discussed below use this same PDF set and tune.

An alternative $q\bar{q} \to 4\ell$ sample was generated at NLO accuracy in QCD using POWHEG-BOX v2 [25–27]. Events were interfaced to PYTHIA 8.186 [28] for the modelling of the parton shower, hadronisation, and underlying event, with parameters set according to the AZNLO tune [29]. The CT10 PDF set [30] was used for the hard-scattering processes, whereas the CTEQ6L1 PDF set [31] was used for the parton shower. A correction to higher-order precision, defined for this process as the ratio of the cross-section at NNLO QCD accuracy to the one at NLO QCD accuracy, was obtained using a MATRIX NNLO QCD prediction [32–35], and applied as a function of $m_{4\ell}$.

A reweighting for virtual NLO electroweak effects [36, 37] was applied as a function of $m_{4\ell}$ to both $q\bar{q} \to 4\ell$ samples. A 100% uncertainty was assigned to this reweighting function to account for non-factorising effects in events with high QCD activity [38]. The real higher-order electroweak contribution to 4ℓ production in association with two jets (which includes vector-boson scattering, but excludes processes involving the Higgs boson) was not included in the sample discussed above but was simulated separately with the SHERPA v2.2.2 generator. The LO-accurate matrix elements were matched to a parton shower based on Catani-Seymour dipole factorisation using the MEPS@NLO prescription.

Uncertainties due to missing higher-order QCD corrections are evaluated for both $q\bar{q} \to 4\ell$ samples [39] using seven variations of the QCD factorisation and renormalisation

scales in the matrix elements by factors of one half and two, avoiding variations in opposite directions. The envelope of the effects of these variations is taken as the uncertainty. For the SHERPA sample, uncertainties from the choice of nominal PDF set are evaluated using 100 replica variations, as well as by reweighting to the alternative `CT14nnlo` [40] and `MMHT2014nnlo` [41] PDF sets, and taking the envelope of these contributions as a combined PDF uncertainty. The effect of the uncertainty in the strong coupling constant α_S is assessed by variations of ± 0.001. For the POWHEG + PYTHIA8 sample, the PDF uncertainty is evaluated using the 26 pairs of upwards and downwards internal PDF variations within `CT10 NLO`, as well as reweighting to the `NNPDF3.0nnlo` and MSTW2008 [42] PDF sets, and taking the envelope of the variations.

The gluon-initiated 4ℓ production process was simulated using SHERPA v2.2.2 [43] at LO precision for up to one additional parton emission, with the parton-shower modelling being the same as for the $q\bar{q} \to 4\ell$ sample described above. The generator requires $m_{\ell\ell} > 10$ GeV for any same-flavour and opposite-charge lepton pair, which removes a small amount of the phase space included in the measurement. This is recovered by the correction to the NLO QCD calculation described below, for all but the m_{12} and m_{34} distributions in the region below 10 GeV, where the prediction from this sample is missing. This is a few percent of the total prediction in the fiducial phase space in this region. The sample includes the $gg \to 4\ell$ box diagram, the s-channel process proceeding via a Higgs boson, $gg\left(\to H^{(*)}\right) \to Z^{(*)}Z^{(*)} \to 4\ell$, and the interference between the two. In the region $m_{4\ell} > 130$ GeV this sample is used to simulate all three contributions. In the region $m_{4\ell} < 130$ GeV, where on-shell Higgs boson production dominates, this sample is only used to simulate the $gg \to 4\ell$ box diagram, with the dedicated samples described below used to simulate Higgs boson production. In this region the interference between the two is negligible and is not simulated. A NLO QCD calculation [44, 45] allowing $m_{4\ell}$ differential K-factors to be calculated is used to correct each of these contributions separately, together with an associated uncertainty. The details are the same as those described in ref. [7]. An additional correction factor of 1.2, taken from the ratio of a NNLO QCD calculation [46, 47] to the NLO prediction for off-shell Higgs production, is assumed to be the same for all three components. Scale and PDF uncertainties are obtained in the same way as for the SHERPA $q\bar{q} \to 4\ell$ sample described above.

In the region $m_{4\ell} < 130$ GeV, where on-shell Higgs boson production is important, and the effect of interference is negligible, dedicated samples are used to model the Higgs boson production processes as accurately as possible. Higgs boson production via gluon-gluon fusion [48], which dominates, was simulated at NNLO accuracy in QCD using the POWHEG NNLOPS program [25, 49–52]. The simulation achieves NNLO accuracy for arbitrary inclusive $gg \to H$ observables by reweighting the Higgs boson rapidity spectrum in `Hj-MiNLO` [48, 53, 54] to that of HNNLO [55]. PYTHIA8 [56] was used with parameters set according to the AZNLO tune to simulate the parton shower and non-perturbative effects. The POWHEG prediction used the `PDF4LHC15nnlo` PDF set [57]. The prediction from the Monte Carlo samples is normalised to the next-to-next-to-next-to-leading-order QCD cross-section plus electroweak corrections at NLO [47, 58–67]. Higgs boson production via vector-boson fusion (VBF) [68], in association with a vector boson (VH) [69], and in association

with a top-quark pair were all simulated with Powheg [25, 51, 52, 68] and interfaced with Pythia8 for the parton shower and non-perturbative effects, with parameters set according to the AZNLO tune. The Powheg prediction used the PDF4LHC15nlo PDF set [57]. For VBF production, the Powheg prediction is accurate to NLO in QCD, and is normalised to an approximate-NNLO QCD cross-section with NLO electroweak corrections [70–72]. For VH production, the Powheg prediction is accurate to NLO in QCD for up to one additional jet, and is normalised to a cross-section calculated at NNLO in QCD with NLO electroweak corrections [73–77]. The uncertainties in on-shell Higgs boson production are the same as reported in ref. [78]. The largest components are from the QCD scale and PDF uncertainties affecting the gluon-gluon fusion component.

Other SM processes making smaller contributions to the final state used in the analysis include triboson production (WWZ, WZZ and ZZZ), collectively referred to as VVV, and $t\bar{t}$ pairs produced in association with vector bosons ($t\bar{t}Z$, $t\bar{t}WW$), collectively referred to as $t\bar{t}V(V)$. The production of triboson events was simulated with Sherpa v2.2.2 using factorised gauge-boson decays. Matrix elements, accurate to NLO for the inclusive process and to LO for up to two additional parton emissions, were matched and merged with the Sherpa parton shower based on Catani-Seymour dipole factorisation using the MEPS@NLO prescription. The virtual QCD corrections for matrix elements at NLO accuracy were provided by the OpenLoops library. Uncertainties are evaluated in the same way as discussed above for the Sherpa $q\bar{q} \to 4\ell$ sample. Two sets of $t\bar{t}V(V)$ samples are used. A sample produced with the MadGraph5_aMC@NLO 2.3.3 [79] generator at NLO with the NNPDF3.0nlo [24] PDF set is used to provide the particle-level predictions to compare with the measurements. The events were interfaced to Pythia 8.210 [56] using the A14 tune [80] and the NNPDF2.3lo PDF set [81]. Uncertainties due to missing higher-order corrections are evaluated as in the Sherpa samples discussed above. Uncertainties in the PDFs are evaluated using the 100 replicas of the NNPDF3.0nlo PDF set. A second sample produced with Sherpa v2.2.0 at LO accuracy, using the MEPS@LO set-up with up to one additional parton, is used to perform the detector corrections. The default Sherpa v2.2.0 parton shower was used along with the NNPDF3.0nnlo PDF set. A flat uncertainty of $\pm 15\%$ is assigned to these samples to cover any differences between them and the MadGraph5_aMC@NLO samples, and also their uncertainties.

A small contribution from double-parton scattering, with the dilepton pairs produced in different parton-parton interactions, is expected to contribute at the level of 0.1%. This is included in the definition of the final state but neglected in the predictions due to the negligible contribution.

To correct for detector effects, generated events were passed through a Geant4-based simulation of the ATLAS detector and trigger [82, 83], and then through the same reconstruction and analysis software as applied to the data. Corrections are applied to simulated leptons to account for differences seen between simulation and data. These include differences in lepton reconstruction, identification, isolation and vertex-matching efficiencies, as well as in the momentum scale and resolution, with associated uncertainties [84, 85]. The effect of multiple proton-proton interactions in the same bunch crossing, known as pile-up, was emulated by overlaying inelastic proton-proton collisions, simulated with Pythia 8.186

using the `NNPDF2.3lo` set of PDFs and the A3 tune [86]. The events are then reweighted to reproduce the distribution of the number of collisions per bunch-crossing observed in the data, which have an average of 33.7 for the total dataset, with an associated uncertainty coming from the uncertainty in the inelastic cross-section.

5 Data analysis

5.1 Event selection

Events are selected by requiring at least one of a set of triggers to accept the event. Each trigger requires the presence of one, two or three electrons or muons satisfying a variety of p_T thresholds [87, 88]. The trigger efficiency increases from around 80% for $m_{4\ell}$ below 80 GeV, to nearly 100% at $m_{4\ell} \sim 200$ GeV and above. Events are required to contain at least one reconstructed pp collision vertex candidate with at least two associated ID tracks. The vertex with the largest sum of p_T^2 of tracks is considered to be the primary interaction vertex.

Electron identification utilises a likelihood-based method, combining information from the shower shapes of clusters in the electromagnetic calorimeters, properties of tracks in the ID, and the quality of the track-cluster matching, the latter being based on spatial separation as well the ratio of the cluster energy to the track momentum. The shower shape variables include variables sensitive to the lateral and longitudinal development of the electromagnetic shower, and variables designed to reject clusters from multiple incident particles. A 'loose' identification working point is used [84], with the additional requirement of a hit in the innermost layer of the pixel detector. Muons are identified using information from various combinations of the MS, the ID and the calorimeters. As with electrons, a 'loose' identification working point is used [85], which focuses on recovering efficiency in poorly instrumented detector regions. In particular, ID tracks identified as muons on the basis of their calorimetric energy deposits or the presence of individual muon segments are included in the region $|\eta| < 0.1$, where the muon spectrometer is only partially instrumented. In addition, stand-alone MS tracks, supplemented using short tracks in the forward pixel detector where possible, are added in the region $2.5 < |\eta| < 2.7$, where ID coverage does not permit full independent ID track reconstruction.

The kinematic requirements described in section 3 for the particle-level selection are also applied to these reconstruction-level[4] electrons and muons, ensuring very little extrapolation into unmeasured regions when correcting for detector effects. The leading and sub-leading leptons must have $p_T > 20$ GeV and > 10 GeV, respectively, to ensure efficient triggering of events. The requirements of $m_{\ell\ell} > 5$ GeV and $\Delta R > 0.05$ between the leptons suppress contributions from J/ψ decays and conversion electrons respectively. To select leptons originating from the primary proton-proton interaction, their tracks are required to have a longitudinal impact parameter, z_0, satisfying $|z_0 \sin(\theta)| < 0.5$ mm from the primary interaction vertex. For MS-only muons, no such requirement is made. To avoid the

---

[4]'Reconstruction-level' refers to the identification and kinematic measurements of final-state object candidates, as defined by measurements with the detector, or full detector simulation, and a subsequent reconstruction software step.

double-counting of particles, if leptons share an ID track, only one survives the selection. Preference is given to higher-p_T leptons and to muons over electrons, unless the muon has no associated MS track, in which case the electron survives. The leptons satisfying the above criteria are referred to as *baseline* leptons and are used to form the quadruplet, as detailed in section 3. Once the quadruplet is formed the following further selection requirements are made. The electrons and muons are required to be isolated from other particles using information from the ID and the calorimeters. The isolation variables form a ratio of the scalar sum of the transverse momenta of all charged particle tracks within a lepton-p_T dependent cone size, with an additional contribution from calorimeter measurements, to the p_T of the lepton. The variables have a correction for pile-up, and another correction for tracks or energy deposits originating from other leptons in the event, in order to retain events with closely spaced prompt leptons. Additionally, the transverse impact parameter significance, $|d_0|/\sigma_{d_0}$, calculated relative to the measured beam-line position must be less than 5 (3) for electrons (muons). The leptons satisfying the above criteria are referred to as *signal* leptons, and they are a subset of the *baseline* leptons.

The overall efficiency to reconstruct, identify, isolate and vertex-match electrons varies from 30% at low p_T and high $|\eta|$ to 98% at high p_T. For muons it varies from 30% at low p_T and high $|\eta|$ to more than 99% at high p_T, and is higher on average than for electrons [89].

5.2 Background estimation

Backgrounds where one or more of the reconstructed leptons entering a quadruplet did not originate from a prompt lepton (non-prompt leptons) are estimated using data-driven methods rather than simulation. The backgrounds are subtracted from the data prior to correcting for detector effects. Simulations suggest that the main source of background events is where the quadruplet is formed by a combination of prompt leptons from Z/γ^* or $t\bar{t}$ production processes, with additional leptons originating from the decay of hadrons.

The background is estimated with a *fake factor* method. The method uses three classes of leptons, the *signal* and *baseline* leptons defined in section 5.1, as well as *baseline-not-signal* leptons, defined as those which pass the baseline selection but fail the signal selection. A quantity called the *fake factor* is defined as the ratio of the number of signal leptons to the number of baseline-not-signal leptons and measured in a dedicated control region in data, which is enriched in non-prompt leptons. The background yield is estimated by applying the fake factor to each baseline-not-signal lepton in events passing an event selection requiring only baseline instead of signal leptons. Four-lepton events containing prompt baseline-not-signal leptons are removed from the estimation by using simulation predictions.

The control region in which the fake factor is evaluated is defined by selecting events containing a same-flavour and opposite-charge lepton pair, with an invariant mass within 15 GeV of m_Z, and at least one other baseline lepton. The leptons from this pair are required to have triggered the event. Events with $Z \to \ell\ell$ decays compose 90% of this sample. The remaining leptons in an event that do not form the candidate Z pair are likely to be non-prompt and to have originated from hadron decays or, to a lesser extent, from jets misidentified as leptons. There is a small contribution of prompt leptons, primarily from WZ decays, and an even smaller contribution from four-prompt-lepton events. These

contributions are subtracted using SHERPA v2.2.2 simulations. After this subtraction, the fake factor is measured in bins of lepton p_T and the number of jets in the event.

An important assumption of the fake-factor method is that the probability of any given lepton to be prompt is uncorrelated with the equivalent probabilities for other leptons in the event. Since this analysis accepts leptons which are separated by as little as $\Delta R = 0.05$, this assumption can break down. For example, cascade decays of b-hadrons can lead to two or more leptons being close to each other. In such cases, the leptons' prompt/non-prompt probabilities are highly correlated. To account for this, if two leptons are found to be within $\Delta R = 0.4$ of each other, one of them is omitted when determining the fake contribution expected from that event. The choice of which lepton to omit depends on the lepton flavour and p_T. If the leptons are different flavours, the electron is omitted, and if the leptons are of the same flavour, the one with the lower transverse momentum is omitted. This approach was validated in closure tests of the method using simulated events.

In order to limit the impact of statistical fluctuations in the non-prompt background, a smoothing procedure based on a variable-span smoothing technique [90] is used to obtain a smoother background shape and reduce the impact of single outlier events. The overall predicted background is 4% of the selected data in the signal region, and falls quickly from 38% for $m_{4\ell}$ between 20 and 60 GeV to around 2.5% for $m_{4\ell}$ above 200 GeV.

Five sources of uncertainty in the background yield are considered. First, the dominant uncertainty for $m_{4\ell} < 150$ GeV and $m_{4\ell} > 350$ GeV comes from the statistical uncertainty of the number of events with four baseline leptons, used as input to the fake-factor method. Second, dominant in the region $150 < m_{4\ell} < 350$ GeV, are the theory uncertainties of the prompt-lepton subtraction in the control region, predominantly from WZ events, which are dominated by QCD scale variations. Third, the uncertainties in the subtracted contribution of genuine four-prompt-lepton events containing baseline-not-signal leptons (which is estimated from simulation) are propagated to the background estimate, which is a sub-dominant contribution. Fourth is the statistical uncertainty of the data in the control region used to measure the fake factors, which is also subdominant. Finally, a very small uncertainty in the smoothing technique is included. The total size of the uncertainty in the predicted number of background events varies between 15% for $m_{4\ell}$ between 20 and 60 GeV and 150% for $m_{4\ell}$ of 1000 GeV.

The background estimation was validated by comparing the prediction of the method to data in dedicated background-enriched phase-space regions. The first validation region is the 'different-flavour validation region', which is defined to be like the signal region, but requires the leptons of one of the pairs to have different flavours. The second is the 'same-charge validation region', which instead requires the leptons in one of the pairs to have the same charge. After application of the estimated background yield, the data and simulation in both validation regions are in agreement within the statistical uncertainties of the data, as shown in figure 2 for the $m_{4\ell}$ observable.

The fake factor method does not account for a very small background contribution from $Z + \Upsilon$ events. These events amount to 0.2% of the selected data, and 0.8% in the $Z \to 4\ell$ region, and are removed prior to correcting for detector effects, using an estimate from PYTHIA8 simulation.
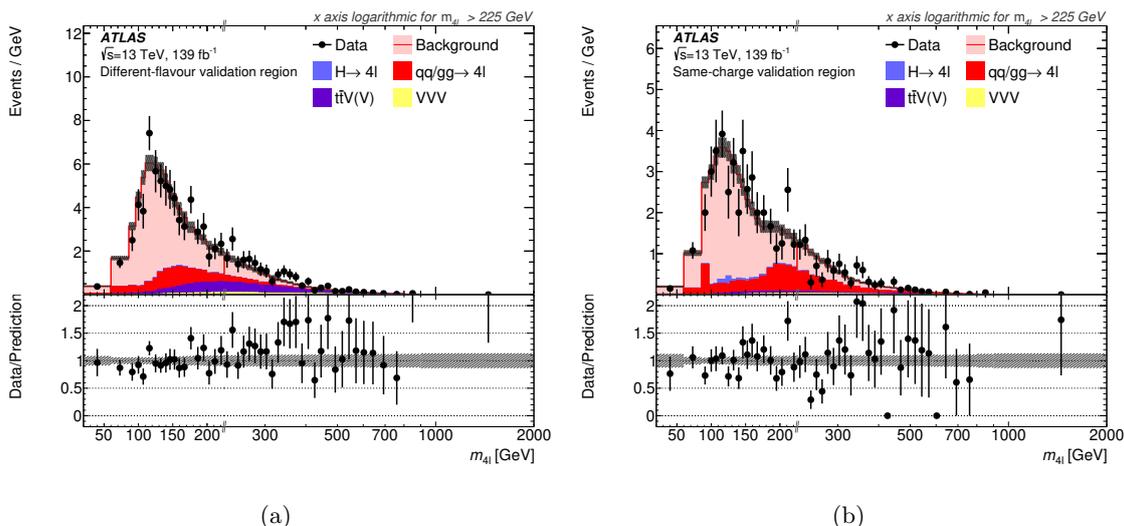
Figure 2. Observed $m_{4\ell}$ distribution compared to the data-driven estimation of the background from non-prompt leptons in the (a) different-flavour and (b) same-charge validation regions. Contributions from events with four prompt leptons, obtained from simulation, are also shown. The hashed band represents the total uncertainty on the background estimation. The x-axis is on a linear scale until $m_{4\ell} = 225$ GeV, where it switches to a logarithmic scale.

5.3 Selected events

Table 1 shows the number of selected events over the full fiducial phase space and in each $m_{4\ell}$ region. Also shown is the predicted contribution from each SM process contributing to the final state, as well as the predicted background contribution from non-prompt leptons. The SHERPA simulation is used for the $q\bar{q} \to 4\ell$ process. Uncertainties in the predictions arise from the sources discussed in sections 4, 5.2 and 5.5.

Figure 3 shows the $m_{4\ell}$ distribution, comparing data with these predictions at reconstruction-level, together with the uncertainties. The distribution shows a number of interesting features. There is a peak in the region $m_{4\ell} \sim m_Z$, dominated by the $Z \to 4\ell$ process, and a peak in the region $m_{4\ell} \sim m_H$, dominated by the $H \to 4\ell$ processes. At the threshold for producing two on-shell Z bosons, $m_{4\ell} \sim 180$ GeV, there is an increase in the cross-section. The cross-section then falls steeply.

5.4 Detector corrections

After subtracting the background due to non-prompt leptons, the measured event yields are corrected for detector effects using a combination of a per-lepton efficiency correction and an iterative Bayesian unfolding technique [91]. The detector effects include the resolution of the measured kinematic variables and the inefficiencies of reconstructing leptons and triggering on the events. The sum of the SM simulations described in section 4 are used to provide the relationship between the particle-level observables defined in section 3 and the reconstruction-level observables defined in section 5.1.

	Region				
	Full	$Z \rightarrow 4\ell$	$H \rightarrow 4\ell$	Off-shell ZZ	On-shell ZZ
$q\bar{q} \rightarrow 4\ell$	6100 ± 500	1490 ± 120	128 ± 10	800 ± 60	3640 ± 280
$gg \rightarrow 4\ell$	680 ± 90	10.8 ± 2.9	3.9 ± 0.7	49 ± 6	620 ± 80
$H \rightarrow 4\ell$	245 ± 20	2.16 ± 0.18	207 ± 17	33.5 ± 3.1	1.98 ± 0.20
VVV	35 ± 4	0.018 ± 0.005	0.127 ± 0.018	2.05 ± 0.22	32.9 ± 3.4
$t\bar{t}V(V)$	123 ± 19	1.37 ± 0.22	1.2 ± 0.2	15.5 ± 2.4	105 ± 16
Background	330 ± 50	44 ± 8	26 ± 5	129 ± 19	139 ± 30
Total Pred.	7500 ± 500	1540 ± 110	367 ± 19	1030 ± 60	4530 ± 290
Data	7755	1452	379	1095	4828

Table 1. Predicted reconstruction-level yields per process and in total, compared with observed data counts, over the full fiducial phase space and in the following regions of $m_{4\ell}$: $Z \rightarrow 4\ell$ ($60 < m_{4\ell} < 100$ GeV), $H \rightarrow 4\ell$ ($120 < m_{4\ell} < 130$ GeV), off-shell ZZ ($20 < m_{4\ell} < 60$ GeV or $100 < m_{4\ell} < 120$ GeV or $130 < m_{4\ell} < 180$ GeV) and on-shell ZZ ($180 < m_{4\ell} < 2000$ GeV). Uncertainties in the predictions include both the statistical and systematic sources. The uncertainty in the total prediction takes into account correlations between processes, and therefore contributions in a given column do not trivially add up in quadrature to give the total. The background row is events with non-prompt leptons, including those from $Z + \Upsilon$ events. The $H \rightarrow 4\ell$ row includes only the on-shell Higgs boson contribution, with off-shell contributions included in $gg \rightarrow 4\ell$.
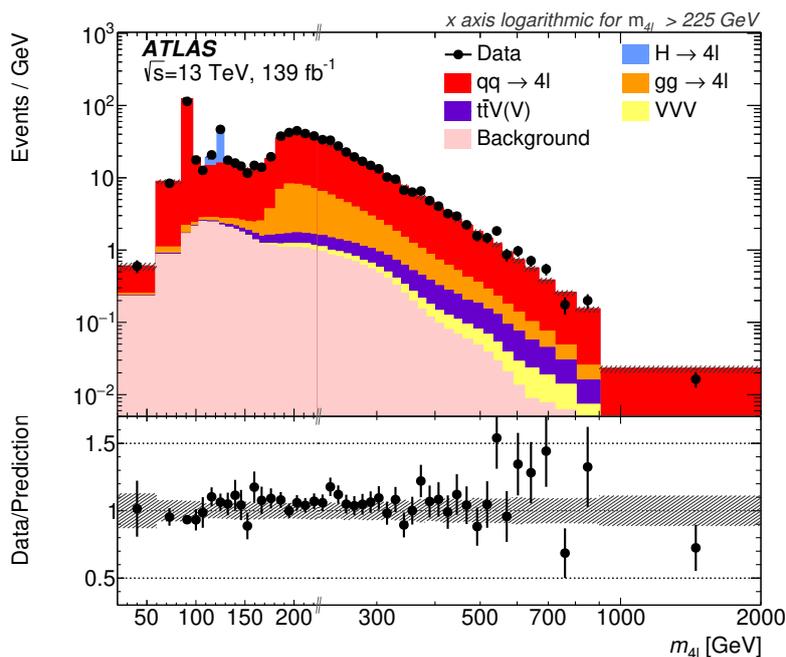

Figure 3. Observed reconstruction-level $m_{4\ell}$ distribution compared with the SM prediction, using SHERPA for the $q\bar{q} \rightarrow 4\ell$ simulation. The statistical uncertainty of the data is displayed as error bars and systematic uncertainties in the prediction are shown as a grey hashed band. The ratio of the data to the prediction is shown in the lower panel. The x-axis is on a linear scale until $m_{4\ell} = 225$ GeV, where it switches to a logarithmic scale, as indicated by the double dashes on the axis. There is one additional data event reconstructed with $m_{4\ell} = 2.14$ TeV, while 0.4 events are expected from simulation for $m_{4\ell} > 2$ TeV.

The first step is a correction for the reconstruction, identification, isolation and vertex-matching efficiency of each lepton in the quadruplet, which is referred to as a pre-unfolding efficiency correction. The efficiency is measured in the simulation as a function of η and p_T for electrons and muons, treating those from τ decays separately, due to a lower $|d_0|/\sigma_{d_0}$ efficiency. It is defined as the ratio of the number of reconstruction-level leptons (that are matched with $\Delta R < 0.05$ to particle-level leptons) to the number of particle-level leptons. A per-event weight is given by: $\prod_{i=1}^{4} [\epsilon_i (p_{Ti}, \eta_i)]^{-1}$, where $\epsilon_i (p_{Ti}, \eta_i)$ is the efficiency for the ith lepton in the quadruplet, treated as uncorrelated between leptons. The efficiency for a given lepton-flavour is obtained from a weighted-average of the efficiency from leptons that originate from τ decays and those that do not, using the $m_{4\ell}$-dependent admixture expected from the simulation. The per-event weight defined above is applied to events in both data and simulation, taking the η and p_T values from the leptons in data and simulation respectively. This ensures there is minimal dependence on the SM description of the lepton kinematics when correcting the data.

The data are then corrected for events that pass the reconstruction-level selection but fail the particle-level selection. This primarily occurs due to resolution effects, and is corrected by a multiplicative factor, known as a fiducial correction, in each bin of each distribution. Then, the iterative Bayesian procedure is applied using the SM particle-level distribution as the initial prior. The data are unfolded using a migration matrix containing probabilities that an event in a given particle-level bin of a distribution is found in a particular reconstruction-level bin of that distribution. This matrix is formed from events that pass both the particle-level and reconstruction-level event selections. This process is iterated with the prior being replaced by the unfolded data from the previous iteration: three iterations are used for all distributions, with the exception of m_{12}, $|\Delta y_{\text{pairs}}|$ and $|\Delta \phi_{\ell\ell}|$ where only two iterations are applied. The iterations chosen represent the optimal compromise between the increase of the statistical uncertainty with too many iterations, and the increase of the residual bias due to over-regularisation with too few iterations.

The final step is to divide the resulting unfolded distribution by the ratio of the number of events passing both particle- and reconstruction-level selections to the number passing the particle-level selections. This is known as an efficiency correction. Since the reconstruction-level selections have already had the pre-unfolding weights applied, this correction is fairly close to one, but it accounts for any residual effects such as resolution and trigger efficiencies.

For sliced variables the distributions are unfolded simultaneously, properly taking into account the migration between regions. The integrated cross-section is obtained by correcting the total number of observed events, after background subtraction and application of pre-unfolding weights, with the fiducial and efficiency corrections calculated for the inclusive phase space. When unfolding the per-region cross-sections the inter-region migrations are accounted for.

The binning of each distribution is driven by the requirement that the fraction of events in a reconstruction-level bin that originate from the same bin at particle-level is at least 60% (70%, 80%) if 25 (20, 14) or more events are predicted for the reconstruction-

level yield of the bin. At least 14 events must be expected in each bin. These requirements ensure that the number of events is approximately Gaussian distributed. There is an additional constraint that bins should be centred on the various resonant peaks in the distributions.

The unfolding method is designed to minimise the dependence on the simulation of the underlying kinematics of the particles. To validate this, a data-driven closure test is performed, where a simulated pseudo-data sample is formed by reweighting the simulation such that the distribution agrees with the data. This pseudo-data sample is then unfolded with the nominal simulation and the resulting unfolded distribution is compared with the input reweighted particle-level prediction. They are in good agreement with each other, and the small differences, averaging much less than 1% but reaching 3% in a few bins in some distributions, are taken as a systematic uncertainty of the final result.

In order to demonstrate that these measurements are robust against the presence of BSM physics in the data and can be used to constrain BSM models, a number of BSM signal injection tests are performed. Pseudo-data consisting of SM+BSM simulations are unfolded with the nominal SM simulation and the result is compared with the particle-level SM+BSM simulation. Any differences are interpreted as a bias in the unfolded SM+BSM result. Overall, the results are found to be extremely robust with only small differences seen, all of them within the experimental uncertainties. Models that predict a broad excess over the SM prediction, such as wide resonances and modifications to SM couplings, lead to very small biases in the unfolded distributions. As an example, the addition of a heavy Higgs boson, with various Higgs masses ranging from 300 GeV to 1400 GeV, and a width of 15% of the mass, is studied. The cross-section of the process is scaled such that the change relative to the SM prediction is equivalent to 2σ of the data uncertainty. The bias in the unfolded result is always less than 20% of the total experimental uncertainty in any given bin, with most cases and bins being considerably less affected. Without the pre-unfolding corrections applied the bias is up to a factor of two larger, indicating that the pre-unfolding step improves the robustness of the unfolding. The same tests are performed with narrow-width heavy Higgs bosons, which lead to predicted enhancements in a single bin only. These tests lead to slightly larger biases due to the more drastic changes in the predicted shapes of distributions. In this case the bias observed is still always within experimental uncertainties, with the maximum being 50% of the total experimental uncertainty (which is dominated by the statistical component) in any given bin. This bias slightly reduces the cross-section in the bin of interest. This implies that limits placed on narrow resonances will be slightly more stringent, or that claims of an excess would be slightly less significant, than they would be without the bias.

5.5 Uncertainties

The statistical uncertainty of the data is dominant for the vast majority of the differential cross-section bins. It is estimated with two approaches: the first is a model-independent approach, using the observed number of events, which is used as the quoted uncertainty in the measurements, and the second uses the expected number of SM events, which is appropriate when testing the observed cross-section against the SM prediction. In the first

approach, 3500 pseudo-datasets are generated by assigning random Poisson-distributed weights of mean one to the data events, and taking the root mean square of the differences between all the unfolded results obtained using the pseudo-datasets. The statistical uncertainties obtained in this way are equivalent to frequentist confidence intervals in the large-sample limit, while in the bins with few entries, the quoted bands are known to be up to 10% narrower than a frequentist confidence interval. In the second approach, 3500 Poisson-distributed pseudo-datasets are generated with a mean equal to the predicted reconstruction-level SM event yield in each bin, unfolding each one and taking the root mean square of the differences between all the unfolded results.

The systematic uncertainties of the measured cross-sections are evaluated by repeating the measurement after applying each associated variation and comparing the unfolded result with the nominal one. Significant contributions arise from uncertainties in the lepton reconstruction, identification, isolation and track-to-vertex matching efficiencies, and momentum resolution and scale. These uncertainties are derived from the data-driven measurements used to determine the factors applied to the simulation [84, 85], as discussed in section 4. Another important source of uncertainty arises from the choice of generator in the simulation of the $q\bar{q} \to 4\ell$ process (the nominal SHERPA prediction and the alternative POWHEG + PYTHIA8 prediction, both introduced in section 4) used to unfold the results. The predominant effect on the measured distributions comes from a known difference between the two generators' modelling of the final-state radiation of photons. When this difference is evaluated the POWHEG + PYTHIA8 prediction is first reweighted to match the SHERPA prediction for the distribution being unfolded. This is to avoid double counting with the data-driven closure test, described in section 5.4. Particularly important in the tails is the uncertainty in the estimate of the background from non-prompt leptons, as described in section 5.2. A flat uncertainty of $\pm 1.7\%$ is assigned as a result of the uncertainty in determining the luminosity for the Run 2 dataset [92, 93]. Smaller uncertainties come from the slight non-closure in the data-driven test for the unfolding, described in section 5.4, the statistical uncertainty of the simulated samples, the uncertainty in the inelastic cross-section, and the other theory uncertainties, the last two both introduced in section 4. The theory uncertainties have small effects on the unfolding due to changes in the shape and normalisation of the various SM contributions. They have a much larger effect on the particle-level predictions that are compared with the data. The dominant uncertainty comes from the scale variations for each process. Figure 4 shows the breakdown of the uncertainties for the measured $m_{4\ell}$ distribution. The statistical uncertainty of the data is the dominant source of uncertainty in all but the third mass bin (at $m_{4\ell} \approx m_Z$), where the uncertainty in lepton efficiencies dominates. The generator uncertainty shows some bin-to-bin fluctuations due to the limited Monte Carlo sample sizes when comparing the unfolding performed with the SHERPA and POWHEG + PYTHIA8 predictions, as well as some real features due to the $m_{4\ell}$-dependence of the differences in the generators' modelling of the final-state radiation of photons.

The covariance matrices for the statistical and systematic uncertainties are available in HEPData for each distribution. The dominant parts of the lepton uncertainties are highly correlated across bins. The background uncertainties are mostly uncorrelated as
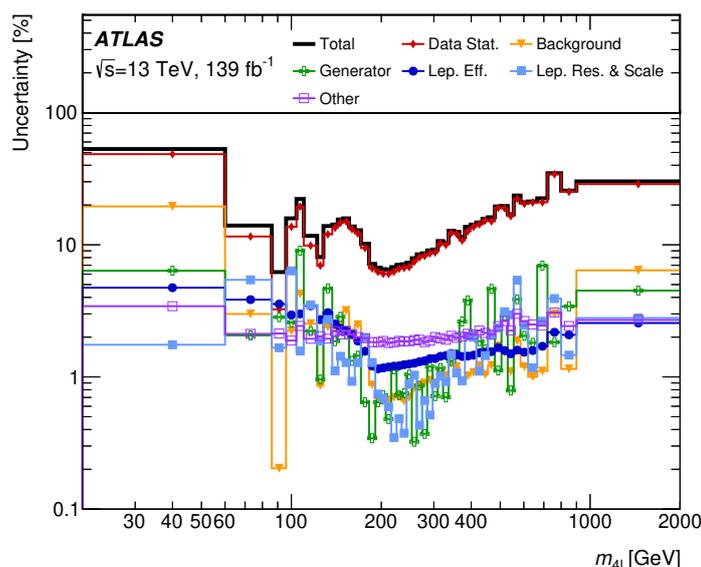
Figure 4. Uncertainty breakdown of the measured cross-section as a function of $m_{4\ell}$. "Lep. Eff." refers to the uncertainties in the lepton efficiencies, "Lep. Res. & Scale" refers to the uncertainties in the lepton resolutions and scales, and the theory uncertainties are included in the "Generator" uncertainty. Contributions from the Monte Carlo statistical uncertainty and uncertainties in the luminosity and the inelastic cross-section are included in "Other".

they are driven by limited sample size. The systematic uncertainty arising from the choice of generator is highly correlated across bins.

For the theoretical uncertainties of the particle-level predictions, the uncertainties from each individual process are treated as uncorrelated and an additional decorrelation of the scale uncertainty between the four $m_{4\ell}$ regions for the $q\bar{q} \to 4\ell$ process is introduced. This strategy is motivated by the fact that each region probes a very different interaction scale, and a different type of process is dominant. This correlation scheme also leads to the most conservative results when interpreting the data.

6 Results

6.1 Measurements

Table 2 gives the measured cross-sections in the full fiducial phase space and in the four $m_{4\ell}$ regions, each dominated by a different process, compared with the theoretical predictions described in section 4. Two predictions are shown, one where the $q\bar{q} \to 4\ell$ process is simulated with SHERPA at NLO accuracy in QCD and one where it is simulated with POWHEG + PYTHIA8 normalised to a prediction at NNLO accuracy in QCD, as described in section 4. All the other SM processes are the same in the two predictions. The SHERPA prediction is generally higher than the POWHEG + PYTHIA8 prediction in all but the on-shell region, where the predictions are very close. The cross-sections measured in data generally agree with both predictions within the quoted uncertainties. The data central

| | Region | | | | |
	Full	$Z \to 4\ell$	$H \to 4\ell$	Off-shell ZZ	On-shell ZZ
Measured	88.9	22.1	4.76	12.4	49.3
fiducial	±1.1 (stat.)	±0.7 (stat.)	±0.29 (stat.)	±0.5 (stat.)	±0.8 (stat.)
cross-section	±2.3 (syst.)	±1.1 (syst.)	±0.18 (syst.)	±0.6 (syst.)	±0.8 (syst.)
[fb]	±1.5 (lumi.)	±0.4 (lumi.)	±0.08 (lumi.)	±0.2 (lumi.)	±0.8 (lumi.)
	±3.0 (total)	±1.3 (total)	±0.35 (total)	±0.8 (total)	±1.3 (total)
SHERPA	86±5	23.6±1.5	4.57±0.21	11.5±0.7	46.0±2.9
POWHEG + PYTHIA8	83±5	21.2±1.3	4.38±0.20	10.7±0.7	46.4±3.0

Table 2. Fiducial cross-sections in fb in the full fiducial phase space and in the following regions of $m_{4\ell}$: $Z \to 4\ell$ ($60 < m_{4\ell} < 100$ GeV), $H \to 4\ell$ ($120 < m_{4\ell} < 130$ GeV), off-shell ZZ ($20 < m_{4\ell} < 60$ GeV or $100 < m_{4\ell} < 120$ GeV or $130 < m_{4\ell} < 180$ GeV) and on-shell ZZ ($180 < m_{4\ell} < 2000$ GeV), compared with particle-level predictions and their uncertainties as described in section 4. Two predictions are shown for the $q\bar{q} \to 4\ell$ process simulated with SHERPA or with POWHEG + PYTHIA8. All other SM processes are the same for the two predictions.

values are above the POWHEG + PYTHIA8 predictions in all regions, and in all but the $Z \to 4\ell$ region for SHERPA. In the on-shell region the SHERPA prediction is a bit more than 1σ below the data. In ref. [94] the $H \to 4\ell$ cross-section is measured by ATLAS in a fiducial phase space that differs slightly from the $H \to 4\ell$ region measured here. The phase space is designed to minimise the contribution from non-$H \to 4\ell$ processes. In the dedicated Higgs boson measurement the cross-section is found to be slightly below the SM prediction. The dedicated Higgs boson measurement differs from the present measurement in using a slightly different phase space, in subtracting non-Higgs boson processes using a data-driven approach, and in including a $\sim 1\%$ contribution from Higgs boson production in association with a b-quark pair in the prediction.

The differential cross-section as a function of $m_{4\ell}$ is shown in figure 5, in much finer bins than those in table 2. The breakdown of the contribution from different SM processes is also shown. The features seen in the reconstruction-level distribution in figure 3 are also present here. The SM predictions agree well with the measurement within uncertainties over the entire $m_{4\ell}$ spectrum, with the same features seen as in the comparisons in table 2. For this distribution, and all the others shown below, two p-values for the observed data given the predicted SM cross-section (using either SHERPA or POWHEG to model the $q\bar{q} \to 4\ell$ contribution) are obtained from the χ^2. This is defined as $\chi^2 = \left[\vec{\sigma}^{\mathrm{meas}} - \vec{\sigma}^{\mathrm{pred}}\right]^T C^{-1} \left[\vec{\sigma}^{\mathrm{meas}} - \vec{\sigma}^{\mathrm{pred}}\right]$, where $\vec{\sigma}^{\mathrm{meas}}$ and $\vec{\sigma}^{\mathrm{pred}}$ are k-dimensional vectors from the measured and predicted differential cross-sections of a given observable respectively, and C is the $k \times k$ total covariance matrix defined by the sum of the statistical and systematic covariances in $\vec{\sigma}^{\mathrm{meas}}$ and $\vec{\sigma}^{\mathrm{pred}}$. The statistical covariance on $\vec{\sigma}^{\mathrm{meas}}$ is obtained from the expected number of SM events, as described in section 5.5. The p-value is the probability for the χ^2, with k degrees of freedom, to have at least the observed value.

In order to study the different $m_{4\ell}$ regions in more detail, Figures 6 and 7 show the cross-section versus m_{12} and m_{34} respectively in each region. In the $H \to 4\ell$ region, the contribution from Higgs boson production is shown separately. The different regions show peaks in different places due to the kinematic constraints of the $m_{4\ell}$ requirements. For all
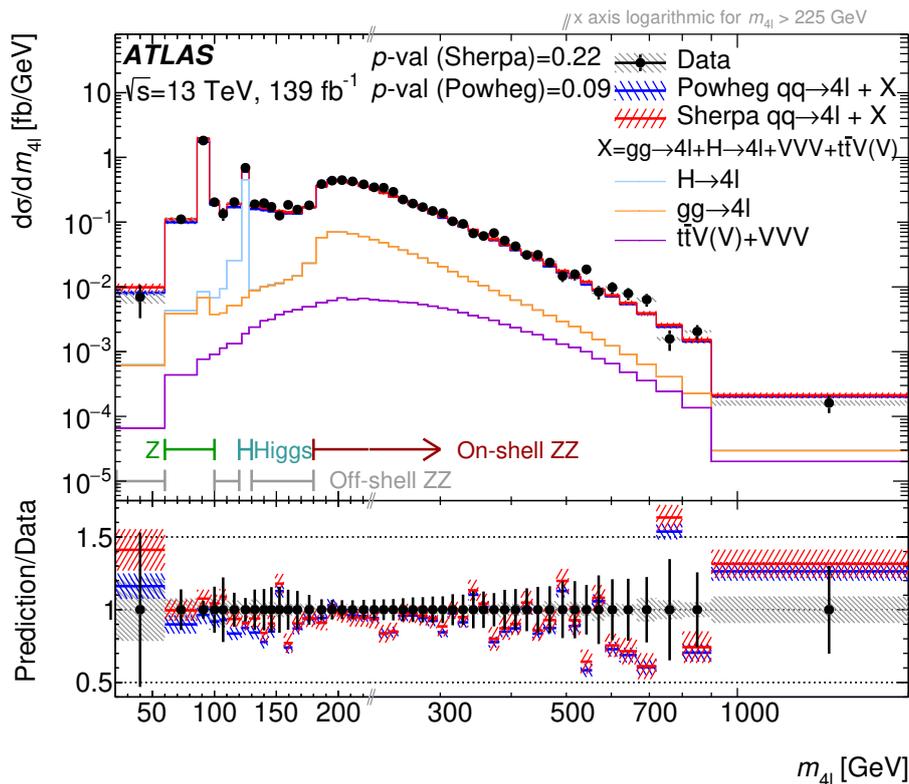
Figure 5. Differential cross-section as a function of $m_{4\ell}$. The measured data (black points) are compared with the SM prediction using either SHERPA (red, with red hashed band for the uncertainty) or POWHEG + PYTHIA8 (blue, with blue hashed band for the uncertainty) to model the $q\bar{q} \to 4\ell$ contribution. The error bars on the data points give the total uncertainty and the grey hashed band gives the systematic uncertainty. The breakdown of the contribution from different SM processes is also shown in successive stacked histograms. The short vertical lines terminating horizontal lines indicate the boundaries of the different $m_{4\ell}$ regions in which the other variables are measured. The p-value is the probability for the χ^2, with the number of degrees of freedom equal to the number of bins in the distribution, to have at least the observed value, given the SM prediction. The lower panel shows the ratio of the SM predictions to the data. The x-axis is on a linear scale until $m_{4\ell} = 225$ GeV, where it switches to a logarithmic scale.

regions but $Z \to 4\ell$ there is a clear enhancement at m_Z for m_{12}. Conversely, m_{34} only has contributions from on-shell Z bosons in the on-shell region. The $Z \to 4\ell$ and off-shell regions are dominated by off-shell photon and Z boson exchange, and the $H \to 4\ell$ region is dominated by off-shell Z production. The data are generally well modelled by the SM predictions within uncertainties, although, as already discussed, the normalisation of the predictions in the on-shell region is lower than the observed measurement, and for the POWHEG + PYTHIA8 prediction it is lower in all the regions, especially the off-shell ZZ region. Combined with some statistical fluctuations in the data this gives some low p-values for some of the distributions, especially for the POWHEG + PYTHIA8 prediction. This is also true for the measurements in figures 8–11. For m_{12} in the on-shell ZZ region, the predictions are below the data for m_{12} below m_Z, and above the data for m_{12} above m_Z.

(a) $Z \rightarrow 4\ell$ region

(b) $H \rightarrow 4\ell$ region

(c) Off-shell ZZ region
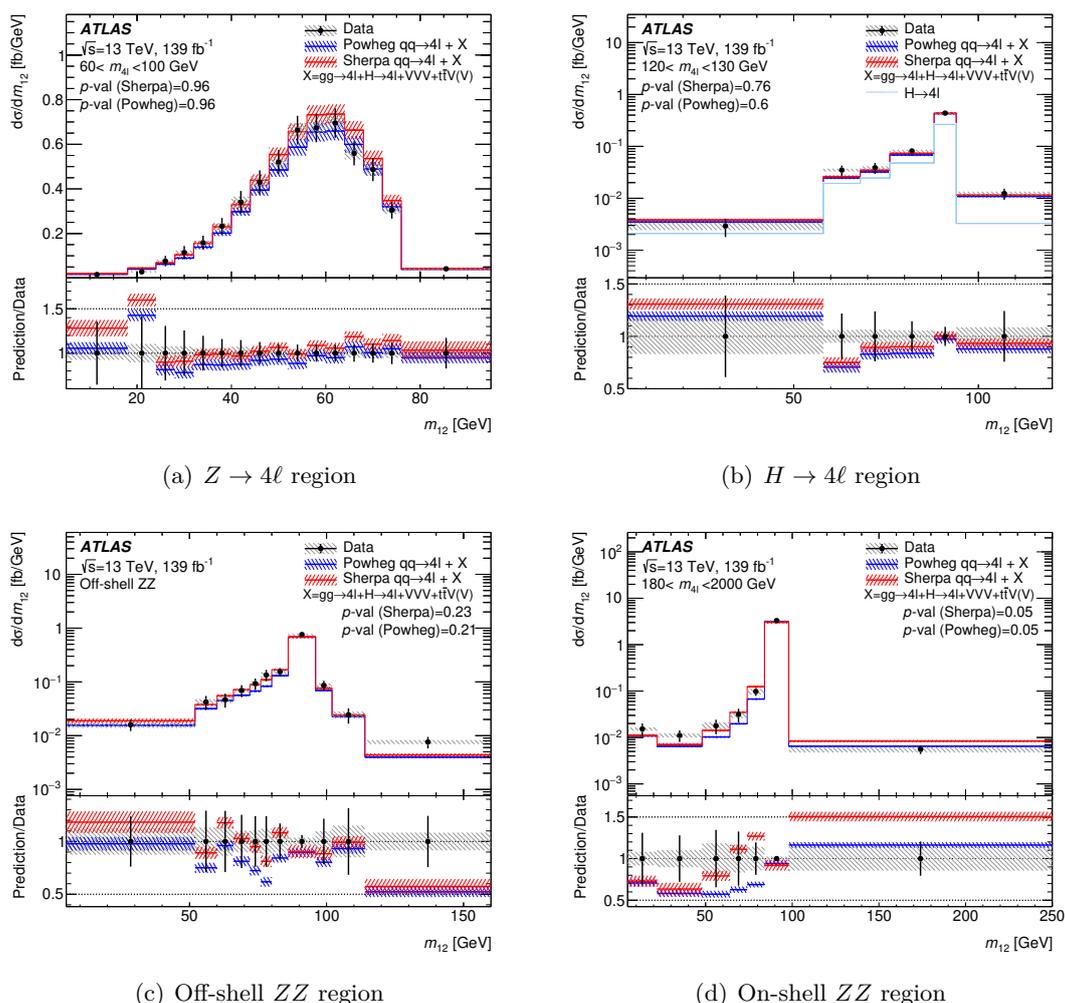
(d) On-shell ZZ region

Figure 6. Differential cross-section as a function of m_{12} in the four $m_{4\ell}$ regions. The measured data (black points) are compared with the SM prediction using either SHERPA (red, with red hashed band for the uncertainty) or POWHEG + PYTHIA8 (blue, with blue hashed band for the uncertainty) to model the $q\bar{q} \rightarrow 4\ell$ contribution. In (b) the contribution from Higgs production is shown in addition to the total SM prediction. The error bars on the data points give the total uncertainty and the grey hashed band gives the systematic uncertainty. The p-value is the probability for the χ^2, with the number of degrees of freedom equal to the number of bins in the distribution, to have at least the observed value, given the SM prediction. The lower panel shows the ratio of the SM predictions to the data.

Here the shapes of the two SM predictions also deviate from each other, indicating differences in the modelling, perhaps related to the modelling of the final-state radiation of photons. The m_{12} and m_{34} measurements provide particular sensitivity to BSM models in which the lepton pairs do not come from Z boson decays, as discussed in section 6.3.

Figure 8 shows the differential cross-sections as a function of $|\Delta\phi_{\text{pairs}}|$, $|\Delta y_{\text{pairs}}|$, $p_{\text{T},12}$, and $p_{\text{T},34}$ in the highest cross-section, on-shell ZZ region. The $|\Delta\phi_{\text{pairs}}|$ distribution peaks at π, with the dilepton pairs back-to-back. The $|\Delta y_{\text{pairs}}|$ distribution peaks at zero, with a

(a) $Z \to 4\ell$ region

(b) $H \to 4\ell$ region
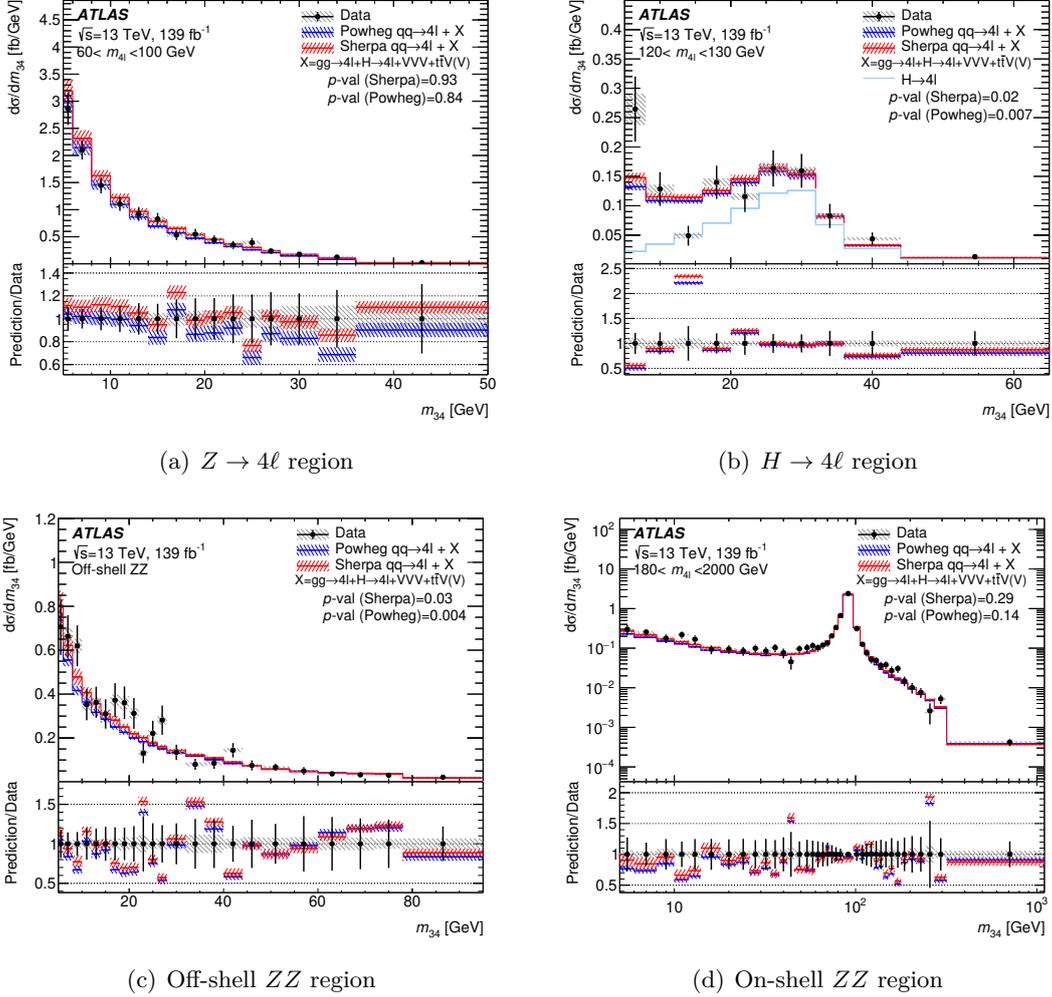
(c) Off-shell ZZ region

(d) On-shell ZZ region

Figure 7. Differential cross-section as a function of m_{34} in the four $m_{4\ell}$ regions. The measured data (black points) are compared with the SM prediction using either SHERPA (red, with red hashed band for the uncertainty) or POWHEG + PYTHIA8 (blue, with blue hashed band for the uncertainty) to model the $q\bar{q} \to 4\ell$ contribution. In (b) the contribution from Higgs production is shown in addition to the total SM prediction. The error bars on the data points give the total uncertainty and the grey hashed band gives the systematic uncertainty. The p-value is the probability for the χ^2, with the number of degrees of freedom equal to the number of bins in the distribution, to have at least the observed value, given the SM prediction. The lower panel shows the ratio of the SM predictions to the data.

(a) $|\Delta\phi_{\mathrm{pairs}}|$

(b) $|\Delta y_{\mathrm{pairs}}|$

(c) $p_{\mathrm{T},12}$

(d) $p_{\mathrm{T},34}$

Figure 8. Differential cross-sections as a function of (a) $|\Delta\phi_{\mathrm{pairs}}|$, (b) $|\Delta y_{\mathrm{pairs}}|$, (c) $p_{\mathrm{T},12}$, and (d) $p_{\mathrm{T},34}$ in the on-shell ZZ region. The measured data (black points) are compared with the SM prediction using either SHERPA (red, with red hashed band for the uncertainty) or POWHEG + PYTHIA8 (blue, with blue hashed band for the uncertainty) to model the $q\bar{q} \to 4\ell$ contribution. The error bars on the data points give the total uncertainty and the grey hashed band gives the systematic uncertainty. The p-value is the probability for the χ^2, with the number of degrees of freedom equal to the number of bins in the distribution, to have at least the observed value, given the SM prediction. The lower 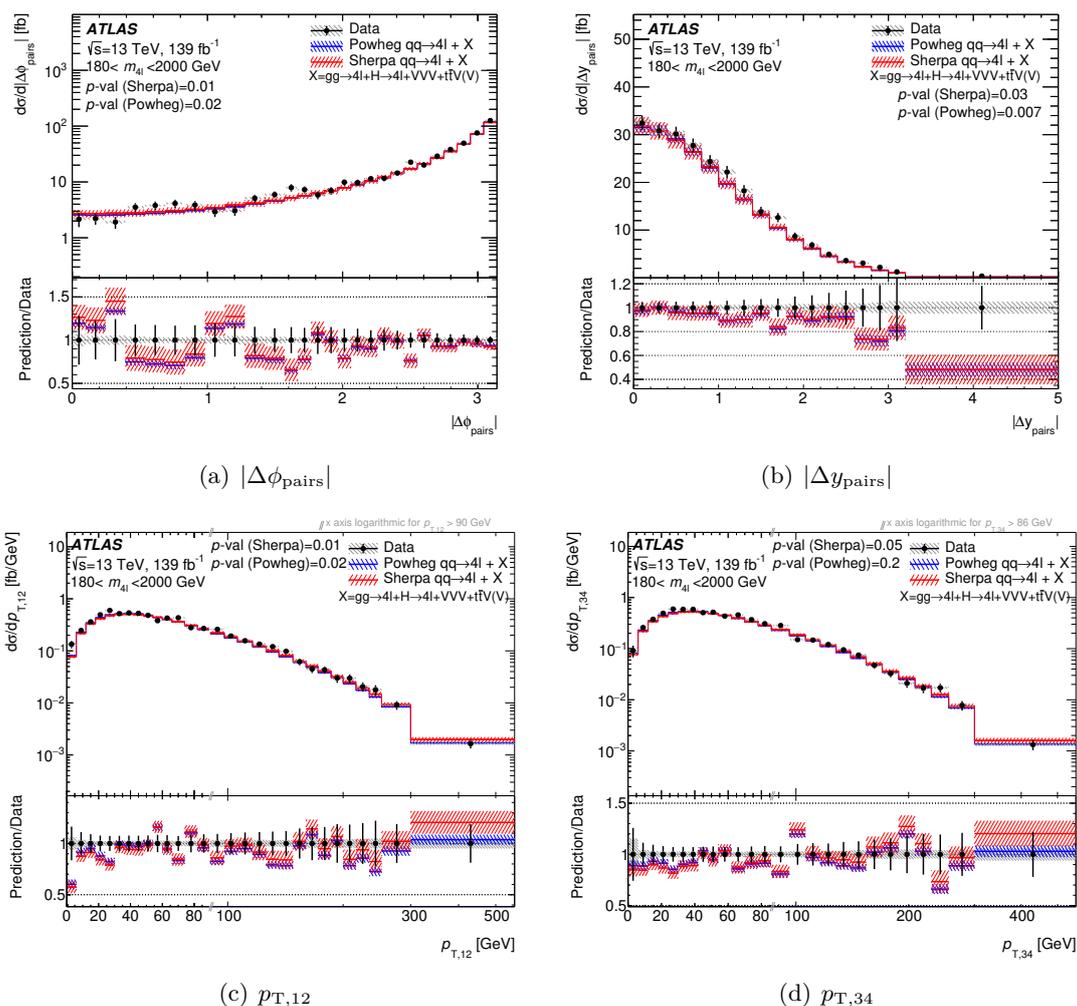panel shows the ratio of the SM predictions to the data. In (c) the x-axis is on a linear scale until $p_{\mathrm{T},12} = 90$ GeV, where it switches to a logarithmic scale; in (d) it switches at $p_{\mathrm{T},34} = 86$ GeV.

tail going out to five. The $p_{\mathrm{T},12}$ and $p_{\mathrm{T},34}$ distributions peak at around 40 GeV. Overall, the SM gives a reasonable description of the kinematics in this region, although the SM prediction is about 20% lower than the data for $2.6 < |\Delta y_{\mathrm{pairs}}| < 3.2$ and 50% lower for $|\Delta y_{\mathrm{pairs}}| > 3.2$, indicating mis-modelling by the simulation in this region of phase space.

Figure 9 shows the cross-section versus $|\Delta\phi_{\ell\ell}|$ for each region, and good agreement with the SM prediction is seen. In each region the cross-section peaks when the two
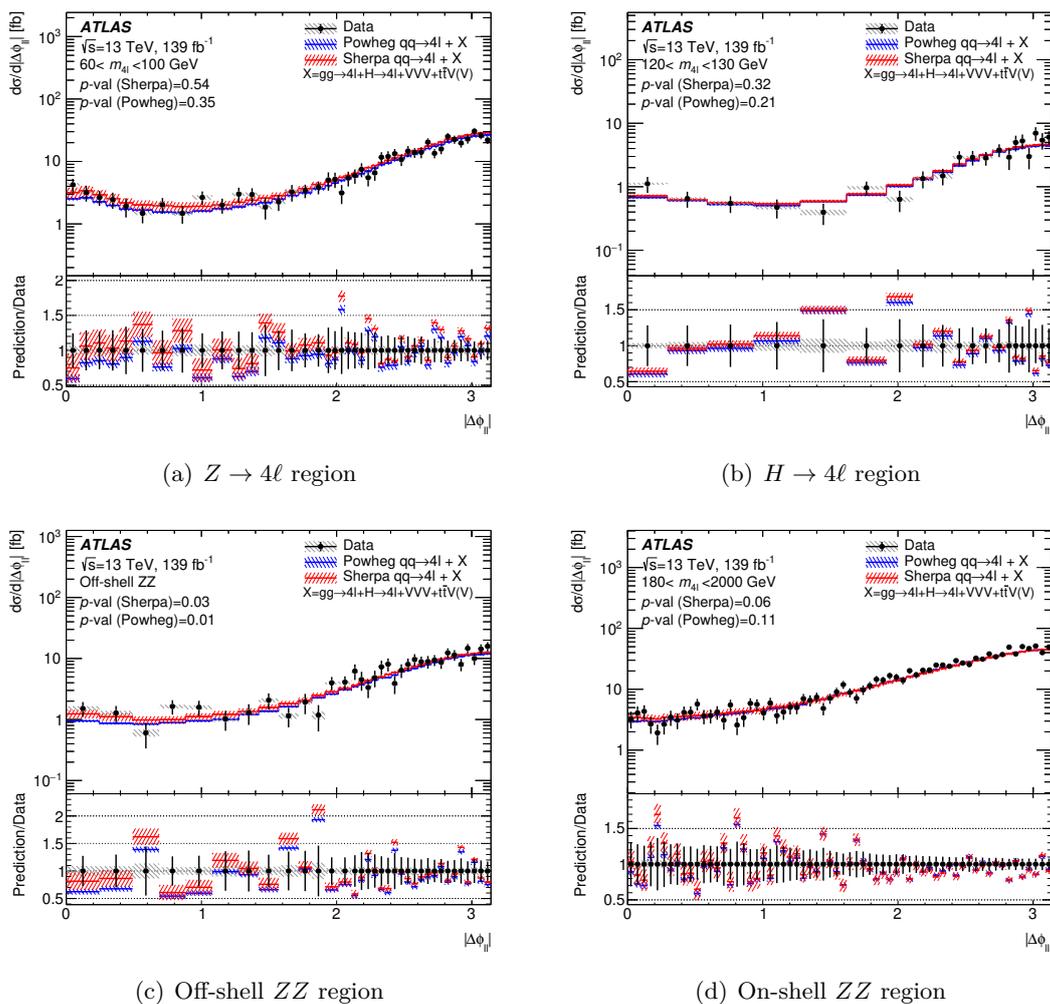
(a) $Z \to 4\ell$ region

(b) $H \to 4\ell$ region

(c) Off-shell ZZ region

(d) On-shell ZZ region

Figure 9. Differential cross-section as a function of $|\Delta\phi_{\ell\ell}|$ in the four $m_{4\ell}$ regions. The measured data (black points) are compared to the SM prediction using either SHERPA (red, with red hashed band for the uncertainty) or POWHEG + PYTHIA8 (blue, with blue hashed band for the uncertainty) to model the $q\bar{q} \to 4\ell$ contribution. The error bars on the data points give the total uncertainty and the grey hashed band gives the systematic uncertainty. The p-value is the probability for the χ^2, with the number of degrees of freedom equal to the number of bins in the distribution, to have at least the observed value, given the SM prediction. The lower panel shows the ratio of the SM predictions to the data.

leading leptons are back-to-back. This variable is sensitive to electroweak corrections to the four-lepton final state [95].

Figures 10 and 11 show $\cos\theta^*_{12}$ and $\cos\theta^*_{34}$ respectively, in all four regions. These variables are sensitive to the polarisation of the decaying bosons. Good agreement with the SM prediction is seen in all regions.

The remaining measured differential cross-sections introduced in section 3.3 are shown in the appendix.
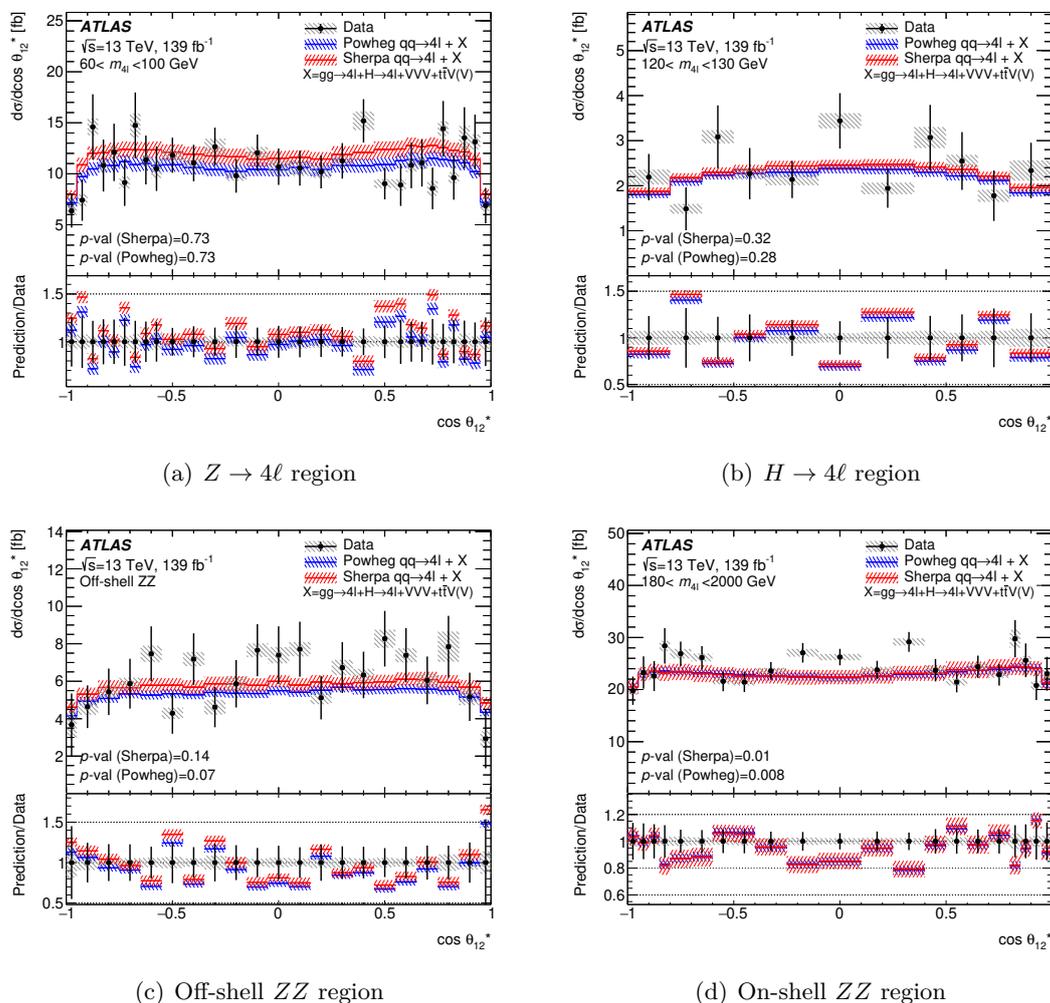
Figure 10. Differential cross-section as a function of $\cos\theta_{12}^*$ in the four $m_{4\ell}$ regions. The measured data (black points) are compared with the SM prediction using either SHERPA (red, with red hashed band for the uncertainty) or POWHEG + PYTHIA8 (blue, with blue hashed band for the uncertainty) to model the $q\bar{q} \to 4\ell$ contribution. The error bars on the data points give the total uncertainty and the grey hashed band gives the systematic uncertainty. The p-value is the probability for the χ^2, with the number of degrees of freedom equal to the number of bins in the distribution, to have at least the observed value, given the SM prediction. The lower panel shows the ratio of the SM predictions to the data.

(a) $Z \to 4\ell$ region

(b) $H \to 4\ell$ region

(c) Off-shell ZZ region

(d) On-shell ZZ region

Figure 11. Differential cross-sections as a function of $\cos\theta_{34}^*$ in the four $m_{4\ell}$ regions. The measured data (black points) are compared with the SM prediction using either SHERPA (red, with red hashed band for the uncertainty) or POWHEG + PYTHIA8 (blue, with blue hashed band for the uncertainty) to model the $q\bar{q} \to 4\ell$ contribution. The error bars on the data points give the total uncertainty and the grey hashed band gives the systematic uncertainty. The p-value is the probability for the χ^2, with the number of degrees of freedom equal to the number of bins in the distribution, to have at least the observed value, given the SM prediction. The lower panel shows the ratio of the SM predictions to the data.
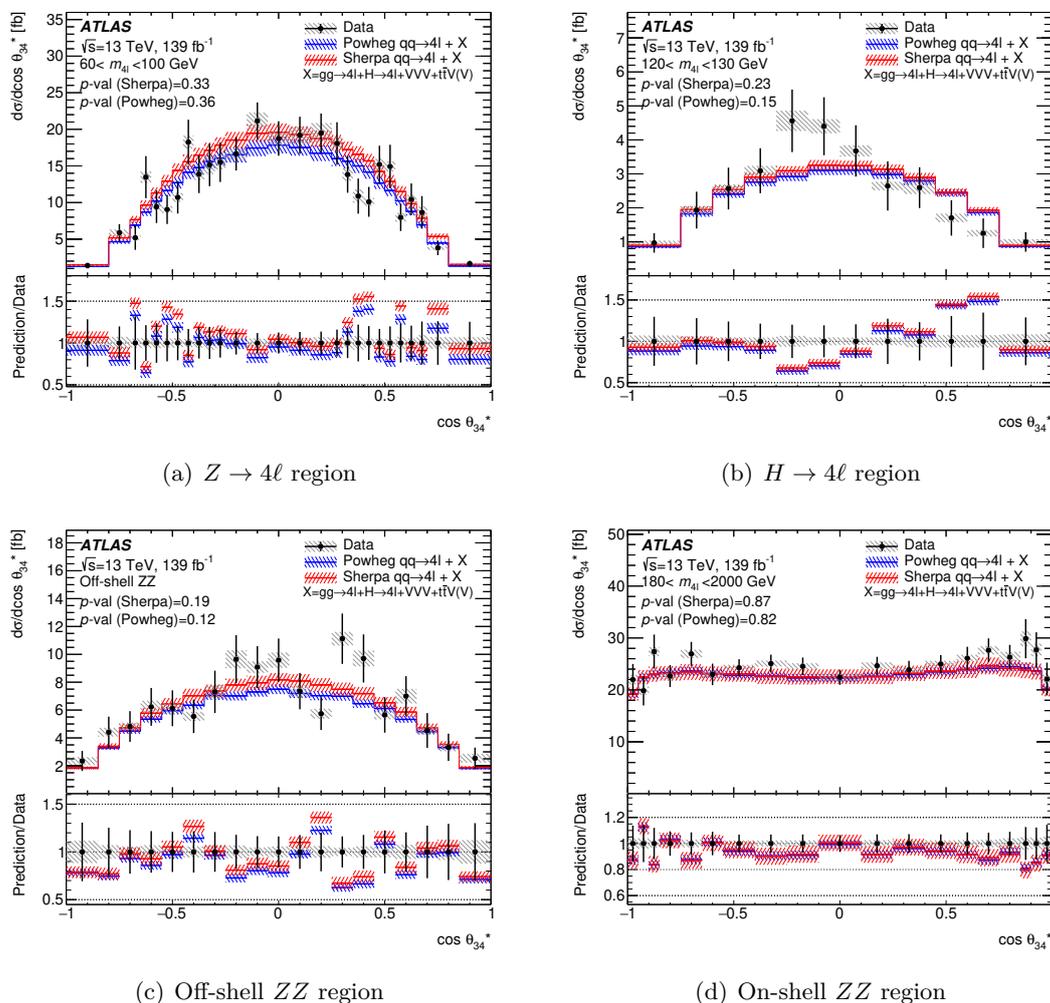
6.2 Extraction of the $Z \to 4\ell$ branching fraction

The $Z \to 4\ell$ branching fraction is extracted using the measured cross-section in the $Z \to 4\ell$ region, $\sigma^{\mathrm{meas}} = 22.1 \pm 1.3$ fb, shown in table 2. An extrapolation is performed using particle-level simulation to a phase space that was used in previous measurements of the branching fraction [7, 9, 96], allowing direct comparison. This phase space is defined by only two requirements: $80 < m_{4\ell} < 100$ GeV and $m_{\ell\ell} > 4$ GeV, with no requirements made on the kinematics of the individual leptons. The definition of the final state is based on leptons before photon radiation (Born level), with no isolation applied and excludes leptons from τ decays. An acceptance factor $A_{\mathrm{fid}} = 0.0852 \pm 0.0015$ is defined as the ratio of simulated particle-level events passing the fiducial selection used for σ^{meas} to those in the extended phase space, calculated using SHERPA. The uncertainty comes from the same sources as discussed in section 4 and is dominated by the scale variations.

The branching fraction is calculated as

$$\mathcal{B}_{Z \to 4\ell} = \frac{\left(\sigma^{\mathrm{meas}} - \sigma^{\mathrm{pred}}_{\mathrm{non}\text{-}q\bar{q} \to 4\ell}\right) \times f_{\mathrm{Z}} \times f_{\mathrm{non}\text{-}\tau}}{\sigma_Z \times A_{\mathrm{fid}}}, \tag{6.1}$$

where $\sigma^{\mathrm{pred}}_{\mathrm{non}\text{-}q\bar{q} \to 4\ell} = 0.22 \pm 0.04$ fb is the predicted fiducial cross-section from sources other than $q\bar{q} \to 4\ell$, obtained from the respective simulations; $f_{\mathrm{Z}} = 0.952 \pm 0.005$ is the fraction of $q\bar{q} \to 4\ell$ coming from single Z production rather than the t-channel ZZ process, obtained from POWHEG-BOX v2; $f_{\mathrm{non}\text{-}\tau} = 0.99186 \pm 0.00014$ is the fraction of events where no leptons originate from τ decays, obtained from SHERPA; and σ_Z is the total cross-section for single-Z production, taken from the ATLAS measurement in ref. [97] using 81 pb^{-1}, with a correction of 0.935 ± 0.001 to account for the different Z mass window. The uncertainties in $\sigma^{\mathrm{pred}}_{\mathrm{non}\text{-}q\bar{q} \to 4\ell}$ and f_{Z} come from the sources discussed in section 4, and are dominated by scale variations, while the uncertainty in $f_{\mathrm{non}\text{-}\tau}$ is statistical only.

Together, these yield a result of

$$\begin{aligned}
\mathcal{B}_{Z \to 4\ell} &= (4.41 \pm 0.13\,(\mathrm{stat.}) \pm 0.23\,(\mathrm{syst.}) \pm 0.09\,(\mathrm{theory}) \pm 0.12\,(\mathrm{lumi.})) \times 10^{-6} \\
&= (4.41 \pm 0.30) \times 10^{-6},
\end{aligned}$$

where the statistical, systematic and luminosity uncertainties come from the measurements of σ^{meas} and σ_Z, and the theory uncertainty includes contributions from A_{fid}, f_{Z}, $f_{\mathrm{non}\text{-}\tau}$ and $\sigma^{\mathrm{pred}}_{\mathrm{non}\text{-}q\bar{q} \to 4\ell}$. Since the measurement of σ_Z was performed with only 81 pb^{-1} of pp collision data, all detector-related systematic uncertainties as well as the luminosity uncertainty are conservatively treated as uncorrelated between σ^{meas} and σ_Z. The measurement is compatible with previous measurements [7, 9, 96] and with the SM prediction of $(4.50 \pm 0.01) \times 10^{-6}$, calculated with POWHEG [96]. The current measurement is the most precise to date, and benefits from an acceptance gain of 130% relative to the previous ATLAS measurement in ref. [7].

6.3 BSM interpretation

The measured cross-sections can be used to constrain BSM models by using the central values and covariance matrices made available in HEPData. For convenience, the SM

particle-level predictions described in this paper are also included, so that comparisons can be made simply by adding BSM simulations to the provided SM predictions. In this section, two well-motivated interpretations are given as examples: constraints on effective field theory parameters and constraints on a model with a Z' boson, where the Z' bosons may be produced in pairs. Limits are set by constructing a likelihood function,

$$\mathcal{L} = \frac{1}{\sqrt{(2\pi)^k |C|}} \exp\left\{-\frac{1}{2}\left[\vec{\sigma}^{\mathrm{meas}} - \vec{\sigma}^{\mathrm{pred}}\left(\vec{\theta}\right)\right]^T C^{-1} \left[\vec{\sigma}^{\mathrm{meas}} - \vec{\sigma}^{\mathrm{pred}}\left(\vec{\theta}\right)\right]\right\} \times \prod_i \mathcal{G}\left(\theta_i, 0, 1\right),$$

(6.2)

where $\vec{\sigma}^{\mathrm{meas}}$ and $\vec{\sigma}^{\mathrm{pred}}$ and C are defined in section 6.1. In this case only the uncertainty in the SM contribution to $\vec{\sigma}^{\mathrm{pred}}$ is included in C. In order to avoid an underestimation of the statistical uncertainty in bins where the data has fluctuated downward, the statistical uncertainty of the expected SM yield is used. It was shown that using the observed statistical uncertainty leads to test statistics with reduced exclusion power and with probability distributions that are far from asymptotic. The BSM theoretical uncertainties are included as nuisance parameters, $\vec{\theta}$, with Gaussian constraints, $\mathcal{G}\left(\theta_i, 0, 1\right)$. Since there are a number of measured differential cross-sections, and the statistical correlation between them is not determined, the variable providing the best expected sensitivity is chosen to set the limits for a given point in BSM parameter space. A variable measured in slices of another variable counts as one observable.

6.3.1 Effective field theory constraints

A SM effective field theory (SMEFT) formalism using the Warsaw basis [98] is considered. The effective Lagrangian is defined as $\mathcal{L}_{\mathrm{SMEFT}} = \mathcal{L}_{\mathrm{SM}} + \sum_i \left(C_i^d / \Lambda^{(d-4)}\right) \mathcal{O}_i^d$, where $\mathcal{O}_i^d$ correspond to operators of dimension d describing the new interactions, the coefficients C_i^d specify the strength of the interactions and are known as Wilson coefficients, and Λ is the scale of the new physics. Only dimension-six operators are considered for this paper as they are the lowest-dimension operators that conserve lepton and baryon number, and the effect of higher-dimensional operators is expected to be suppressed. Since at energies well below Λ only the ratio $C_i^{(d=6)}/\Lambda^2$ is accessible, Λ is absorbed into the Wilson coefficients, and they are redefined as $c_i = C_i^{(d=6)}/\Lambda^2$.

The `SMEFTsim` package [99] is used for the SMEFT implementations of `FeynRules` [100]. Monte Carlo samples were simulated with MadGraph5_aMC@NLO 2.6.5 + Pythia 8.243 at LO precision in QCD [79], with the `NNPDF3.0nlo` set of PDFs. Uncertainties come from missing higher-order QCD corrections, PDFs and from the uncertainty in α_{S}, using the same strategy as is used for the SM $q\bar{q} \to 4\ell$ predictions, described in section 4.

The set-up allows the separate generation of the SM only, BSM only and interference contributions, with the total predicted cross-section given by

$$\vec{\sigma}^{\mathrm{pred}} = \vec{\sigma}^{\mathrm{SM}} \times \left(1 + c_i \cdot \vec{\sigma}^{\mathrm{INT}}/\vec{\sigma}^{\mathrm{LO\ SM}} + c_i^2 \cdot \vec{\sigma}^{\mathrm{BSM}}/\vec{\sigma}^{\mathrm{LO\ SM}}\right),$$

(6.3)

where $\vec{\sigma}^{\mathrm{SM}}$ is the most accurate SM predicted cross-section, described in section 4, using Sherpa for the $q\bar{q} \to 4\ell$ prediction, $c_i \cdot \vec{\sigma}^{\mathrm{INT}}$ is the interference term between the SM and BSM contributions, also referred to as the linear term, and $c_i^2 \cdot \vec{\sigma}^{\mathrm{BSM}}$ is the BSM-only

cross-section, also referred to as the quadratic term. Since the BSM contributions are LO cross-sections, they are scaled by the ratio of $\vec{\sigma}^{\text{SM}}$ to $\vec{\sigma}^{\text{LO SM}}$, which is the LO SM prediction given in the above set-up, where the assumption is that higher-order effects are the same for SM contributions as they are for contributions from new physics. A minimal flavour-violating scenario is assumed and the full list of 59 dimension-six operators can be found in ref. [98]. Only the following 22 coefficients that give non-negligible contributions to the four-lepton final state are considered:

- three affecting Higgs couplings: c_{HG}, $\tilde{c}_{HG}$, c_{HD};

- one affecting gauge boson couplings: c_{HWB};

- seven affecting the $Z \to \ell\ell$ vertex: c_{Hd}, c_{Hu}, c_{He}, $c_{Hl}^{(1)}$, $c_{Hl}^{(3)}$, $c_{Hq}^{(1)}$, $c_{Hq}^{(3)}$;

- eleven from four-fermion interactions (contact terms): c_{ed}, c_{ee}, c_{eu}, c_{ld}, c_{le}, c_{ll}, $c_{ll}^{(1)}$, $c_{lq}^{(1)}$, $c_{lq}^{(3)}$, c_{lu}, c_{qe}.

Each one is considered separately with the others set to zero.

The test statistic is based on a ratio of profiled likelihoods [101],

$$q = -2 \ln \frac{\mathcal{L}(c, \hat{\hat{\vec{\theta}}}(c))}{\mathcal{L}(\hat{c}, \hat{\vec{\theta}})} \,, \tag{6.4}$$

where c is the Wilson coefficient, $\hat{c}$ and $\hat{\vec{\theta}}$ are the unconditional maximum-likelihood estimators, and $\hat{\hat{\vec{\theta}}}$ is the conditional maximum likelihood estimated under the c hypothesis. The value of the test statistic is used to compare the different probabilities of hypotheses to construct a likelihood scan over c. For simplicity the uncertainties are taken to be fixed at the SM value, $c = 0$, rather than scaling with c. It has been shown that this leads to very similar results and is much less computationally expensive. In the case that the signal results in a small enhancement relative to the SM yield, with a dominant linear (interference) term, the use of uncertainties fixed at the SM value results in an asymptotic test statistic. For large, local enhancements or cases where the quadratic term dominates, the behaviour becomes non-asymptotic. For this reason Monte Carlo toys are used to evaluate the distribution of the test statistic when obtaining 95% confidence level (CL) intervals.

Two sets of results are presented: those where the full predicted cross-section from eq. (6.3) is used, referred to as the full EFT model, and those where the quadratic term in eq. (6.3) is neglected, referred to as the linear-only model. Since the linear terms of the missing dimension-eight operators in the effective Lagrangian expansion are at the same order in an expansion in $1/\Lambda$ as the quadratic terms of the dimension-six operators, large differences indicate that the neglected dimension-eight operators may play a non-negligible role. Tables 3 and 4 show the observed and expected exclusion limits at 95% CL for the 22 Wilson coefficients, for the full EFT model and for the model with only linear terms, respectively. Also shown in the tables is the most sensitive observable that is used to set the limit. The results are also presented graphically in figure 12. When comparing the

results in tables 3 and 4, the coefficients fall into four categories: those (c_{HD}, c_{HWB}, c_{He}, $c_{Hl}^{(1)}$, $c_{Hq}^{(3)}$, $c_{Hl}^{(3)}$ and $c_{ll}^{(1)}$) that have a negligible contribution from the quadratic term and therefore have very similar limits whether or not the quadratic term is included; those ($c_{Hq}^{(1)}$ and $c_{lq}^{(3)}$) that, because of the quadratic term, make small positive contributions to the total prediction, enhancing (lessening) the positive (negative) linear contribution at positive (negative) values of the coefficient, and hence shifting both the lower and upper limits to slightly lower values; those (c_{HG} and c_{Hu}) that have more stringent limits when using the linear-only terms because of the presence of double maxima in the likelihood scans when the quadratic term is included; and the remaining 11 coefficients that have non-negligible contributions from the quadratic term and hence more stringent limits when they are included (including $\tilde{c}_{HG}$, which has zero contribution from the linear term). The differences seen in the limits in the last category indicate that dimension-eight terms may not be negligible.

In general the observed limits are compatible with the expected limits. One exception is the observed lower limit on $c_{lq}^{(1)}$, which is significantly less stringent than the expected limit for the results using linear-only terms. This is an artifact of the simple model of the scale uncertainty affecting the EFT prediction. In general, for a large EFT signal that is incompatible with the data, the EFT scale uncertainty's nuisance parameter is pulled in order to bring the prediction closer to the observation. The nuisance parameter's constraint term penalises this behaviour in the likelihood. However, for large negative values of $c_{lq}^{(1)}$ the size and shape of the scale uncertainty's effect on the signal prediction are related in a way that produces a prediction precisely imitating the statistical fluctuations in the measured cross-section, increasing the likelihood. This leads to a larger than expected observed lower limit on $c_{lq}^{(1)}$.

Limits have already been placed on c_{HG}, $\tilde{c}_{HG}$ and c_{HWB}, in a measurement of the $H \to 4\ell$ cross-section [102]. For c_{HG} the limits are more stringent in the $H \to 4\ell$ cross-section analysis, but for $\tilde{c}_{HG}$ the limits are very similar, with this paper providing slightly tighter constraints. For c_{HWB} the constraints from this paper are significantly more stringent with $[-0.20, 0.21]$ expected and $[-0.29, 0.13]$ observed compared to $[-1.09, 0.99]$ expected and $[-1.06, 0.99]$ observed in the $H \to 4\ell$ cross-section paper. The improvement can be understood as being due to the fact that changes in c_{HWB} affect the entire $m_{4\ell}$ spectrum, not just the region close to m_H. Limits on the coefficients affecting the $Z \to \ell\ell$ vertex have been obtained previously from a global fit to LEP and LHC data [103], and are generally one or two orders of magnitude more stringent than the limits in this paper.

6.3.2 $B - L$ gauge model constraints

The data are used to set limits on a model in which the global baryon-number-minus-lepton-number ($B - L$) symmetry is treated as a local gauge symmetry and spontaneously broken [104]. This model predicts a Z', the gauge boson of the new local symmetry, and an exotic Higgs boson h_2, from the symmetry breaking, that mixes with the SM Higgs boson, with a mixing angle α. The new Higgs boson and the SM Higgs boson can decay into ZZ or $Z'Z'$, with the gauge bosons decaying into lepton pairs.

Coefficient	Observable	95% CL Expected [TeV^{-2}]	95% CL Observed [TeV^{-2}]
c_{HG}	m_{34} vs. $m_{4\ell}$	$[-0.18, -0.027] \cup [-0.014, 0.011]$	$[-0.20, -0.029] \cup [-0.010, 0.012]$
$\tilde{c}_{HG}$	m_{34} vs. $m_{4\ell}$	$[-0.031, 0.031]$	$[-0.033, 0.033]$
c_{HD}	m_{34} vs. $m_{4\ell}$	$[-0.45, 0.44]$	$[-0.60, 0.29]$
c_{HWB}	m_{34} vs. $m_{4\ell}$	$[-0.20, 0.21]$	$[-0.29, 0.13]$
c_{Hd}	$p_{\mathrm{T},12}$ vs. $m_{4\ell}$	$[-4.9, 9.8]$	$[-2.6, 8.3]$
c_{Hu}	$|\Delta\phi_{\ell\ell}|$ vs. $m_{4\ell}$	$[-11, 2.8]$	$[-13, -6.9] \cup [-1.5, 4.4]$
c_{He}	$|\Delta\phi_{\mathrm{pairs}}|$ vs. $m_{4\ell}$	$[-0.46, 0.49]$	$[-0.70, 0.21]$
$c_{Hl}^{(1)}$	$|\Delta\phi_{\mathrm{pairs}}|$ vs. $m_{4\ell}$	$[-0.39, 0.37]$	$[-0.19, 0.55]$
$c_{Hl}^{(3)}$	$|\Delta\phi_{\ell\ell}|$ vs. $m_{4\ell}$	$[-0.28, 0.29]$	$[-0.47, 0.12]$
$c_{Hq}^{(1)}$	m_{34} vs. $m_{4\ell}$	$[-0.93, 0.69]$	$[-1.6, 0.43]$
$c_{Hq}^{(3)}$	$|\Delta\phi_{\mathrm{pairs}}|$ vs. $m_{4\ell}$	$[-0.34, 0.33]$	$[-0.15, 0.52]$
c_{ed}	m_{34} vs. $m_{4\ell}$	$[-0.49, 0.39]$	$[-0.51, 0.41]$
c_{ee}	m_{34} vs. $m_{4\ell}$	$[-38, 35]$	$[-33, 42]$
c_{eu}	$m_{4\ell}$	$[-0.21, 0.35]$	$[-0.14, 0.21]$
c_{ld}	m_{34} vs. $m_{4\ell}$	$[-0.40, 0.34]$	$[-0.41, 0.36]$
c_{le}	m_{34} vs. $m_{4\ell}$	$[-23, 22]$	$[-21, 26]$
c_{ll}	m_{34} vs. $m_{4\ell}$	$[-23, 21]$	$[-20, 25]$
$c_{ll}^{(1)}$	$|\Delta\phi_{\mathrm{pairs}}|$ vs. $m_{4\ell}$	$[-0.34, 0.33]$	$[-0.17, 0.50]$
$c_{lq}^{(1)}$	$m_{4\ell}$	$[-0.14, 0.28]$	$[-0.086, 0.17]$
$c_{lq}^{(3)}$	m_{34} vs. $m_{4\ell}$	$[-0.083, 0.071]$	$[-0.064, 0.081]$
c_{lu}	$m_{4\ell}$	$[-0.24, 0.32]$	$[-0.16, 0.20]$
c_{qe}	$m_{4\ell}$	$[-0.17, 0.21]$	$[-0.11, 0.14]$

Table 3. The expected and observed confidence intervals at 95% CL for the SMEFT Wilson coefficients, including both the linear and quadratic terms. The most sensitive observable indicated for each coefficient is used for the constraints. Only one coefficient is fitted at a time, with all others set to zero.

The sensitivity of previous LHC measurements to this model was presented in ref. [105], where four-lepton measurements were seen to provide significant constraints. One of the scans from that study is repeated here using all the measured observables, to derive exclusion limits in the plane of $\sin\alpha$ versus the mass of h_2, m_{h_2}, for a low-mass (35 GeV) Z' which is weakly coupled to the SM ($g' = 10^{-3}$). In this scenario, depending on the other parameters, ZZ and $Z'Z'$ production via one of the Higgs bosons may lead to contributions to the cross-sections measured in this paper.

BSM events were generated using Herwig 7.2 [106, 107]. Interference terms, and the impact of the model on SM decays of the SM Higgs, are not taken into account. The impact of this on the limits is expected to be negligible.

Coefficient	Observable	95% CL Expected [TeV^{-2}]	95% CL Observed [TeV^{-2}]
c_{HG}	m_{34} vs. $m_{4\ell}$	$[-0.011, 0.013]$	$[-0.0090, 0.015]$
$\tilde{c}_{HG}$	m_{34} vs. $m_{4\ell}$	—	—
c_{HD}	m_{34} vs. $m_{4\ell}$	$[-0.46, 0.45]$	$[-0.63, 0.28]$
c_{HWB}	m_{34} vs. $m_{4\ell}$	$[-0.21, 0.20]$	$[-0.29, 0.13]$
c_{Hd}	$p_{\mathrm{T},12}$ vs. $m_{4\ell}$	$[-10, 10]$	$[-3.0, 18]$
c_{Hu}	$|\Delta\phi_{\ell\ell}|$ vs. $m_{4\ell}$	$[-3.5, 3.7]$	$[-1.6, 6.1]$
c_{He}	$|\Delta\phi_{\mathrm{pairs}}|$ vs. $m_{4\ell}$	$[-0.47, 0.46]$	$[-0.75, 0.21]$
$c_{Hl}^{(1)}$	$|\Delta\phi_{\mathrm{pairs}}|$ vs. $m_{4\ell}$	$[-0.37, 0.38]$	$[-0.19, 0.57]$
$c_{Hl}^{(3)}$	$|\Delta\phi_{\ell\ell}|$ vs. $m_{4\ell}$	$[-0.29, 0.29]$	$[-0.51, 0.12]$
$c_{Hq}^{(1)}$	m_{34} vs. $m_{4\ell}$	$[-0.81, 0.78]$	$[-1.1, 0.47]$
$c_{Hq}^{(3)}$	$|\Delta\phi_{\mathrm{pairs}}|$ vs. $m_{4\ell}$	$[-0.34, 0.35]$	$[-0.15, 0.53]$
c_{ed}	m_{34} vs. $m_{4\ell}$	$[-1.3, 1.8]$	$[-1.0, 2.3]$
c_{ee}	m_{34} vs. $m_{4\ell}$	$[-59, 65]$	$[-25, 100]$
c_{eu}	$m_{4\ell}$	$[-0.62, 0.45]$	$[-0.36, 0.63]$
c_{ld}	m_{34} vs. $m_{4\ell}$	$[-1.8, 2.5]$	$[-1.3, 3.0]$
c_{le}	m_{34} vs. $m_{4\ell}$	$[-63, 68]$	$[-18, 130]$
c_{ll}	m_{34} vs. $m_{4\ell}$	$[-39, 43]$	$[-17, 70]$
$c_{ll}^{(1)}$	$|\Delta\phi_{\mathrm{pairs}}|$ vs. $m_{4\ell}$	$[-0.34, 0.34]$	$[-0.18, 0.50]$
$c_{lq}^{(1)}$	$m_{4\ell}$	$[-0.76, 0.40]$	$[-4.1, 0.53]$
$c_{lq}^{(3)}$	m_{34} vs. $m_{4\ell}$	$[-0.059, 0.083]$	$[-0.050, 0.098]$
c_{lu}	$m_{4\ell}$	$[-1.4, 0.99]$	$[-0.78, 1.4]$
c_{qe}	$m_{4\ell}$	$[-1.1, 0.83]$	$[-0.72, 1.2]$

Table 4. The expected and observed confidence intervals at 95% CL for the SMEFT Wilson coefficients, including only linear terms. The most sensitive observable indicated for each coefficient is used for the constraints. Only one coefficient is fitted at a time, with all others set to zero.

The likelihood function defined in eq. (6.2) is used to define the test statistic, $\tilde{q}$, as

$$
\tilde{q} = \begin{cases} -2\ln\frac{\mathcal{L}(\mu,\hat{\hat{\theta}}(\mu))}{\mathcal{L}(0,\hat{\hat{\theta}}(0))} & \hat{\mu} < 0, \\ -2\ln\frac{\mathcal{L}(\mu,\hat{\hat{\theta}}(\mu))}{\mathcal{L}(\hat{\mu},\hat{\theta})} & 0 \le \hat{\mu} \le \mu, \\ 0 & \hat{\mu} > \mu, \end{cases} \tag{6.5}
$$

where μ determines the strength of the signal process, with $\mu = 0$ corresponding to the SM hypothesis and $\mu = 1$ being the nominal signal hypothesis. The CL$_\mathrm{s}$ method [108] is then used to derive the 95% CL exclusion contour in the $(\sin\alpha, m_{h_2})$ plane as shown in
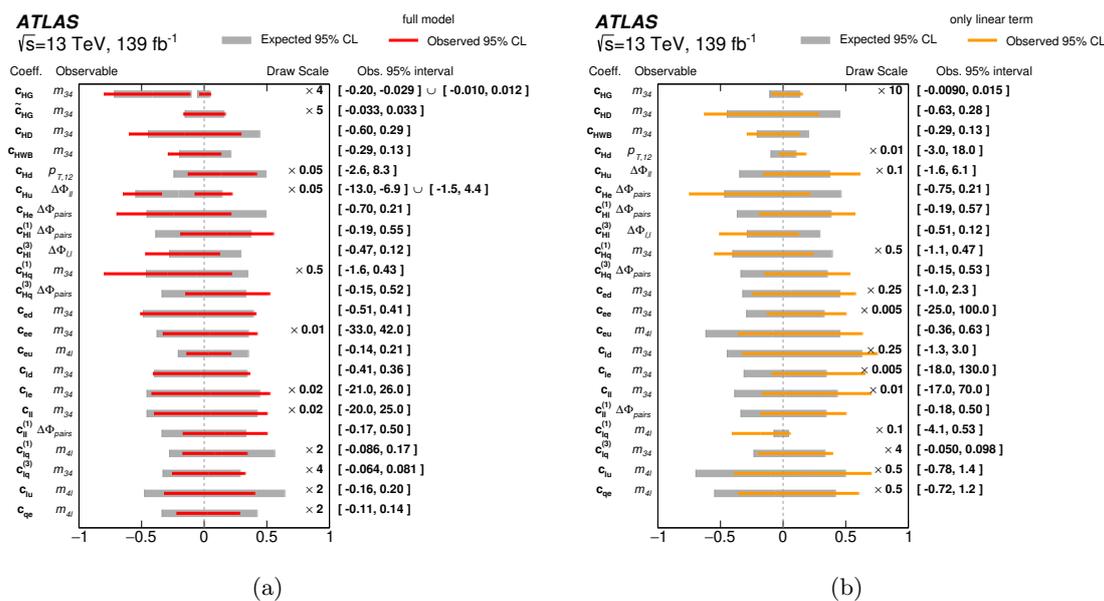
Figure 12. The expected and observed confidence intervals at 95% CL for the SMEFT Wilson coefficients, which are in units of TeV^{-2}, for (a) the full model and (b) only the linear terms. The multiplicative number shown to the right of plotted points indicates a scaling factor that is applied to the limit for the purpose of the plot, in order to show all coefficients on the same scale. The most sensitive observable indicated for each coefficient is used for the constraints. Only one coefficient is fitted at a time, with all others set to zero.

figure 13(a).[5] Figure 13(b) displays for each $(\sin\alpha, m_{h_2})$ point the observable which has the highest expected sensitivity and was therefore used to set the limit. The most sensitive observable changes in the region $m_{h_2} \sim 125$ GeV since the phenomenology of the model changes as the mass of the exotic Higgs boson approaches that of the SM Higgs boson. In order to demonstrate the power of the different variables, a similar scan was performed using the $m_{4\ell}$ distribution only, and the expected limits on $\sin\alpha$ weakened from 0.28 to 0.46 at high m_{h_2}. As can be seen in figure 13(b), improvements at high m_{h_2} come mostly from including measurements of m_{12}. The previous study [105] only covers $\sin\alpha > 0.4$ for most values of m_{h_2}, and provides no constraints for $m_{h_2} > 600$ GeV. The new overall limits significantly improve on this, excluding $\sin\alpha > 0.28$ for most of the plane, even at high m_{h_2}, and, for example, for $m_{h_2} = 500$ GeV, the limit on $\sin\alpha$ improves from 0.5 to 0.26.

---

[5]The asymptotic formulae from ref. [101] are used, and their validity is checked by using pseudo-data simulations for a number of points in the $(\sin\alpha, m_{h_2})$ plane.
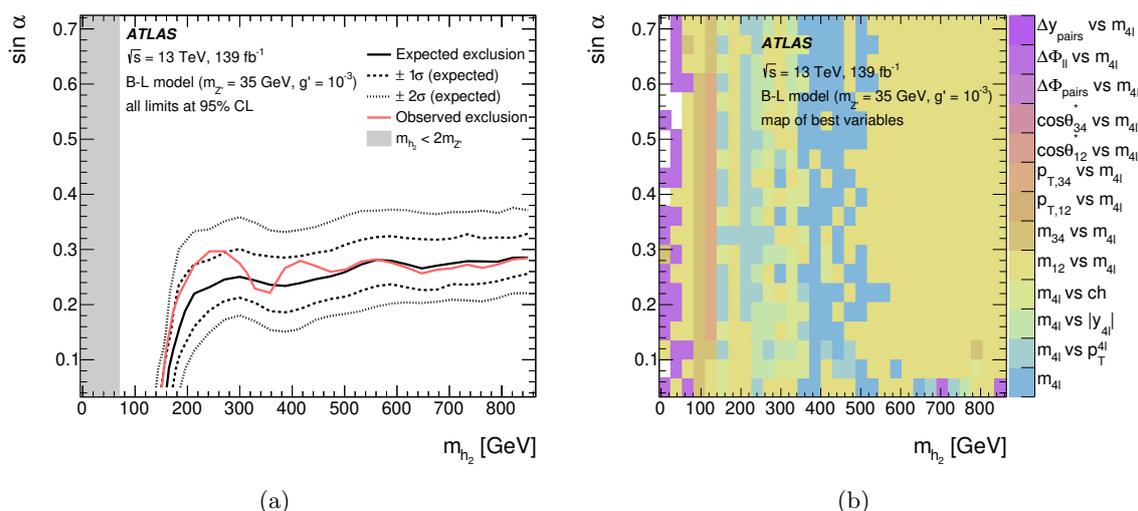
Figure 13. (a) Exclusion contour at 95% confidence level for the $B - L$ gauge model [104] in the plane of $\sin \alpha$ versus m_{h_2} for $m_{Z'} = 35$ GeV and $g' = 10^{-3}$. The red line shows the observed exclusion and the solid black line shows the expected exclusion, with the dashed black lines indicating the $\pm 1\sigma$ and $\pm 2\sigma$ uncertainty bands. The region above and to the left of the lines is excluded, up to the grey band, which shows the region $m_{h_2} < 2m_{Z'}$, where the four-lepton final state has no sensitivity. (b) Colour palette indicating which observable has the highest expected sensitivity at each point in the parameter space and is used to set the limit.

7 Conclusion

Measurements of inclusive and differential fiducial cross-sections in four-lepton events are presented using 139 fb^{-1} of $\sqrt{s} = 13$ TeV proton-proton collisions, collected by the ATLAS detector during Run 2 of the LHC. Included are measurements of the four-lepton invariant mass, the dilepton masses, and other kinematic variables of the four leptons and dilepton pairs, including angular correlations. The measured phase-space is significantly increased compared to previous measurements with four leptons, in particular reducing requirements that specifically enhance the contribution from SM ZZ production. The methodology used to correct for detector effects was developed to have minimal bias in the case of possible BSM contributions to the final-state. The measured cross-sections are compared with state-of-the-art SM predictions and are found to be in agreement.

The final state has contributions from a number of SM processes, including $Z \to 4\ell$, $H \to 4\ell$ and the dominant quark-induced t-channel $q\bar{q} \to 4\ell$ process. The region dominated by $Z \to 4\ell$ production is used to extract the most precise measurement of the $Z \to 4\ell$ branching fraction to date, $\mathcal{B}_{Z\to4\ell} = (4.41 \pm 0.13\,(\text{stat.}) \pm 0.23\,(\text{syst.}) \pm 0.09\,(\text{theory}) \pm 0.12\,(\text{lumi.})) \times 10^{-6}$. The result is consistent with previous measurements and with the SM prediction.

Various BSM effects can contribute to the final state. The data are used to constrain SMEFT coefficients and a model based on a spontaneously broken $B - L$ gauge symmetry. All necessary information for a detailed reinterpretation has been made public so it can be used to probe further BSM models in the future.

A Further measurements

This appendix shows the differential cross-sections that are not included in section 6.1. In each case the data are compared with the SM predictions. Two predictions are shown, one where the $q\bar{q} \to 4\ell$ process is simulated with SHERPA and one where it is simulated with POWHEG + PYTHIA8. All the other processes are the same for both predictions.

Figure 14 shows the $m_{4\ell}$ distribution separately for the three channels 4μ, $4e$ and $2e2\mu$; figures 15 and 16 show it in slices of $p_{\mathrm{T},4\ell}$ and $|y_{4\ell}|$ respectively. The SM predictions describe the data well for most of the distributions. However, the POWHEG + PYTHIA8 prediction in the highest-p_{T} slice in figure 15, and in the off-shell ZZ region in the $0.9 < |y_{4\ell}| < 1.2$ slice in figure 16, is below the data.

Figures 17, 18, 19, 20 respectively show $p_{\mathrm{T},12}$, $p_{\mathrm{T},34}$, $|\Delta\phi_{\mathrm{pairs}}|$ and $|\Delta y_{\mathrm{pairs}}|$ separately in the $Z \to 4\ell$, $H \to 4\ell$ and off-shell ZZ regions. The on-shell ZZ region is shown in section 6.1. The data are well described by the SM predictions. The p-values for the $|\Delta\phi_{\mathrm{pairs}}|$ distribution in the off-shell ZZ region are low, which is mainly driven by statistical fluctuations in the data, together with predictions that are lower than the observations at low $|\Delta\phi_{\mathrm{pairs}}|$ values, especially for the POWHEG + PYTHIA8 prediction.

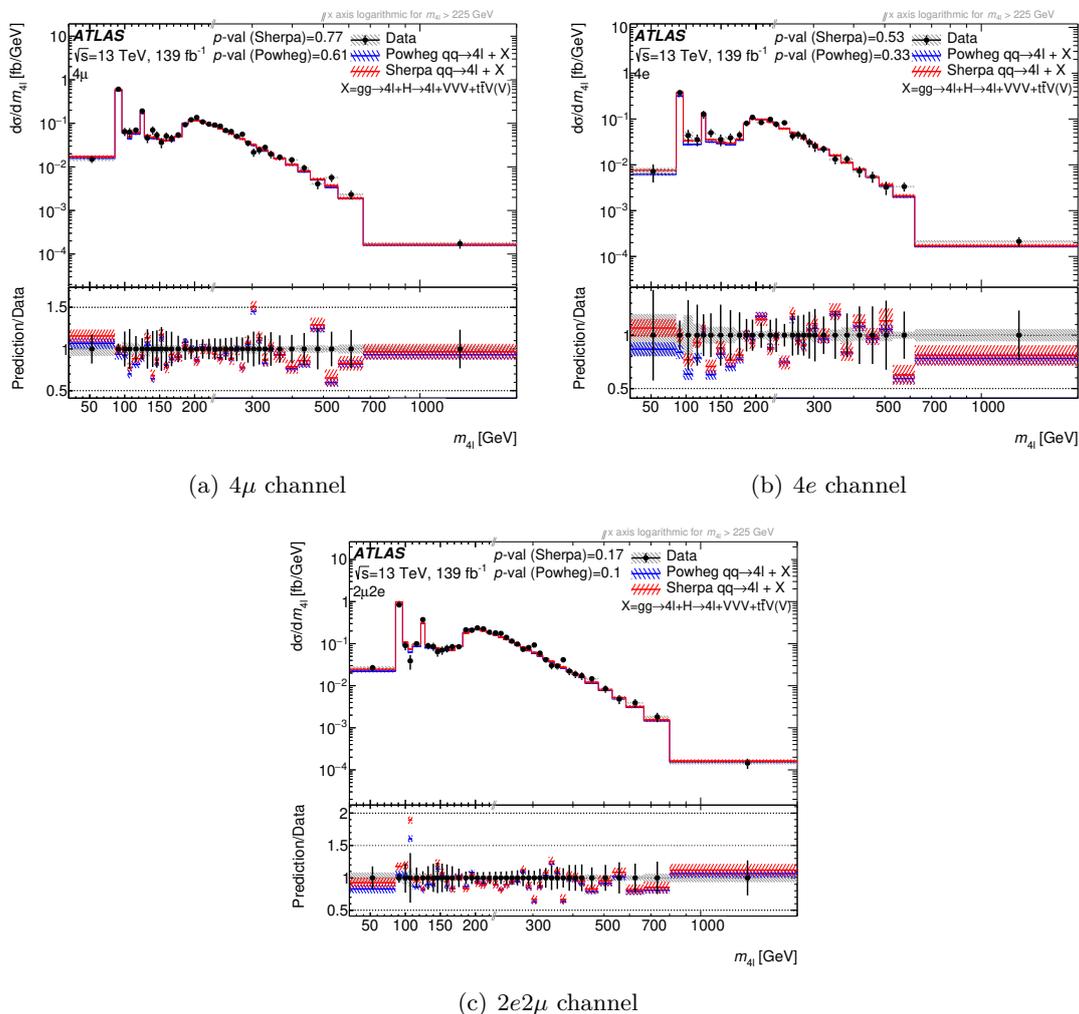(a) 4μ channel

(b) $4e$ channel

(c) $2e2\mu$ channel

Figure 14. Differential cross-section as a function of $m_{4\ell}$ for each lepton flavour channel. The measured data (black points) are compared with the SM prediction using either SHERPA (red, with red hashed band for the uncertainty) or POWHEG + PYTHIA8 (blue, with blue hashed band for the uncertainty) to model the $q\bar{q} \to 4\ell$ contribution. The error bars on the data points give the total uncertainty and the grey hashed band gives the systematic uncertainty. The p-value is the probability for the χ^2, with the number of degrees of freedom equal to the number of bins in the distribution, to have at least the observed value, given the SM prediction. The lower panel shows the ratio of the SM predictions to the data. The x-axis is on a linear scale until $m_{4\ell} = 225$ GeV, where it switches to a logarithmic scale.
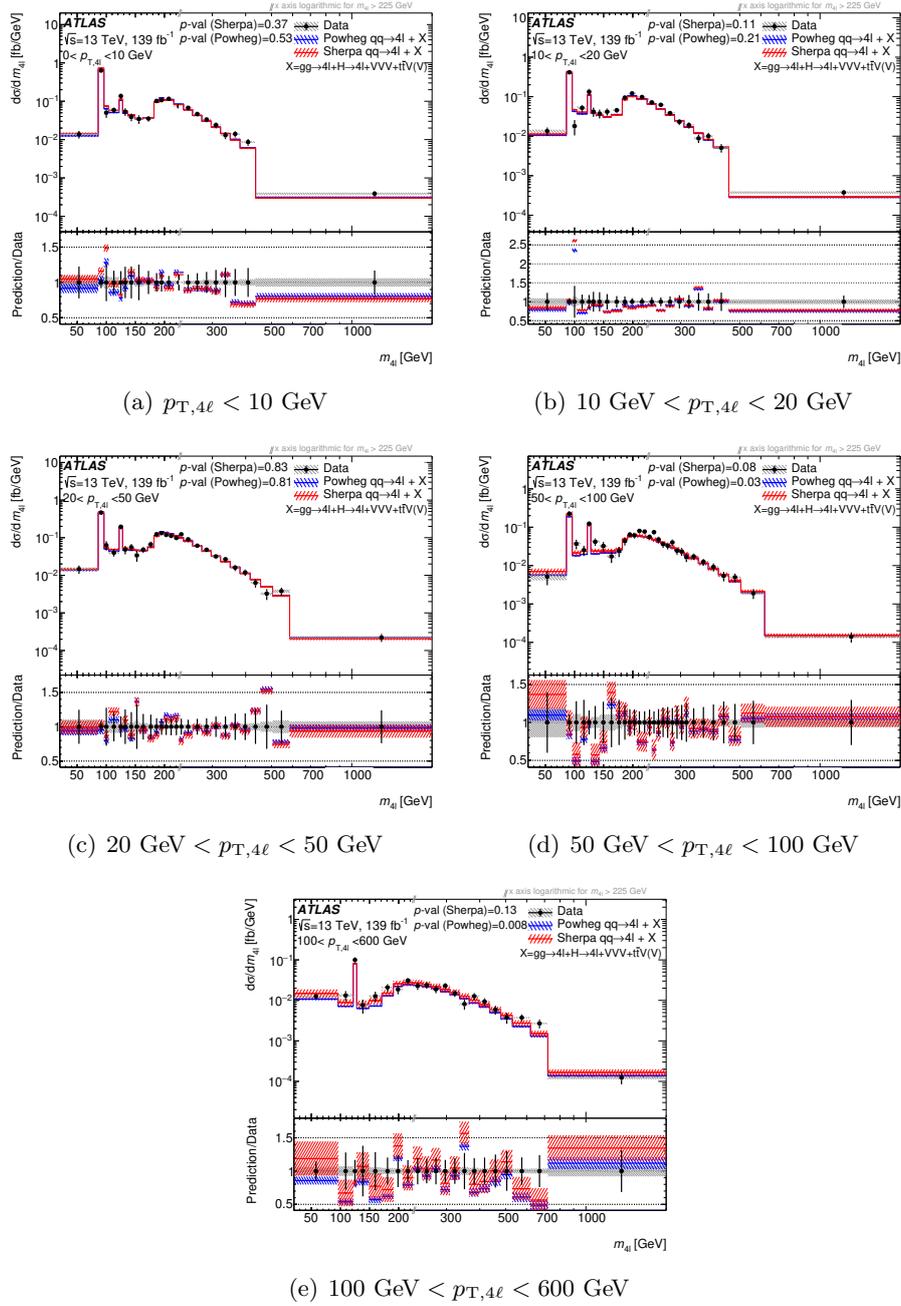
(a) $p_{T,4\ell} < 10$ GeV

(b) 10 GeV $< p_{T,4\ell} < 20$ GeV

(c) 20 GeV $< p_{T,4\ell} < 50$ GeV

(d) 50 GeV $< p_{T,4\ell} < 100$ GeV

(e) 100 GeV $< p_{T,4\ell} < 600$ GeV

Figure 15. Differential cross-section as a function of $m_{4\ell}$ in $p_{T,4\ell}$ slices. The measured data (black points) are compared with the SM prediction using either SHERPA (red, with red hashed band for the uncertainty) or POWHEG + PYTHIA8 (blue, with blue hashed band for the uncertainty) to model the $q\bar{q} \to 4\ell$ contribution. The error bars on the data points give the total uncertainty and the grey hashed band gives the systematic uncertainty. The p-value is the probability for the χ^2, with the number of degrees of freedom equal to the number of bins in the distribution, to have at least the observed value, given the SM prediction. The lower panel shows the ratio of the SM predictions to the data. The x-axis is on a linear scale until $m_{4\ell} = 234$ GeV for the $p_{T,4\ell} < 10$ GeV slice and $m_{4\ell} = 225$ GeV for all other slices, when it switches to a logarithmic scale.

(a) $|y_{4\ell}| < 0.3$

(b) $0.3 < |y_{4\ell}| < 0.6$

(c) $0.6 < |y_{4\ell}| < 0.9$

(d) $0.9 < |y_{4\ell}| < 1.2$
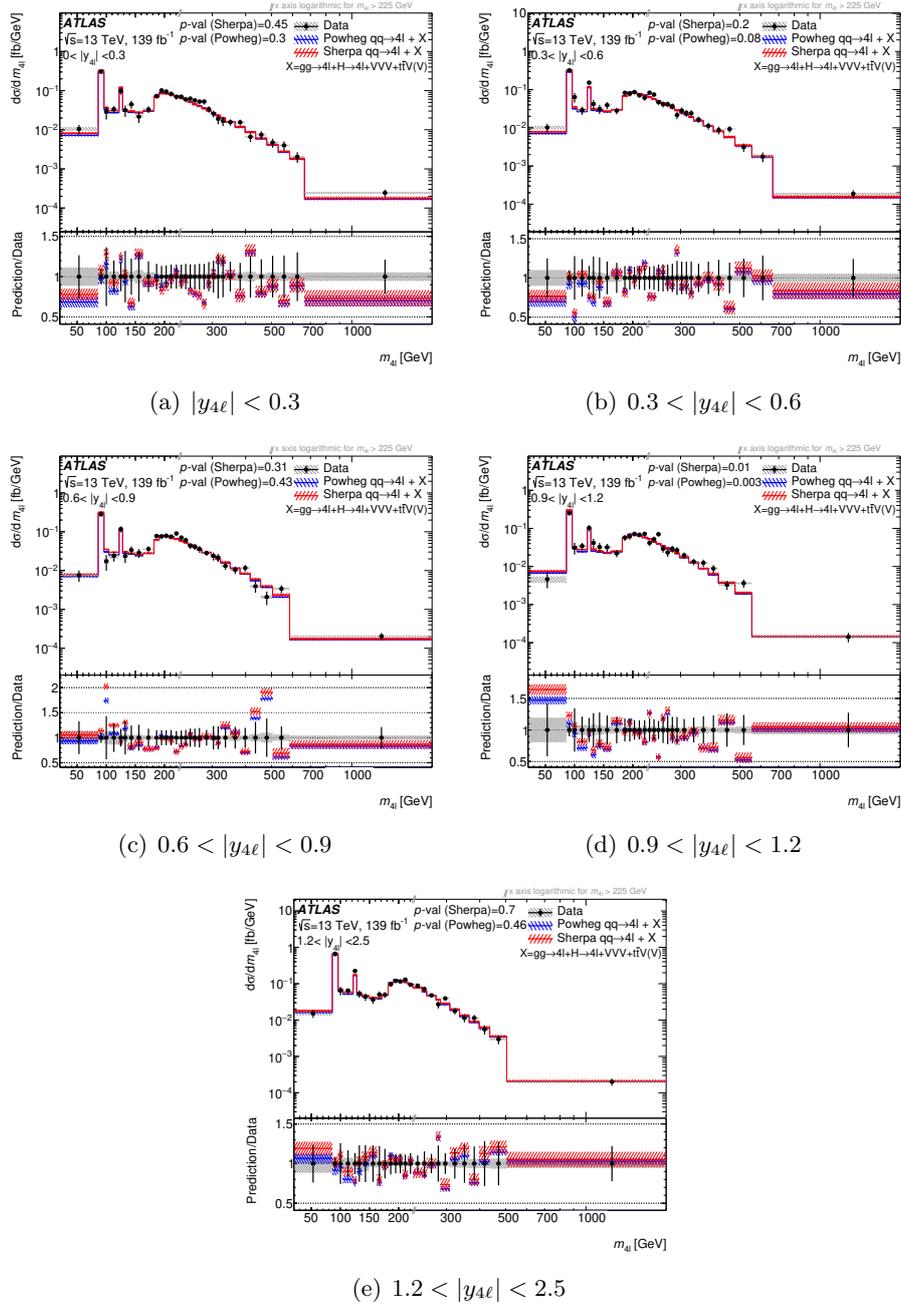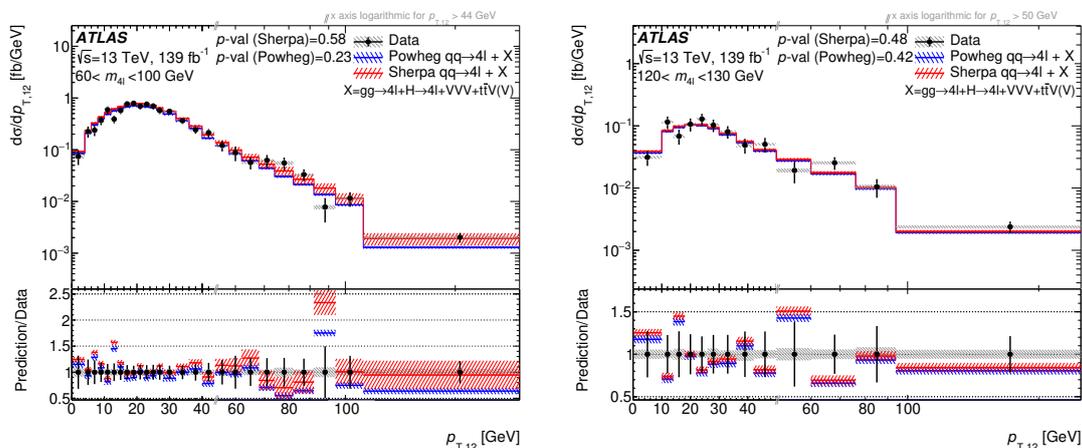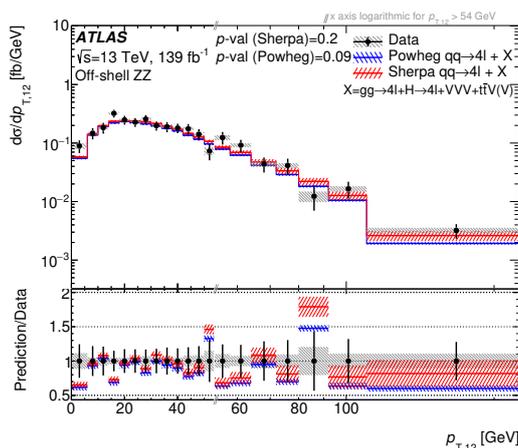
(e) $1.2 < |y_{4\ell}| < 2.5$

Figure 16. Differential cross-section as a function of $m_{4\ell}$ in $|y_{4\ell}|$ slices. The measured data (black points) are compared with the SM prediction using either Sherpa (red, with red hashed band for the uncertainty) or Powheg + Pythia8 (blue, with blue hashed band for the uncertainty) to model the $q\bar{q} \to 4\ell$ contribution. The error bars on the data points give the total uncertainty and the grey hashed band gives the systematic uncertainty. The p-value is the probability for the χ^2, with the number of degrees of freedom equal to the number of bins in the distribution, to have at least the observed value, given the SM prediction. The lower panel shows the ratio of the SM predictions to the data. The x-axis is on a linear scale until $m_{4\ell} = 225$ GeV, where it switches to a logarithmic scale.
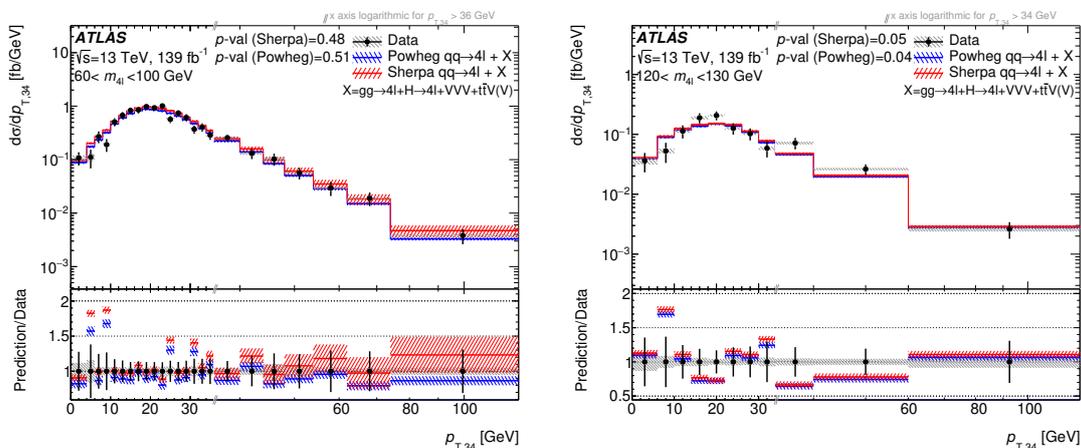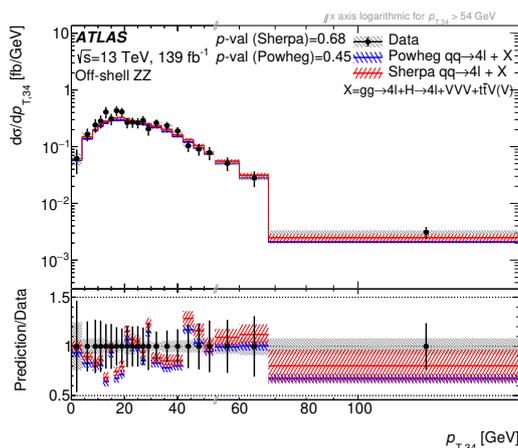
(a) $Z \to 4\ell$ region

(b) $H \to 4\ell$ region

(c) Off-shell ZZ region

Figure 17. Differential cross-section as a function of $p_{\mathrm{T},12}$ in $m_{4\ell}$ regions. The measured data (black points) are compared with the SM prediction using either SHERPA (red, with red hashed band for the uncertainty) or POWHEG + PYTHIA8 (blue, with blue hashed band for the uncertainty) to model the $q\bar{q} \to 4\ell$ contribution. The error bars on the data points give the total uncertainty and the grey hashed band gives the systematic uncertainty. The p-value is the probability for the χ^2, with the number of degrees of freedom equal to the number of bins in the distribution, to have at least the observed value, given the SM prediction. The lower panel shows the ratio of the SM predictions to the data. In (a) the x-axis is on a linear scale until $p_{\mathrm{T},12} = 44$ GeV, where it switches to a logarithmic scale; in (b) it switches at $p_{\mathrm{T},12} = 50$ GeV, and in (c) at $p_{\mathrm{T},12} = 54$ GeV.

(a) $Z \to 4\ell$ region

(b) $H \to 4\ell$ region

(c) Off-shell ZZ region

Figure 18. Differential cross-section as a function of $p_{\mathrm{T},34}$ in $m_{4\ell}$ regions. The measured data (black points) are compared with the SM prediction using either SHERPA (red, with red hashed band for the uncertainty) or POWHEG + PYTHIA8 (blue, with blue hashed band for the uncertainty) to model the $q\bar{q} \to 4\ell$ contribution. The error bars on the data points give the total uncertainty and the grey hashed band gives the systematic uncertainty. The p-value is the probability for the χ^2, with the number of degrees of freedom equal to the number of bins in the distribution, to have at least the observed value, given the SM prediction. The lower panel shows the ratio of the SM predictions to the data. In (a) the x-axis is on a linear scale until $p_{\mathrm{T},34} = 36$ GeV, where it switches to a logarithmic scale; in (b) it switches at $p_{\mathrm{T},34} = 34$ GeV, and in (c) at $p_{\mathrm{T},34} = 54$ GeV.

(a) $Z \to 4\ell$ region

(b) $H \to 4\ell$ region

(c) Off-shell ZZ region

Figure 19. Differential cross-section as a function of $|\Delta\phi_{\mathrm{pairs}}|$ in $m_{4\ell}$ regions. The measured data (black points) are compared with the SM prediction using either SHERPA (red, with red hashed band for the uncertainty) or POWHEG + PYTHIA8 (blue, with blue hashed band for the uncertainty) to model the $q\bar{q} \to 4\ell$ contribution. The error bars on the data points give the total uncertainty and the grey hashed band gives the systematic uncertainty. The p-value is the probability for the χ^2, with the number of degrees of freedom equal to the number of bins in the distribution, to have at least the observed value, given the SM prediction. The lower panel shows the ratio of the SM predictions to the data.

(a) $Z \to 4\ell$ region
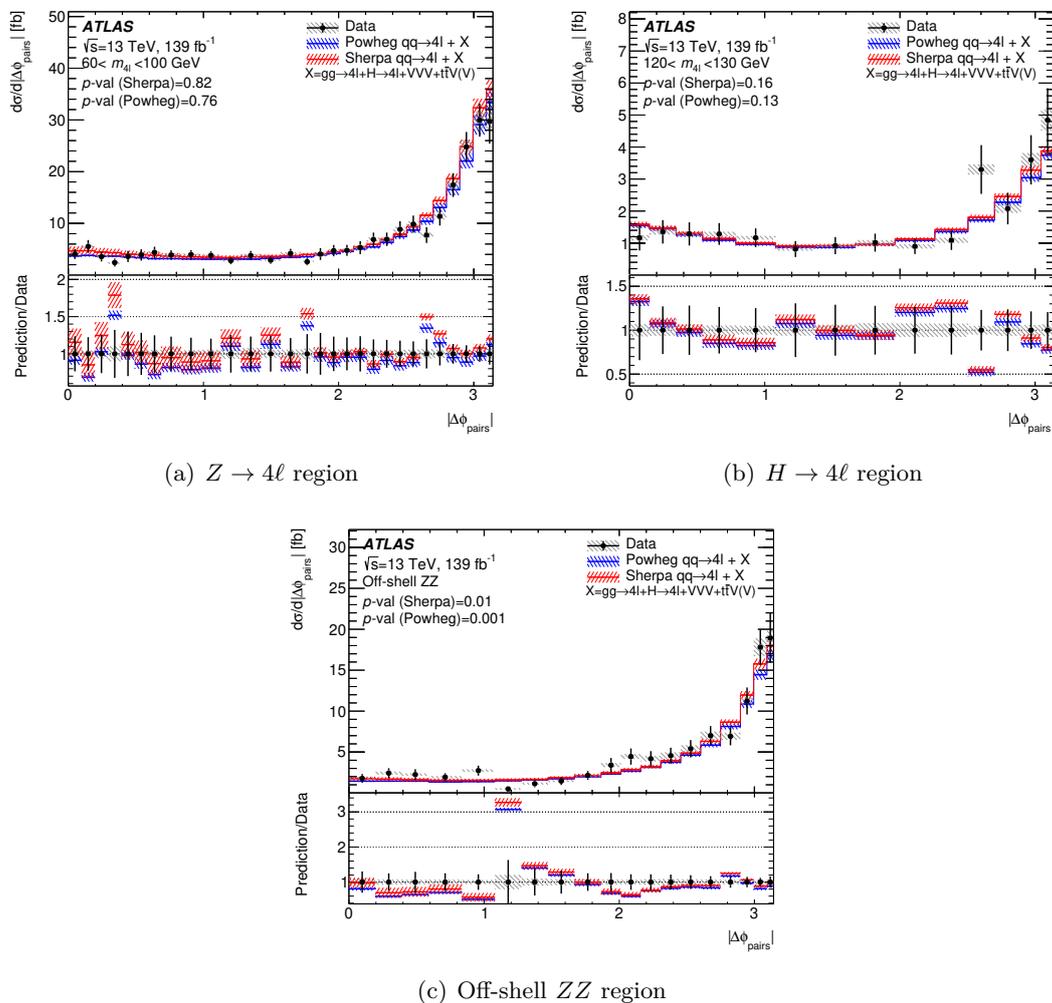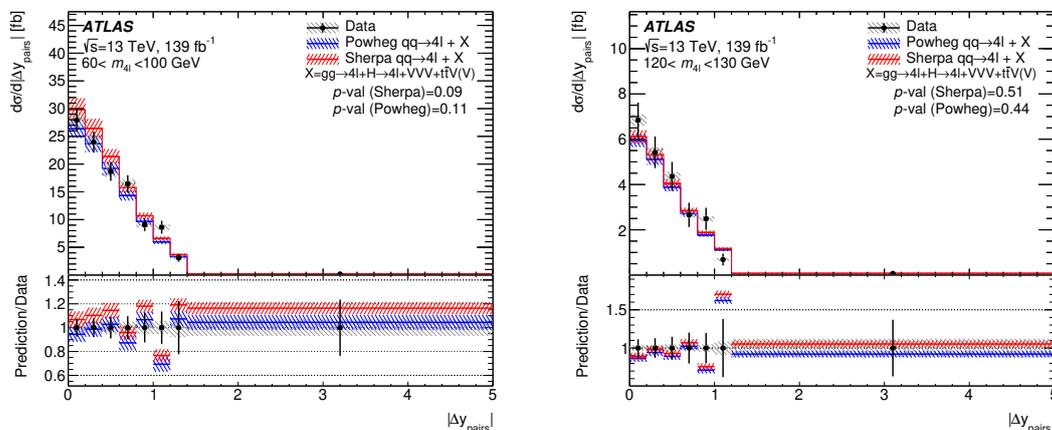
(b) $H \to 4\ell$ region
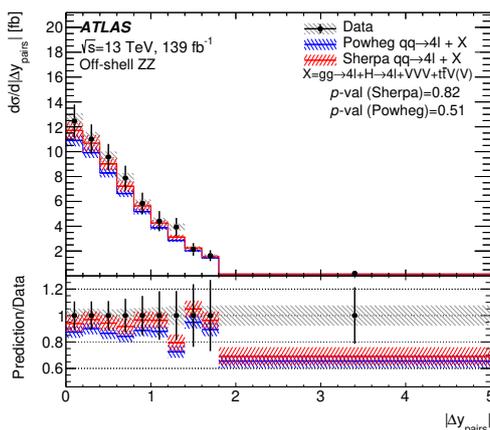

(c) Off-shell ZZ region

Figure 20. Differential cross-section as a function of $|\Delta y_{\mathrm{pairs}}|$ in $m_{4\ell}$ regions. The measured data (black points) are compared with the SM prediction using either SHERPA (red, with red hashed band for the uncertainty) or POWHEG + PYTHIA8 (blue, with blue hashed band for the uncertainty) to model the $q\bar{q} \to 4\ell$ contribution. The error bars on the data points give the total uncertainty and the grey hashed band gives the systematic uncertainty. The p-value is the probability for the χ^2, with the number of degrees of freedom equal to the number of bins in the distribution, to have at least the observed value, given the SM prediction. The lower panel shows the ratio of the SM predictions to the data.

Acknowledgments

References

[1] ATLAS collaboration, *The ATLAS Experiment at the CERN Large Hadron Collider*, 2008 *JINST* **3** S08003 [INSPIRE].

[2] ATLAS IBL collaboration, *Production and integration of the ATLAS Insertable B-Layer*, 2018 *JINST* **13** T05008 [arXiv:1803.00844] [INSPIRE].

[3] L. Evans and P. Bryant, eds., *LHC Machine*, 2008 *JINST* **3** S08001 [INSPIRE].

[4] Particle Data Group collaboration, *Review of Particle Physics*, *PTEP* **2020** (2020) 083C01 [INSPIRE].

[5] GAMBIT collaboration, *Combined collider constraints on neutralinos and charginos*, *Eur. Phys. J. C* **79** (2019) 395 [arXiv:1809.02097] [INSPIRE].

[6] G. Brooijmans et al., *Les Houches 2019 Physics at TeV Colliders: New Physics Working Group Report*, in *11th Les Houches Workshop on Physics at TeV Colliders: PhysTeV Les Houches*, arXiv:2002.12220 [INSPIRE].

[7] ATLAS collaboration, *Measurement of the four-lepton invariant mass spectrum in* 13 *TeV proton-proton collisions with the ATLAS detector*, *JHEP* **04** (2019) 048 [arXiv:1902.05892] [INSPIRE].

[8] ATLAS collaboration, $ZZ \rightarrow \ell^+\ell^-\ell'^+\ell'^-$ *cross-section measurements and search for anomalous triple gauge couplings in 13 TeV pp collisions with the ATLAS detector*, *Phys. Rev. D* **97** (2018) 032005 [arXiv:1709.07703] [INSPIRE].

[9] CMS collaboration, *Measurements of the* pp → ZZ *production cross section and the* Z → 4ℓ *branching fraction, and constraints on anomalous triple gauge couplings at* $\sqrt{s} = 13$ *TeV*, *Eur. Phys. J. C* **78** (2018) 165 [*Erratum ibid.* **78** (2018) 515] [arXiv:1709.08601] [INSPIRE].

[10] CMS collaboration, *Measurements of* pp → ZZ *production cross sections and constraints on anomalous triple gauge couplings at* $\sqrt{s} = 13$ *TeV*, *Eur. Phys. J. C* **81** (2021) 200 [arXiv:2009.01186] [INSPIRE].

[11] E. Maguire, L. Heinrich and G. Watt, *HEPData: a repository for high energy physics data*, *J. Phys. Conf. Ser.* **898** (2017) 102006 [arXiv:1704.05473] [INSPIRE].

[12] C. Bierlich et al., *Robust Independent Validation of Experiment and Theory: Rivet version 3*, *SciPost Phys.* **8** (2020) 026 [arXiv:1912.05451] [INSPIRE].

[13] ATLAS collaboration, *Performance of the ATLAS trigger system in 2015*, *Eur. Phys. J. C* **77** (2017) 317 [arXiv:1611.09661] [INSPIRE].

[14] *Proposal for truth particle observable definitions in physics measurements*, Tech. Rep. ATL-PHYS-PUB-2015-013, CERN, Geneva (Jun, 2015).

[15] Sherpa collaboration, *Event generation with Sherpa 2.2*, *SciPost Phys.* **7** (2019) 034 [arXiv:1905.09127] [INSPIRE].

[16] T. Gleisberg and S. Hoeche, *Comix, a new matrix element generator*, *JHEP* **12** (2008) 039 [arXiv:0808.3674] [INSPIRE].

[17] S. Schumann and F. Krauss, *A parton shower algorithm based on Catani-Seymour dipole factorisation*, *JHEP* **03** (2008) 038 [arXiv:0709.1027] [INSPIRE].

[18] S. Hoeche, F. Krauss, M. Schönherr and F. Siegert, *A critical appraisal of NLO+PS matching methods*, *JHEP* **09** (2012) 049 [arXiv:1111.1220] [INSPIRE].

[19] S. Hoeche, F. Krauss, M. Schönherr and F. Siegert, *QCD matrix elements + parton showers: The NLO case*, *JHEP* **04** (2013) 027 [arXiv:1207.5030] [INSPIRE].

[20] S. Catani, F. Krauss, R. Kuhn and B.R. Webber, *QCD matrix elements + parton showers*, *JHEP* **11** (2001) 063 [hep-ph/0109231] [INSPIRE].

[21] S. Hoeche, F. Krauss, S. Schumann and F. Siegert, *QCD matrix elements and truncated showers*, *JHEP* **05** (2009) 053 [arXiv:0903.1219] [INSPIRE].

[22] F. Cascioli, P. Maierhöfer and S. Pozzorini, *Scattering Amplitudes with Open Loops*, *Phys. Rev. Lett.* **108** (2012) 111601 [arXiv:1111.5206] [InSPIRE].

[23] A. Denner, S. Dittmaier and L. Hofer, *Collier: a fortran-based Complex One-Loop LIbrary in Extended Regularizations*, *Comput. Phys. Commun.* **212** (2017) 220 [arXiv:1604.06792] [InSPIRE].

[24] NNPDF collaboration, *Parton distributions for the LHC Run II*, *JHEP* **04** (2015) 040 [arXiv:1410.8849] [InSPIRE].

[25] S. Alioli, P. Nason, C. Oleari and E. Re, *A general framework for implementing NLO calculations in shower Monte Carlo programs: the POWHEG BOX*, *JHEP* **06** (2010) 043 [arXiv:1002.2581] [InSPIRE].

[26] T. Melia, P. Nason, R. Röntsch and G. Zanderighi, W^+W^-, WZ and ZZ production in the POWHEG BOX, *JHEP* **11** (2011) 078 [arXiv:1107.5051] [InSPIRE].

[27] P. Nason and G. Zanderighi, W^+W^-, WZ and ZZ production in the POWHEG-BOX-V2, *Eur. Phys. J. C* **74** (2014) 2702 [arXiv:1311.1365] [InSPIRE].

[28] T. Sjöstrand, S. Mrenna and P.Z. Skands, *A brief introduction to PYTHIA 8.1*, *Comput. Phys. Commun.* **178** (2008) 852 [arXiv:0710.3820] [InSPIRE].

[29] ATLAS collaboration, *Measurement of the Z/γ^* boson transverse momentum distribution in pp collisions at $\sqrt{s} = 7$ TeV with the ATLAS detector*, *JHEP* **09** (2014) 145 [arXiv:1406.3660] [InSPIRE].

[30] H.-L. Lai et al., *New parton distributions for collider physics*, *Phys. Rev. D* **82** (2010) 074024 [arXiv:1007.2241] [InSPIRE].

[31] J. Pumplin, D.R. Stump, J. Huston, H.L. Lai, P.M. Nadolsky and W.K. Tung, *New generation of parton distributions with uncertainties from global QCD analysis*, *JHEP* **07** (2002) 012 [hep-ph/0201195] [InSPIRE].

[32] F. Cascioli et al., *ZZ production at hadron colliders in NNLO QCD*, *Phys. Lett. B* **735** (2014) 311 [arXiv:1405.2219] [InSPIRE].

[33] M. Grazzini, S. Kallweit and D. Rathlev, *ZZ production at the LHC: fiducial cross sections and distributions in NNLO QCD*, *Phys. Lett. B* **750** (2015) 407 [arXiv:1507.06257] [InSPIRE].

[34] M. Grazzini, S. Kallweit and M. Wiesemann, *Fully differential NNLO computations with MATRIX*, *Eur. Phys. J. C* **78** (2018) 537 [arXiv:1711.06631] [InSPIRE].

[35] S. Kallweit and M. Wiesemann, *ZZ production at the LHC: NNLO predictions for $2\ell2\nu$ and 4ℓ signatures*, *Phys. Lett. B* **786** (2018) 382 [arXiv:1806.05941] [InSPIRE].

[36] B. Biedermann, A. Denner, S. Dittmaier, L. Hofer and B. Jäger, *Electroweak corrections to $pp \to \mu^+\mu^- e^+ e^- + X$ at the LHC: a Higgs background study*, *Phys. Rev. Lett.* **116** (2016) 161803 [arXiv:1601.07787] [InSPIRE].

[37] B. Biedermann, A. Denner, S. Dittmaier, L. Hofer and B. Jäger, *Next-to-leading-order electroweak corrections to the production of four charged leptons at the LHC*, *JHEP* **01** (2017) 033 [arXiv:1611.05338] [InSPIRE].

[38] S. Gieseke, T. Kasprzik and J.H. Kühn, *Vector-boson pair production and electroweak corrections in HERWIG++*, *Eur. Phys. J. C* **74** (2014) 2988 [arXiv:1401.3964] [InSPIRE].

[39] E. Bothmann, M. Schönherr and S. Schumann, *Reweighting QCD matrix-element and parton-shower calculations*, *Eur. Phys. J. C* **76** (2016) 590 [arXiv:1606.08753] [INSPIRE].

[40] S. Dulat et al., *New parton distribution functions from a global analysis of quantum chromodynamics*, *Phys. Rev. D* **93** (2016) 033006 [arXiv:1506.07443] [INSPIRE].

[41] L.A. Harland-Lang, A.D. Martin, P. Motylinski and R.S. Thorne, *Parton distributions in the LHC era: MMHT 2014 PDFs*, *Eur. Phys. J. C* **75** (2015) 204 [arXiv:1412.3989] [INSPIRE].

[42] A.D. Martin, W.J. Stirling, R.S. Thorne and G. Watt, *Parton distributions for the LHC*, *Eur. Phys. J. C* **63** (2009) 189 [arXiv:0901.0002] [INSPIRE].

[43] F. Cascioli, S. Höche, F. Krauss, P. Maierhöfer, S. Pozzorini and F. Siegert, *Precise Higgs-background predictions: merging NLO QCD and squared quark-loop corrections to four-lepton + 0,1 jet production*, *JHEP* **01** (2014) 046 [arXiv:1309.0500] [INSPIRE].

[44] F. Caola, K. Melnikov, R. Röntsch and L. Tancredi, *QCD corrections to ZZ production in gluon fusion at the LHC*, *Phys. Rev. D* **92** (2015) 094028 [arXiv:1509.06734] [INSPIRE].

[45] F. Caola, M. Dowling, K. Melnikov, R. Röntsch and L. Tancredi, *QCD corrections to vector boson pair production in gluon fusion including interference effects with off-shell Higgs at the LHC*, *JHEP* **07** (2016) 087 [arXiv:1605.04610] [INSPIRE].

[46] G. Passarino, *Higgs CAT*, *Eur. Phys. J. C* **74** (2014) 2866 [arXiv:1312.2397] [INSPIRE].

[47] LHC HIGGS CROSS SECTION WORKING GROUP collaboration, *Handbook of LHC Higgs Cross Sections: 4. Deciphering the Nature of the Higgs Sector*, arXiv:1610.07922 [INSPIRE].

[48] J.M. Campbell, R.K. Ellis, R. Frederix, P. Nason, C. Oleari and C. Williams, *NLO Higgs boson production plus one and two jets using the POWHEG BOX, MadGraph4 and MCFM*, *JHEP* **07** (2012) 092 [arXiv:1202.5475] [INSPIRE].

[49] K. Hamilton, P. Nason, E. Re and G. Zanderighi, *NNLOPS simulation of Higgs boson production*, *JHEP* **10** (2013) 222 [arXiv:1309.0017] [INSPIRE].

[50] K. Hamilton, P. Nason and G. Zanderighi, *Finite quark-mass effects in the NNLOPS POWHEG+MiNLO Higgs generator*, *JHEP* **05** (2015) 140 [arXiv:1501.04637] [INSPIRE].

[51] P. Nason, *A new method for combining NLO QCD with shower Monte Carlo algorithms*, *JHEP* **11** (2004) 040 [hep-ph/0409146] [INSPIRE].

[52] S. Frixione, P. Nason and C. Oleari, *Matching NLO QCD computations with Parton Shower simulations: the POWHEG method*, *JHEP* **11** (2007) 070 [arXiv:0709.2092] [INSPIRE].

[53] K. Hamilton, P. Nason and G. Zanderighi, *MINLO: multi-scale improved NLO*, *JHEP* **10** (2012) 155 [arXiv:1206.3572] [INSPIRE].

[54] K. Hamilton, P. Nason, C. Oleari and G. Zanderighi, *Merging H/W/Z + 0 and 1 jet at NLO with no merging scale: a path to parton shower + NNLO matching*, *JHEP* **05** (2013) 082 [arXiv:1212.4504] [INSPIRE].

[55] S. Catani and M. Grazzini, *Next-to-Next-to-Leading-Order Subtraction Formalism in Hadron Collisions and its Application to Higgs Boson Production at the Large Hadron Collider*, *Phys. Rev. Lett.* **98** (2007) 222002 [hep-ph/0703012] [INSPIRE].

[56] T. Sjöstrand et al., *An introduction to PYTHIA 8.2*, *Comput. Phys. Commun.* **191** (2015) 159 [arXiv:1410.3012] [INSPIRE].

[57] J. Butterworth et al., *PDF4LHC recommendations for LHC Run II*, *J. Phys. G* **43** (2016) 023001 [arXiv:1510.03865] [INSPIRE].

[58] C. Anastasiou et al., *High precision determination of the gluon fusion Higgs boson cross-section at the LHC*, *JHEP* **05** (2016) 058 [arXiv:1602.00695] [INSPIRE].

[59] C. Anastasiou, C. Duhr, F. Dulat, F. Herzog and B. Mistlberger, *Higgs Boson Gluon-Fusion Production in QCD at Three Loops*, *Phys. Rev. Lett.* **114** (2015) 212001 [arXiv:1503.06056] [INSPIRE].

[60] F. Dulat, A. Lazopoulos and B. Mistlberger, *iHixs 2 — Inclusive Higgs cross sections*, *Comput. Phys. Commun.* **233** (2018) 243 [arXiv:1802.00827] [INSPIRE].

[61] R.V. Harlander and K.J. Ozeren, *Finite top mass effects for hadronic Higgs production at next-to-next-to-leading order*, *JHEP* **11** (2009) 088 [arXiv:0909.3420] [INSPIRE].

[62] R.V. Harlander and K.J. Ozeren, *Top mass effects in Higgs production at next-to-next-to-leading order QCD: Virtual corrections*, *Phys. Lett. B* **679** (2009) 467 [arXiv:0907.2997] [INSPIRE].

[63] R.V. Harlander, H. Mantler, S. Marzani and K.J. Ozeren, *Higgs production in gluon fusion at next-to-next-to-leading order QCD for finite top mass*, *Eur. Phys. J. C* **66** (2010) 359 [arXiv:0912.2104] [INSPIRE].

[64] A. Pak, M. Rogal and M. Steinhauser, *Finite top quark mass effects in NNLO Higgs boson production at LHC*, *JHEP* **02** (2010) 025 [arXiv:0911.4662] [INSPIRE].

[65] S. Actis, G. Passarino, C. Sturm and S. Uccirati, *NLO electroweak corrections to Higgs boson production at hadron colliders*, *Phys. Lett. B* **670** (2008) 12 [arXiv:0809.1301] [INSPIRE].

[66] S. Actis, G. Passarino, C. Sturm and S. Uccirati, *NNLO computational techniques: The cases $H \to \gamma\gamma$ and $H \to gg$*, *Nucl. Phys. B* **811** (2009) 182 [arXiv:0809.3667] [INSPIRE].

[67] M. Bonetti, K. Melnikov and L. Tancredi, *Higher order corrections to mixed QCD-EW contributions to Higgs boson production in gluon fusion*, *Phys. Rev. D* **97** (2018) 056017 [*Erratum ibid.* **97** (2018) 099906] [arXiv:1801.10403] [INSPIRE].

[68] P. Nason and C. Oleari, *NLO Higgs boson production via vector-boson fusion matched with shower in POWHEG*, *JHEP* **02** (2010) 037 [arXiv:0911.5299] [INSPIRE].

[69] G. Luisoni, P. Nason, C. Oleari and F. Tramontano, *$HW^{\pm}/HZ$ + 0 and 1 jet at NLO with the POWHEG BOX interfaced to GoSam and their merging within MiNLO*, *JHEP* **10** (2013) 083 [arXiv:1306.2542] [INSPIRE].

[70] M. Ciccolini, A. Denner and S. Dittmaier, *Strong and Electroweak Corrections to the Production of Higgs + 2 Jets via Weak Interactions at the Large Hadron Collider*, *Phys. Rev. Lett.* **99** (2007) 161803 [arXiv:0707.0381] [INSPIRE].

[71] M. Ciccolini, A. Denner and S. Dittmaier, *Electroweak and QCD corrections to Higgs production via vector-boson fusion at the CERN LHC*, *Phys. Rev. D* **77** (2008) 013002 [arXiv:0710.4749] [INSPIRE].

[72] P. Bolzoni, F. Maltoni, S.-O. Moch and M. Zaro, *Higgs Boson Production via Vector-Boson Fusion at Next-to-Next-to-Leading Order in QCD*, *Phys. Rev. Lett.* **105** (2010) 011801 [arXiv:1003.4451] [INSPIRE].

[73] M.L. Ciccolini, S. Dittmaier and M. Krämer, *Electroweak radiative corrections to associated WH and ZH production at hadron colliders*, *Phys. Rev. D* **68** (2003) 073003 [hep-ph/0306234] [INSPIRE].

[74] O. Brein, A. Djouadi and R. Harlander, *NNLO QCD corrections to the Higgs-strahlung processes at hadron colliders*, *Phys. Lett. B* **579** (2004) 149 [hep-ph/0307206] [INSPIRE].

[75] O. Brein, R. Harlander, M. Wiesemann and T. Zirke, *Top-quark mediated effects in hadronic Higgs-Strahlung*, *Eur. Phys. J. C* **72** (2012) 1868 [arXiv:1111.0761] [INSPIRE].

[76] A. Denner, S. Dittmaier, S. Kallweit and A. Mück, *HAWK 2.0: A Monte Carlo program for Higgs production in vector-boson fusion and Higgs strahlung at hadron colliders*, *Comput. Phys. Commun.* **195** (2015) 161 [arXiv:1412.5390] [INSPIRE].

[77] O. Brein, R.V. Harlander and T.J.E. Zirke, *vh@nnlo — Higgs Strahlung at hadron colliders*, *Comput. Phys. Commun.* **184** (2013) 998 [arXiv:1210.5347] [INSPIRE].

[78] ATLAS collaboration, *Measurement of the Higgs boson coupling properties in the $H \to ZZ^* \to 4\ell$ decay channel at $\sqrt{s} = 13$ TeV with the ATLAS detector*, *JHEP* **03** (2018) 095 [arXiv:1712.02304] [INSPIRE].

[79] J. Alwall et al., *The automated computation of tree-level and next-to-leading order differential cross sections, and their matching to parton shower simulations*, *JHEP* **07** (2014) 079 [arXiv:1405.0301] [INSPIRE].

[80] *ATLAS PYTHIA 8 tunes to 7 TeV data*, Tech. Rep. ATL-PHYS-PUB-2014-021, CERN, Geneva (Nov, 2014).

[81] R.D. Ball et al., *Parton distributions with LHC data*, *Nucl. Phys. B* **867** (2013) 244 [arXiv:1207.1303] [INSPIRE].

[82] GEANT4 collaboration, *GEANT4 — a simulation toolkit*, *Nucl. Instrum. Meth. A* **506** (2003) 250 [INSPIRE].

[83] ATLAS collaboration, *The ATLAS Simulation Infrastructure*, *Eur. Phys. J. C* **70** (2010) 823 [arXiv:1005.4568] [INSPIRE].

[84] ATLAS collaboration, *Electron and photon performance measurements with the ATLAS detector using the 2015-2017 LHC proton-proton collision data*, 2019 *JINST* **14** P12006 [arXiv:1908.00005] [INSPIRE].

[85] ATLAS collaboration, *Muon reconstruction performance of the ATLAS detector in proton-proton collision data at $\sqrt{s} = 13$ TeV*, *Eur. Phys. J. C* **76** (2016) 292 [arXiv:1603.05598] [INSPIRE].

[86] ATLAS collaboration, *The PYTHIA 8 A3 tune description of ATLAS minimum bias and inelastic measurements incorporating the Donnachie-Landshoff diffractive model*, Tech. Rep. ATL-PHYS-PUB-2016-017, CERN, Geneva (Aug, 2016).

[87] ATLAS collaboration, *Performance of electron and photon triggers in ATLAS during LHC Run 2*, *Eur. Phys. J. C* **80** (2020) 47 [arXiv:1909.00761] [INSPIRE].

[88] ATLAS collaboration, *Performance of the ATLAS muon triggers in Run 2*, 2020 *JINST* **15** P09015 [arXiv:2004.13447] [INSPIRE].

[89] ATLAS collaboration, *Muon reconstruction and identification efficiency in ATLAS using the full Run 2 pp collision data set at $\sqrt{s} = 13$ TeV*, arXiv:2012.00578 [INSPIRE].

[90] J.H. Friedman, *A variable span smoother*, Tech. Rep. SLAC-PUB-3477. STAN-LCS-005, SLAC, Stanford, CA, U.S.A. (1984).

[91] G. D'Agostini, *A multidimensional unfolding method based on Bayes' theorem*, *Nucl. Instrum. Meth. A* **362** (1995) 487 [INSPIRE].

[92] ATLAS collaboration, *Luminosity determination in pp collisions at $\sqrt{s} = 13$ TeV using the ATLAS detector at the LHC*, Tech. Rep. ATLAS-CONF-2019-021, CERN, Geneva (Jun, 2019).

[93] G. Avoni et al., *The new LUCID-2 detector for luminosity measurement and monitoring in ATLAS*, 2018 *JINST* **13** P07017 [INSPIRE].

[94] ATLAS collaboration, *Measurements of the Higgs boson inclusive and differential fiducial cross sections in the 4ℓ decay channel at $\sqrt{s} = 13$ TeV*, *Eur. Phys. J. C* **80** (2020) 942 [arXiv:2004.03969] [INSPIRE].

[95] C. Gütschow and M. Schönherr, *Four lepton production and the accuracy of QED FSR*, *Eur. Phys. J. C* **81** (2021) 48 [arXiv:2007.15360] [INSPIRE].

[96] ATLAS collaboration, *Measurements of Four-Lepton Production at the Z Resonance in pp Collisions at $\sqrt{s} = 7$ and 8 TeV with ATLAS*, *Phys. Rev. Lett.* **112** (2014) 231806 [arXiv:1403.5657] [INSPIRE].

[97] ATLAS collaboration, *Measurement of $W^{\pm}$ and Z-boson production cross sections in pp collisions at $\sqrt{s} = 13$ TeV with the ATLAS detector*, *Phys. Lett. B* **759** (2016) 601 [arXiv:1603.09222] [INSPIRE].

[98] B. Grzadkowski, M. Iskrzynski, M. Misiak and J. Rosiek, *Dimension-six terms in the Standard Model Lagrangian*, *JHEP* **10** (2010) 085 [arXiv:1008.4884] [INSPIRE].

[99] I. Brivio, Y. Jiang and M. Trott, *The SMEFTsim package, theory and tools*, *JHEP* **12** (2017) 070 [arXiv:1709.06492] [INSPIRE].

[100] A. Alloul, N.D. Christensen, C. Degrande, C. Duhr and B. Fuks, *FEYNRULES 2.0 — A complete toolbox for tree-level phenomenology*, *Comput. Phys. Commun.* **185** (2014) 2250 [arXiv:1310.1921] [INSPIRE].

[101] G. Cowan, K. Cranmer, E. Gross and O. Vitells, *Asymptotic formulae for likelihood-based tests of new physics*, *Eur. Phys. J. C* **71** (2011) 1554 [*Erratum ibid.* **73** (2013) 2501] [arXiv:1007.1727] [INSPIRE].

[102] ATLAS collaboration, *Higgs boson production cross-section measurements and their EFT interpretation in the 4ℓ decay channel at $\sqrt{s} = 13$ TeV with the ATLAS detector*, *Eur. Phys. J. C* **80** (2020) 957 [*Erratum ibid.* **81** (2021) 29] [*Erratum ibid.* **81** (2021) 398] [arXiv:2004.03447] [INSPIRE].

[103] J. Ellis, C.W. Murphy, V. Sanz and T. You, *Updated global SMEFT fit to Higgs, diboson and electroweak data*, *JHEP* **06** (2018) 146 [arXiv:1803.03252] [INSPIRE].

[104] F.F. Deppisch, W. Liu and M. Mitra, *Long-lived heavy neutrinos from Higgs decays*, *JHEP* **08** (2018) 181 [arXiv:1804.04075] [INSPIRE].

[105] S. Amrith, J.M. Butterworth, F.F. Deppisch, W. Liu, A. Varma and D. Yallup, *LHC constraints on a $B - L$ gauge model using CONTUR*, *JHEP* **05** (2019) 154 [arXiv:1811.11452] [INSPIRE].

[106] M. Bähr et al., *Herwig++ physics and manual*, *Eur. Phys. J. C* **58** (2008) 639 [arXiv:0803.0883] [INSPIRE].

[107] J. Bellm et al., *Herwig 7.0/Herwig++ 3.0 release note*, *Eur. Phys. J. C* **76** (2016) 196 [arXiv:1512.01178] [INSPIRE].

[108] A.L. Read, *Presentation of search results: the CL_S technique*, *J. Phys. G* **28** (2002) 2693 [INSPIRE].

[109] ATLAS collaboration, *ATLAS Computing Acknowledgements*, Tech. Rep. ATL-SOFT-PUB-2020-001, CERN, Geneva (May, 2020).

The ATLAS collaboration

G. Aad[102], B. Abbott[128], D.C. Abbott[103], A. Abed Abud[36], K. Abeling[53], D.K. Abhayasinghe[94],
S.H. Abidi[167], O.S. AbouZeid[40], N.L. Abraham[156], H. Abramowicz[161], H. Abreu[160],
Y. Abulaiti[6], B.S. Acharya[67a,67b,o], B. Achkar[53], L. Adam[100], C. Adam Bourdarios[5],
L. Adamczyk[84a], L. Adamek[167], J. Adelman[121], A. Adiguzel[12c,ad], S. Adorni[54], T. Adye[143],
A.A. Affolder[145], Y. Afik[160], C. Agapopoulou[65], M.N. Agaras[38], A. Aggarwal[119],
C. Agheorghiesei[27c], J.A. Aguilar-Saavedra[139f,139a,ac], A. Ahmad[36], F. Ahmadov[80],
W.S. Ahmed[104], X. Ai[18], G. Aielli[74a,74b], S. Akatsuka[86], M. Akbiyik[100], T.P.A. Åkesson[97],
E. Akilli[54], A.V. Akimov[111], K. Al Khoury[65], G.L. Alberghi[23b,23a], J. Albert[176],
M.J. Alconada Verzini[161], S. Alderweireldt[36], M. Aleksa[36], I.N. Aleksandrov[80], C. Alexa[27b],
T. Alexopoulos[10], A. Alfonsi[120], F. Alfonsi[23b,23a], M. Alhroob[128], B. Ali[141], S. Ali[158],
M. Aliev[166], G. Alimonti[69a], C. Allaire[36], B.M.M. Allbrooke[156], B.W. Allen[131], P.P. Allport[21],
A. Aloisio[70a,70b], F. Alonso[89], C. Alpigiani[148], E. Alunno Camelia[74a,74b], M. Alvarez Estevez[99],
M.G. Alviggi[70a,70b], Y. Amaral Coutinho[81b], A. Ambler[104], L. Ambroz[134], C. Amelung[36],
D. Amidei[106], S.P. Amor Dos Santos[139a], S. Amoroso[46], C.S. Amrouche[54], F. An[79],
C. Anastopoulos[149], N. Andari[144], T. Andeen[11], J.K. Anders[20], S.Y. Andrean[45a,45b],
A. Andreazza[69a,69b], V. Andrei[61a], C.R. Anelli[176], S. Angelidakis[9], A. Angerami[39],
A.V. Anisenkov[122b,122a], A. Annovi[72a], C. Antel[54], M.T. Anthony[149], E. Antipov[129],
M. Antonelli[51], D.J.A. Antrim[18], F. Anulli[73a], M. Aoki[82], J.A. Aparisi Pozo[174], M.A. Aparo[156],
L. Aperio Bella[46], N. Aranzabal[36], V. Araujo Ferraz[81a], R. Araujo Pereira[81b], C. Arcangeletti[51],
A.T.H. Arce[49], J-F. Arguin[110], S. Argyropoulos[52], J.-H. Arling[46], A.J. Armbruster[36],
A. Armstrong[171], O. Arnaez[167], H. Arnold[120], Z.P. Arrubarrena Tame[114], G. Artoni[134],
H. Asada[117], K. Asai[126], S. Asai[163], T. Asawatavonvanich[165], N. Asbah[59],
E.M. Asimakopoulou[172], L. Asquith[156], J. Assahsah[35e], K. Assamagan[29], R. Astalos[28a],
R.J. Atkin[33a], M. Atkinson[173], N.B. Atlay[19], H. Atmani[65], P.A. Atmasiddha[106], K. Augsten[141],
V.A. Austrup[182], G. Avolio[36], M.K. Ayoub[15a], G. Azuelos[110,ak], D. Babal[28a], H. Bachacou[144],
K. Bachas[162], F. Backman[45a,45b], P. Bagnaia[73a,73b], M. Bahmani[85], H. Bahrasemani[152],
A.J. Bailey[174], V.R. Bailey[173], J.T. Baines[143], C. Bakalis[10], O.K. Baker[183], P.J. Bakker[120],
E. Bakos[16], D. Bakshi Gupta[8], S. Balaji[157], R. Balasubramanian[120], E.M. Baldin[122b,122a],
P. Balek[180], F. Balli[144], W.K. Balunas[134], J. Balz[100], E. Banas[85], M. Bandieramonte[138],
A. Bandyopadhyay[19], Sw. Banerjee[181,j], L. Barak[161], W.M. Barbe[38], E.L. Barberio[105],
D. Barberis[55b,55a], M. Barbero[102], G. Barbour[95], T. Barillari[115], M-S. Barisits[36], J. Barkeloo[131],
T. Barklow[153], R. Barnea[160], B.M. Barnett[143], R.M. Barnett[18], Z. Barnovska-Blenessy[60a],
A. Baroncelli[60a], G. Barone[29], A.J. Barr[134], L. Barranco Navarro[45a,45b], F. Barreiro[99],
J. Barreiro Guimarães da Costa[15a], U. Barron[161], S. Barsov[137], F. Bartels[61a], R. Bartoldus[153],
G. Bartolini[102], A.E. Barton[90], P. Bartos[28a], A. Basalaev[46], A. Basan[100], A. Bassalat[65,ah],
M.J. Basso[167], R.L. Bates[57], S. Batlamous[35f], J.R. Batley[32], B. Batool[151], M. Battaglia[145],
M. Bauce[73a,73b], F. Bauer[144,*], P. Bauer[24], H.S. Bawa[31], A. Bayirli[12c], J.B. Beacham[49],
T. Beau[135], P.H. Beauchemin[170], F. Becherer[52], P. Bechtle[24], H.C. Beck[53], H.P. Beck[20,q],
K. Becker[178], C. Becot[46], A. Beddall[12d], A.J. Beddall[12a], V.A. Bednyakov[80], M. Bedognetti[120],
C.P. Bee[155], T.A. Beermann[182], M. Begalli[81b], M. Begel[29], A. Behera[155], J.K. Behr[46],
F. Beisiegel[24], M. Belfkir[5], A.S. Bell[95], G. Bella[161], L. Bellagamba[23b], A. Bellerive[34], P. Bellos[9],
K. Beloborodov[122b,122a], K. Belotskiy[112], N.L. Belyaev[112], D. Benchekroun[35a], N. Benekos[10],
Y. Benhammou[161], D.P. Benjamin[6], M. Benoit[29], J.R. Bensinger[26], S. Bentvelsen[120],
L. Beresford[134], M. Beretta[51], D. Berge[19], E. Bergeaas Kuutmann[172], N. Berger[5],
B. Bergmann[141], L.J. Bergsten[26], J. Beringer[18], S. Berlendis[7], G. Bernardi[135], C. Bernius[153],
F.U. Bernlochner[24], T. Berry[94], P. Berta[100], A. Berthold[48], I.A. Bertram[90],

O. Bessidskaia Bylund[182], N. Besson[144], S. Bethke[115], A. Betti[42], A.J. Bevan[93], J. Beyer[115],
S. Bhatta[155], D.S. Bhattacharya[177], P. Bhattarai[26], V.S. Bhopatkar[6], R. Bi[138], R.M. Bianchi[138],
O. Biebel[114], D. Biedermann[19], R. Bielski[36], K. Bierwagen[100], N.V. Biesuz[72a,72b], M. Biglietti[75a],
T.R.V. Billoud[141], M. Bindi[53], A. Bingul[12d], C. Bini[73a,73b], S. Biondi[23b,23a], C.J. Birch-sykes[101],
M. Birman[180], T. Bisanz[36], J.P. Biswal[3], D. Biswas[181,j], A. Bitadze[101], C. Bittrich[48],
K. Bjørke[133], T. Blazek[28a], I. Bloch[46], C. Blocker[26], A. Blue[57], U. Blumenschein[93],
G.J. Bobbink[120], V.S. Bobrovnikov[122b,122a], S.S. Bocchetta[97], D. Bogavac[14],
A.G. Bogdanchikov[122b,122a], C. Bohm[45a], V. Boisvert[94], P. Bokan[172,53], T. Bold[84a],
A.E. Bolz[61b], M. Bomben[135], M. Bona[93], J.S. Bonilla[131], M. Boonekamp[144], C.D. Booth[94],
A.G. Borbély[57], H.M. Borecka-Bielska[91], L.S. Borgna[95], A. Borisov[123], G. Borissov[90],
D. Bortoletto[134], D. Boscherini[23b], M. Bosman[14], J.D. Bossio Sola[104], K. Bouaouda[35a],
J. Boudreau[138], E.V. Bouhova-Thacker[90], D. Boumediene[38], A. Boveia[127], J. Boyd[36], D. Boye[33c],
I.R. Boyko[80], A.J. Bozson[94], J. Bracinik[21], N. Brahimi[60d,60c], G. Brandt[182], O. Brandt[32],
F. Braren[46], B. Brau[103], J.E. Brau[131], W.D. Breaden Madden[57], K. Brendlinger[46], R. Brener[160],
L. Brenner[36], R. Brenner[172], S. Bressler[180], B. Brickwedde[100], D.L. Briglin[21], D. Britton[57],
D. Britzger[115], I. Brock[24], R. Brock[107], G. Brooijmans[39], W.K. Brooks[146d], E. Brost[29],
P.A. Bruckman de Renstrom[85], B. Brüers[46], D. Bruncko[28b], A. Bruni[23b], G. Bruni[23b],
M. Bruschi[23b], N. Bruscino[73a,73b], L. Bryngemark[153], T. Buanes[17], Q. Buat[155], P. Buchholz[151],
A.G. Buckley[57], I.A. Budagov[80], M.K. Bugge[133], O. Bulekov[112], B.A. Bullard[59], T.J. Burch[121],
S. Burdin[91], C.D. Burgard[120], A.M. Burger[129], B. Burghgrave[8], J.T.P. Burr[46], C.D. Burton[11],
J.C. Burzynski[103], V. Büscher[100], E. Buschmann[53], P.J. Bussey[57], J.M. Butler[25], C.M. Buttar[57],
J.M. Butterworth[95], P. Butti[36], W. Buttinger[143], C.J. Buxo Vazquez[107], A. Buzatu[158],
A.R. Buzykaev[122b,122a], G. Cabras[23b,23a], S. Cabrera Urbán[174], D. Caforio[56], H. Cai[138],
V.M.M. Cairo[153], O. Cakir[4a], N. Calace[36], P. Calafiura[18], G. Calderini[135], P. Calfayan[66],
G. Callea[57], L.P. Caloba[81b], A. Caltabiano[74a,74b], S. Calvente Lopez[99], D. Calvet[38], S. Calvet[38],
T.P. Calvet[102], M. Calvetti[72a,72b], R. Camacho Toro[135], S. Camarda[36], D. Camarero Munoz[99],
P. Camarri[74a,74b], M.T. Camerlingo[75a,75b], D. Cameron[133], C. Camincher[36], S. Campana[36],
M. Campanelli[95], A. Camplani[40], V. Canale[70a,70b], A. Canesse[104], M. Cano Bret[78],
J. Cantero[129], T. Cao[161], Y. Cao[173], M. Capua[41b,41a], R. Cardarelli[74a], F. Cardillo[174],
G. Carducci[41b,41a], I. Carli[142], T. Carli[36], G. Carlino[70a], B.T. Carlson[138], E.M. Carlson[176,168a],
L. Carminati[69a,69b], R.M.D. Carney[153], S. Caron[119], E. Carquin[146d], S. Carrá[46],
G. Carratta[23b,23a], J.W.S. Carter[167], T.M. Carter[50], M.P. Casado[14,g], A.F. Casha[167],
E.G. Castiglia[183], F.L. Castillo[174], L. Castillo Garcia[14], V. Castillo Gimenez[174],
N.F. Castro[139a,139e], A. Catinaccio[36], J.R. Catmore[133], A. Cattai[36], V. Cavaliere[29],
V. Cavasinni[72a,72b], E. Celebi[12b], F. Celli[134], K. Cerny[130], A.S. Cerqueira[81a], A. Cerri[156],
L. Cerrito[74a,74b], F. Cerutti[18], A. Cervelli[23b,23a], S.A. Cetin[12b], Z. Chadi[35a], D. Chakraborty[121],
J. Chan[181], W.S. Chan[120], W.Y. Chan[91], J.D. Chapman[32], B. Chargeishvili[159b],
D.G. Charlton[21], T.P. Charman[93], M. Chatterjee[20], C.C. Chau[34], S. Che[127], S. Chekanov[6],
S.V. Chekulaev[168a], G.A. Chelkov[80,af], B. Chen[79], C. Chen[60a], C.H. Chen[79], H. Chen[15c],
H. Chen[29], J. Chen[60a], J. Chen[39], J. Chen[26], S. Chen[136], S.J. Chen[15c], X. Chen[15b], Y. Chen[60a],
Y-H. Chen[46], H.C. Cheng[63a], H.J. Cheng[15a], A. Cheplakov[80], E. Cheremushkina[123],
R. Cherkaoui El Moursli[35f], E. Cheu[7], K. Cheung[64], T.J.A. Chevalérias[144], L. Chevalier[144],
V. Chiarella[51], G. Chiarelli[72a], G. Chiodini[68a], A.S. Chisholm[21], A. Chitan[27b], I. Chiu[163],
Y.H. Chiu[176], M.V. Chizhov[80], K. Choi[11], A.R. Chomont[73a,73b], Y. Chou[103], Y.S. Chow[120],
L.D. Christopher[33e], M.C. Chu[63a], X. Chu[15a,15d], J. Chudoba[140], J.J. Chwastowski[85],
L. Chytka[130], D. Cieri[115], K.M. Ciesla[85], V. Cindro[92], I.A. Cioară[27b], A. Ciocio[18],
F. Cirotto[70a,70b], Z.H. Citron[180,k], M. Citterio[69a], D.A. Ciubotaru[27b], B.M. Ciungu[167],
A. Clark[54], P.J. Clark[50], S.E. Clawson[101], C. Clement[45a,45b], L. Clissa[23b,23a], Y. Coadou[102],

M. Cobal[67a,67c], A. Coccaro[55b], J. Cochran[79], R. Coelho Lopes De Sa[103], H. Cohen[161],
A.E.C. Coimbra[36], B. Cole[39], A.P. Colijn[120], J. Collot[58], P. Conde Muiño[139a,139h],
S.H. Connell[33c], I.A. Connelly[57], S. Constantinescu[27b], F. Conventi[70a,al], A.M. Cooper-Sarkar[134],
F. Cormier[175], K.J.R. Cormier[167], L.D. Corpe[95], M. Corradi[73a,73b], E.E. Corrigan[97],
F. Corriveau[104,aa], M.J. Costa[174], F. Costanza[5], D. Costanzo[149], G. Cowan[94], J.W. Cowley[32],
J. Crane[101], K. Cranmer[125], R.A. Creager[136], S. Crépé-Renaudin[58], F. Crescioli[135],
M. Cristinziani[24], V. Croft[170], G. Crosetti[41b,41a], A. Cueto[5], T. Cuhadar Donszelmann[171],
H. Cui[15a,15d], A.R. Cukierman[153], W.R. Cunningham[57], S. Czekierda[85], P. Czodrowski[36],
M.M. Czurylo[61b], M.J. Da Cunha Sargedas De Sousa[60b], J.V. Da Fonseca Pinto[81b],
C. Da Via[101], W. Dabrowski[84a], F. Dachs[36], T. Dado[47], S. Dahbi[33e], T. Dai[106],
C. Dallapiccola[103], M. Dam[40], G. D'amen[29], V. D'Amico[75a,75b], J. Damp[100], J.R. Dandoy[136],
M.F. Daneri[30], M. Danninger[152], V. Dao[36], G. Darbo[55b], O. Dartsi[5], A. Dattagupta[131],
T. Daubney[46], S. D'Auria[69a,69b], C. David[168b], T. Davidek[142], D.R. Davis[49], I. Dawson[149],
K. De[8], R. De Asmundis[70a], M. De Beurs[120], S. De Castro[23b,23a], N. De Groot[119], P. de Jong[120],
H. De la Torre[107], A. De Maria[15c], D. De Pedis[73a], A. De Salvo[73a], U. De Sanctis[74a,74b],
M. De Santis[74a,74b], A. De Santo[156], J.B. De Vivie De Regie[65], D.V. Dedovich[80], A.M. Deiana[42],
J. Del Peso[99], Y. Delabat Diaz[46], D. Delgove[65], F. Deliot[144], C.M. Delitzsch[7],
M. Della Pietra[70a,70b], D. Della Volpe[54], A. Dell'Acqua[36], L. Dell'Asta[74a,74b], M. Delmastro[5],
C. Delporte[65], P.A. Delsart[58], S. Demers[183], M. Demichev[80], G. Demontigny[110], S.P. Denisov[123],
L. D'Eramo[121], D. Derendarz[85], J.E. Derkaoui[35e], F. Derue[135], P. Dervan[91], K. Desch[24],
K. Dette[167], C. Deutsch[24], M.R. Devesa[30], P.O. Deviveiros[36], F.A. Di Bello[73a,73b],
A. Di Ciaccio[74a,74b], L. Di Ciaccio[5], C. Di Donato[70a,70b], A. Di Girolamo[36],
G. Di Gregorio[72a,72b], A. Di Luca[76a,76b], B. Di Micco[75a,75b], R. Di Nardo[75a,75b],
K.F. Di Petrillo[59], R. Di Sipio[167], C. Diaconu[102], F.A. Dias[120], T. Dias Do Vale[139a],
M.A. Diaz[146a], F.G. Diaz Capriles[24], J. Dickinson[18], M. Didenko[166], E.B. Diehl[106], J. Dietrich[19],
S. Díez Cornell[46], C. Diez Pardos[151], A. Dimitrievska[18], W. Ding[15b], J. Dingfelder[24],
S.J. Dittmeier[61b], F. Dittus[36], F. Djama[102], T. Djobava[159b], J.I. Djuvsland[17],
M.A.B. Do Vale[147], M. Dobre[27b], D. Dodsworth[26], C. Doglioni[97], J. Dolejsi[142], Z. Dolezal[142],
M. Donadelli[81c], B. Dong[60c], J. Donini[38], A. D'onofrio[15c], M. D'Onofrio[91], J. Dopke[143],
A. Doria[70a], M.T. Dova[89], A.T. Doyle[57], E. Drechsler[152], E. Dreyer[152], T. Dreyer[53],
A.S. Drobac[170], D. Du[60b], T.A. du Pree[120], Y. Duan[60d], F. Dubinin[111], M. Dubovsky[28a],
A. Dubreuil[54], E. Duchovni[180], G. Duckeck[114], O.A. Ducu[36,27b], D. Duda[115], A. Dudarev[36],
A.C. Dudder[100], E.M. Duffield[18], M. D'uffizi[101], L. Duflot[65], M. Dührssen[36], C. Dülsen[182],
M. Dumancic[180], A.E. Dumitriu[27b], M. Dunford[61a], S. Dungs[47], A. Duperrin[102],
H. Duran Yildiz[4a], M. Düren[56], A. Durglishvili[159b], D. Duschinger[48], B. Dutta[46], D. Duvnjak[1],
G.I. Dyckes[136], M. Dyndal[36], S. Dysch[101], B.S. Dziedzic[85], M.G. Eggleston[49], T. Eifert[8],
G. Eigen[17], K. Einsweiler[18], T. Ekelof[172], H. El Jarrari[35f], V. Ellajosyula[172], M. Ellert[172],
F. Ellinghaus[182], A.A. Elliot[93], N. Ellis[36], J. Elmsheuser[29], M. Elsing[36], D. Emeliyanov[143],
A. Emerman[39], Y. Enari[163], M.B. Epland[49], J. Erdmann[47], A. Ereditato[20], P.A. Erland[85],
M. Errenst[182], M. Escalier[65], C. Escobar[174], O. Estrada Pastor[174], E. Etzion[161], G. Evans[139a],
H. Evans[66], M.O. Evans[156], A. Ezhilov[137], F. Fabbri[57], L. Fabbri[23b,23a], V. Fabiani[119],
G. Facini[178], R.M. Fakhrutdinov[123], S. Falciano[73a], P.J. Falke[24], S. Falke[36], J. Faltova[142],
Y. Fang[15a], Y. Fang[15a], G. Fanourakis[44], M. Fanti[69a,69b], M. Faraj[67a,67c], A. Farbin[8],
A. Farilla[75a], E.M. Farina[71a,71b], T. Farooque[107], S.M. Farrington[50], P. Farthouat[36], F. Fassi[35f],
P. Fassnacht[36], D. Fassouliotis[9], M. Faucci Giannelli[50], W.J. Fawcett[32], L. Fayard[65],
O.L. Fedin[137,p], W. Fedorko[175], A. Fehr[20], M. Feickert[173], L. Feligioni[102], A. Fell[149], C. Feng[60b],
M. Feng[49], M.J. Fenton[171], A.B. Fenyuk[123], S.W. Ferguson[43], J. Ferrando[46], A. Ferrari[172],
P. Ferrari[120], R. Ferrari[71a], D.E. Ferreira de Lima[61b], A. Ferrer[174], D. Ferrere[54], C. Ferretti[106],

F. Fiedler[100], A. Filipčič[92], F. Filthaut[119], K.D. Finelli[25], M.C.N. Fiolhais[139a,139c,a],
L. Fiorini[174], F. Fischer[114], J. Fischer[100], W.C. Fisher[107], T. Fitschen[21], I. Fleck[151],
P. Fleischmann[106], T. Flick[182], B.M. Flierl[114], L. Flores[136], L.R. Flores Castillo[63a],
F.M. Follega[76a,76b], N. Fomin[17], J.H. Foo[167], G.T. Forcolin[76a,76b], B.C. Forland[66],
A. Formica[144], F.A. Förster[14], A.C. Forti[101], E. Fortin[102], M.G. Foti[134], D. Fournier[65], H. Fox[90],
P. Francavilla[72a,72b], S. Francescato[73a,73b], M. Franchini[23b,23a], S. Franchino[61a], D. Francis[36],
L. Franco[5], L. Franconi[20], M. Franklin[59], G. Frattari[73a,73b], A.N. Fray[93], P.M. Freeman[21],
B. Freund[110], W.S. Freund[81b], E.M. Freundlich[47], D.C. Frizzell[128], D. Froidevaux[36],
J.A. Frost[134], M. Fujimoto[126], C. Fukunaga[164], E. Fullana Torregrosa[174], T. Fusayasu[116],
J. Fuster[174], A. Gabrielli[23b,23a], A. Gabrielli[36], S. Gadatsch[54], P. Gadow[115], G. Gagliardi[55b,55a],
L.G. Gagnon[110], G.E. Gallardo[134], E.J. Gallas[134], B.J. Gallop[143], R. Gamboa Goni[93],
K.K. Gan[127], S. Ganguly[180], J. Gao[60a], Y. Gao[50], Y.S. Gao[31,m], F.M. Garay Walls[146a],
C. García[174], J.E. García Navarro[174], J.A. García Pascual[15a], C. Garcia-Argos[52],
M. Garcia-Sciveres[18], R.W. Gardner[37], N. Garelli[153], S. Gargiulo[52], C.A. Garner[167],
V. Garonne[133], S.J. Gasiorowski[148], P. Gaspar[81b], A. Gaudiello[55b,55a], G. Gaudio[71a],
P. Gauzzi[73a,73b], I.L. Gavrilenko[111], A. Gavrilyuk[124], C. Gay[175], G. Gaycken[46], E.N. Gazis[10],
A.A. Geanta[27b], C.M. Gee[145], C.N.P. Gee[143], J. Geisen[97], M. Geisen[100], C. Gemme[55b],
M.H. Genest[58], C. Geng[106], S. Gentile[73a,73b], S. George[94], T. Geralis[44], L.O. Gerlach[53],
P. Gessinger-Befurt[100], G. Gessner[47], M. Ghasemi Bostanabad[176], M. Ghneimat[151], A. Ghosh[65],
A. Ghosh[78], B. Giacobbe[23b], S. Giagu[73a,73b], N. Giangiacomi[167], P. Giannetti[72a],
A. Giannini[70a,70b], G. Giannini[14], S.M. Gibson[94], M. Gignac[145], D.T. Gil[84b], B.J. Gilbert[39],
D. Gillberg[34], G. Gilles[182], N.E.K. Gillwald[46], D.M. Gingrich[3,ak], M.P. Giordani[67a,67c],
P.F. Giraud[144], G. Giugliarelli[67a,67c], D. Giugni[69a], F. Giuli[74a,74b], S. Gkaitatzis[162],
I. Gkialas[9,h], E.L. Gkougkousis[14], P. Gkountoumis[10], L.K. Gladilin[113], C. Glasman[99],
J. Glatzer[14], P.C.F. Glaysher[46], A. Glazov[46], G.R. Gledhill[131], I. Gnesi[41b,c],
M. Goblirsch-Kolb[26], D. Godin[110], S. Goldfarb[105], T. Golling[54], D. Golubkov[123],
A. Gomes[139a,139b], R. Goncalves Gama[53], R. Gonçalo[139a,139c], G. Gonella[131], L. Gonella[21],
A. Gongadze[80], F. Gonnella[21], J.L. Gonski[39], S. González de la Hoz[174], S. Gonzalez Fernandez[14],
R. Gonzalez Lopez[91], C. Gonzalez Renteria[18], R. Gonzalez Suarez[172], S. Gonzalez-Sevilla[54],
G.R. Gonzalvo Rodriguez[174], L. Goossens[36], N.A. Gorasia[21], P.A. Gorbounov[124], H.A. Gordon[29],
B. Gorini[36], E. Gorini[68a,68b], A. Gorišek[92], A.T. Goshaw[49], M.I. Gostkin[80], C.A. Gottardo[119],
M. Gouighri[35b], A.G. Goussiou[148], N. Govender[33c], C. Goy[5], I. Grabowska-Bold[84a],
E.C. Graham[91], J. Gramling[171], E. Gramstad[133], S. Grancagnolo[19], M. Grandi[156],
V. Gratchev[137], P.M. Gravila[27f], F.G. Gravili[68a,68b], C. Gray[57], H.M. Gray[18], C. Grefe[24],
K. Gregersen[97], I.M. Gregor[46], P. Grenier[153], K. Grevtsov[46], C. Grieco[14], N.A. Grieser[128],
A.A. Grillo[145], K. Grimm[31,l], S. Grinstein[14,w], J.-F. Grivaz[65], S. Groh[100], E. Gross[180],
J. Grosse-Knetter[53], Z.J. Grout[95], C. Grud[106], A. Grummer[118], J.C. Grundy[134], L. Guan[106],
W. Guan[181], C. Gubbels[175], J. Guenther[77], A. Guerguichon[65], J.G.R. Guerrero Rojas[174],
F. Guescini[115], D. Guest[77], R. Gugel[100], A. Guida[46], T. Guillemin[5], S. Guindon[36], J. Guo[60c],
W. Guo[106], Y. Guo[60a], Z. Guo[102], R. Gupta[46], S. Gurbuz[12c], G. Gustavino[128], M. Guth[52],
P. Gutierrez[128], C. Gutschow[95], C. Guyot[144], C. Gwenlan[134], C.B. Gwilliam[91], E.S. Haaland[133],
A. Haas[125], C. Haber[18], H.K. Hadavand[8], A. Hadef[100], M. Haleem[177], J. Haley[129], J.J. Hall[149],
G. Halladjian[107], G.D. Hallewell[102], K. Hamano[176], H. Hamdaoui[35f], M. Hamer[24],
G.N. Hamity[50], K. Han[60a], L. Han[15c], L. Han[60a], S. Han[18], Y.F. Han[167], K. Hanagaki[82,u],
M. Hance[145], D.M. Handl[114], M.D. Hank[37], R. Hankache[135], E. Hansen[97], J.B. Hansen[40],
J.D. Hansen[40], M.C. Hansen[24], P.H. Hansen[40], E.C. Hanson[101], K. Hara[169], T. Harenberg[182],
S. Harkusha[108], P.F. Harrison[178], N.M. Hartman[153], N.M. Hartmann[114], Y. Hasegawa[150],
A. Hasib[50], S. Hassani[144], S. Haug[20], R. Hauser[107], M. Havranek[141], C.M. Hawkes[21],

R.J. Hawkings[36], S. Hayashida[117], D. Hayden[107], C. Hayes[106], R.L. Hayes[175], C.P. Hays[134],
J.M. Hays[93], H.S. Hayward[91], S.J. Haywood[143], F. He[60a], Y. He[165], M.P. Heath[50], V. Hedberg[97],
A.L. Heggelund[133], N.D. Hehir[93], C. Heidegger[52], K.K. Heidegger[52], W.D. Heidorn[79],
J. Heilman[34], S. Heim[46], T. Heim[18], B. Heinemann[46,ai], J.G. Heinlein[136], J.J. Heinrich[131],
L. Heinrich[36], J. Hejbal[140], L. Helary[46], A. Held[125], S. Hellesund[133], C.M. Helling[145],
S. Hellman[45a,45b], C. Helsens[36], R.C.W. Henderson[90], L. Henkelmann[32],
A.M. Henriques Correia[36], H. Herde[26], Y. Hernández Jiménez[33e], H. Herr[100], M.G. Herrmann[114],
T. Herrmann[48], G. Herten[52], R. Hertenberger[114], L. Hervas[36], G.G. Hesketh[95], N.P. Hessey[168a],
H. Hibi[83], S. Higashino[82], E. Higón-Rodriguez[174], K. Hildebrand[37], J.C. Hill[32], K.K. Hill[29],
K.H. Hiller[46], S.J. Hillier[21], M. Hils[48], I. Hinchliffe[18], F. Hinterkeuser[24], M. Hirose[132],
S. Hirose[169], D. Hirschbuehl[182], B. Hiti[92], O. Hladik[140], J. Hobbs[155], R. Hobincu[27e], N. Hod[180],
M.C. Hodgkinson[149], A. Hoecker[36], D. Hohn[52], D. Hohov[65], T. Holm[24], T.R. Holmes[37],
M. Holzbock[115], L.B.A.H. Hommels[32], T.M. Hong[138], J.C. Honig[52], A. Hönle[115],
B.H. Hooberman[173], W.H. Hopkins[6], Y. Horii[117], P. Horn[48], L.A. Horyn[37], S. Hou[158],
A. Hoummada[35a], J. Howarth[57], J. Hoya[89], M. Hrabovsky[130], J. Hrivnac[65], A. Hrynevich[109],
T. Hryn'ova[5], P.J. Hsu[64], S.-C. Hsu[148], Q. Hu[39], S. Hu[60c], Y.F. Hu[15a,15d,am], D.P. Huang[95],
X. Huang[15c], Y. Huang[60a], Y. Huang[15a], Z. Hubacek[141], F. Hubaut[102], M. Huebner[24],
F. Huegging[24], T.B. Huffman[134], M. Huhtinen[36], R. Hulsken[58], R.F.H. Hunter[34],
N. Huseynov[80,ab], J. Huston[107], J. Huth[59], R. Hyneman[153], S. Hyrych[28a], G. Iacobucci[54],
G. Iakovidis[29], I. Ibragimov[151], L. Iconomidou-Fayard[65], P. Iengo[36], R. Ignazzi[40], R. Iguchi[163],
T. Iizawa[54], Y. Ikegami[82], M. Ikeno[82], N. Ilic[119,167,aa], F. Iltzsche[48], H. Imam[35a],
G. Introzzi[71a,71b], M. Iodice[75a], K. Iordanidou[168a], V. Ippolito[73a,73b], M.F. Isacson[172],
M. Ishino[163], W. Islam[129], C. Issever[19,46], S. Istin[160], J.M. Iturbe Ponce[63a], R. Iuppa[76a,76b],
A. Ivina[180], J.M. Izen[43], V. Izzo[70a], P. Jacka[140], P. Jackson[1], R.M. Jacobs[46], B.P. Jaeger[152],
V. Jain[2], G. Jäkel[182], K.B. Jakobi[100], K. Jakobs[52], T. Jakoubek[180], J. Jamieson[57],
K.W. Janas[84a], R. Jansky[54], M. Janus[53], P.A. Janus[84a], G. Jarlskog[97], A.E. Jaspan[91],
N. Javadov[80,ab], T. Javůrek[36], M. Javurkova[103], F. Jeanneau[144], L. Jeanty[131], J. Jejelava[159a],
P. Jenni[52,d], N. Jeong[46], S. Jézéquel[5], J. Jia[155], Z. Jia[15c], H. Jiang[79], Y. Jiang[60a], Z. Jiang[153],
S. Jiggins[52], F.A. Jimenez Morales[38], J. Jimenez Pena[115], S. Jin[15c], A. Jinaru[27b],
O. Jinnouchi[165], H. Jivan[33e], P. Johansson[149], K.A. Johns[7], C.A. Johnson[66], E. Jones[178],
R.W.L. Jones[90], S.D. Jones[156], T.J. Jones[91], J. Jovicevic[36], X. Ju[18], J.J. Junggeburth[115],
A. Juste Rozas[14,w], A. Kaczmarska[85], M. Kado[73a,73b], H. Kagan[127], M. Kagan[153], A. Kahn[39],
C. Kahra[100], T. Kaji[179], E. Kajomovitz[160], C.W. Kalderon[29], A. Kaluza[100],
A. Kamenshchikov[123], M. Kaneda[163], N.J. Kang[145], S. Kang[79], Y. Kano[117], J. Kanzaki[82],
L.S. Kaplan[181], D. Kar[33e], K. Karava[134], M.J. Kareem[168b], I. Karkanias[162], S.N. Karpov[80],
Z.M. Karpova[80], V. Kartvelishvili[90], A.N. Karyukhin[123], E. Kasimi[162], A. Kastanas[45a,45b],
C. Kato[60d], J. Katzy[46], K. Kawade[150], K. Kawagoe[88], T. Kawaguchi[117], T. Kawamoto[144],
G. Kawamura[53], E.F. Kay[176], F.I. Kaya[170], S. Kazakos[14], V.F. Kazanin[122b,122a],
J.M. Keaveney[33a], R. Keeler[176], J.S. Keller[34], E. Kellermann[97], D. Kelsey[156], J.J. Kempster[21],
J. Kendrick[21], K.E. Kennedy[39], O. Kepka[140], S. Kersten[182], B.P. Kerševan[92],
S. Ketabchi Haghighat[167], F. Khalil-Zada[13], M. Khandoga[144], A. Khanov[129],
A.G. Kharlamov[122b,122a], T. Kharlamova[122b,122a], E.E. Khoda[175], T.J. Khoo[77], G. Khoriauli[177],
E. Khramov[80], J. Khubua[159b], S. Kido[83], M. Kiehn[36], E. Kim[165], Y.K. Kim[37], N. Kimura[95],
A. Kirchhoff[53], D. Kirchmeier[48], J. Kirk[143], A.E. Kiryunin[115], T. Kishimoto[163], D.P. Kisliuk[167],
V. Kitali[46], C. Kitsaki[10], O. Kivernyk[24], T. Klapdor-Kleingrothaus[52], M. Klassen[61a], C. Klein[34],
M.H. Klein[106], M. Klein[91], U. Klein[91], K. Kleinknecht[100], P. Klimek[36], A. Klimentov[29],
F. Klimpel[36], T. Klingl[24], T. Klioutchnikova[36], F.F. Klitzner[114], P. Kluit[120], S. Kluth[115],
E. Kneringer[77], E.B.F.G. Knoops[102], A. Knue[52], D. Kobayashi[88], M. Kobel[48], M. Kocian[153],

T. Kodama[163], P. Kodys[142], D.M. Koeck[156], P.T. Koenig[24], T. Koffas[34], N.M. Köhler[36],
M. Kolb[144], I. Koletsou[5], T. Komarek[130], T. Kondo[82], K. Köneke[52], A.X.Y. Kong[1],
A.C. König[119], T. Kono[126], V. Konstantinides[95], N. Konstantinidis[95], B. Konya[97],
R. Kopeliansky[66], S. Koperny[84a], K. Korcyl[85], K. Kordas[162], G. Koren[161], A. Korn[95],
I. Korolkov[14], E.V. Korolkova[149], N. Korotkova[113], O. Kortner[115], S. Kortner[115],
V.V. Kostyukhin[149,166], A. Kotsokechagia[65], A. Kotwal[49], A. Koulouris[10],
A. Kourkoumeli-Charalampidi[71a,71b], C. Kourkoumelis[9], E. Kourlitis[6], V. Kouskoura[29],
R. Kowalewski[176], W. Kozanecki[101], A.S. Kozhin[123], V.A. Kramarenko[113], G. Kramberger[92],
D. Krasnopevtsev[60a], M.W. Krasny[135], A. Krasznahorkay[36], D. Krauss[115], J.A. Kremer[100],
J. Kretzschmar[91], K. Kreul[19], P. Krieger[167], F. Krieter[114], S. Krishnamurthy[103], A. Krishnan[61b],
M. Krivos[142], K. Krizka[18], K. Kroeninger[47], H. Kroha[115], J. Kroll[140], J. Kroll[136],
K.S. Krowpman[107], U. Kruchonak[80], H. Krüger[24], N. Krumnack[79], M.C. Kruse[49],
J.A. Krzysiak[85], A. Kubota[165], O. Kuchinskaia[166], S. Kuday[4b], D. Kuechler[46], J.T. Kuechler[46],
S. Kuehn[36], T. Kuhl[46], V. Kukhtin[80], Y. Kulchitsky[108,ae], S. Kuleshov[146b], Y.P. Kulinich[173],
M. Kuna[58], A. Kupco[140], T. Kupfer[47], O. Kuprash[52], H. Kurashige[83], L.L. Kurchaninov[168a],
Y.A. Kurochkin[108], A. Kurova[112], M.G. Kurth[15a,15d], E.S. Kuwertz[36], M. Kuze[165],
A.K. Kvam[148], J. Kvita[130], T. Kwan[104], C. Lacasta[174], F. Lacava[73a,73b], D.P.J. Lack[101],
H. Lacker[19], D. Lacour[135], E. Ladygin[80], R. Lafaye[5], B. Laforge[135], T. Lagouri[146c], S. Lai[53],
I.K. Lakomiec[84a], J.E. Lambert[128], S. Lammers[66], W. Lampl[7], C. Lampoudis[162], E. Lançon[29],
U. Landgraf[52], M.P.J. Landon[93], V.S. Lang[52], J.C. Lange[53], R.J. Langenberg[103],
A.J. Lankford[171], F. Lanni[29], K. Lantzsch[24], A. Lanza[71a], A. Lapertosa[55b,55a], J.F. Laporte[144],
T. Lari[69a], F. Lasagni Manghi[23b,23a], M. Lassnig[36], V. Latonova[140], T.S. Lau[63a], A. Laudrain[100],
A. Laurier[34], M. Lavorgna[70a,70b], S.D. Lawlor[94], M. Lazzaroni[69a,69b], B. Le[101],
E. Le Guirriec[102], A. Lebedev[79], M. LeBlanc[7], T. LeCompte[6], F. Ledroit-Guillon[58],
A.C.A. Lee[95], C.A. Lee[29], G.R. Lee[17], L. Lee[59], S.C. Lee[158], S. Lee[79], B. Lefebvre[168a],
H.P. Lefebvre[94], M. Lefebvre[176], C. Leggett[18], K. Lehmann[152], N. Lehmann[20],
G. Lehmann Miotto[36], W.A. Leight[46], A. Leisos[162,v], M.A.L. Leite[81c], C.E. Leitgeb[114],
R. Leitner[142], K.J.C. Leney[42], T. Lenz[24], S. Leone[72a], C. Leonidopoulos[50], A. Leopold[135],
C. Leroy[110], R. Les[107], C.G. Lester[32], M. Levchenko[137], J. Levêque[5], D. Levin[106],
L.J. Levinson[180], D.J. Lewis[21], B. Li[15b], B. Li[106], C-Q. Li[60c,60d], F. Li[60c], H. Li[60a], H. Li[60b],
J. Li[60c], K. Li[148], L. Li[60c], M. Li[15a,15d], Q.Y. Li[60a], S. Li[60d,60c,b], X. Li[46], Y. Li[46], Z. Li[60b],
Z. Li[134], Z. Li[104], Z. Li[91], Z. Liang[15a], M. Liberatore[46], B. Liberti[74a], K. Lie[63c], S. Lim[29],
C.Y. Lin[32], K. Lin[107], R.A. Linck[66], R.E. Lindley[7], J.H. Lindon[21], A. Linss[46], A.L. Lionti[54],
E. Lipeles[136], A. Lipniacka[17], T.M. Liss[173,aj], A. Lister[175], J.D. Little[8], B. Liu[79], B.X. Liu[152],
H.B. Liu[29], J.B. Liu[60a], J.K.K. Liu[37], K. Liu[60d,60c], M. Liu[60a], M.Y. Liu[60a], P. Liu[15a], X. Liu[60a],
Y. Liu[46], Y. Liu[15a,15d], Y.L. Liu[106], Y.W. Liu[60a], M. Livan[71a,71b], A. Lleres[58],
J. Llorente Merino[152], S.L. Lloyd[93], C.Y. Lo[63b], E.M. Lobodzinska[46], P. Loch[7],
S. Loffredo[74a,74b], T. Lohse[19], K. Lohwasser[149], M. Lokajicek[140], J.D. Long[173], R.E. Long[90],
I. Longarini[73a,73b], L. Longo[36], I. Lopez Paz[101], A. Lopez Solis[149], J. Lorenz[114],
N. Lorenzo Martinez[5], A.M. Lory[114], A. Lösle[52], X. Lou[45a,45b], X. Lou[15a], A. Lounis[65], J. Love[6],
P.A. Love[90], J.J. Lozano Bahilo[174], M. Lu[60a], Y.J. Lu[64], H.J. Lubatti[148], C. Luci[73a,73b],
F.L. Lucio Alves[15c], A. Lucotte[58], F. Luehring[66], I. Luise[155], L. Luminari[73a], B. Lund-Jensen[154],
N.A. Luongo[131], M.S. Lutz[161], D. Lynn[29], H. Lyons[91], R. Lysak[140], E. Lytken[97], F. Lyu[15a],
V. Lyubushkin[80], T. Lyubushkina[80], H. Ma[29], L.L. Ma[60b], Y. Ma[95], D.M. Mac Donell[176],
G. Maccarrone[51], C.M. Macdonald[149], J.C. MacDonald[149], J. Machado Miguens[136], R. Madar[38],
W.F. Mader[48], M. Madugoda Ralalage Don[129], N. Madysa[48], J. Maeda[83], T. Maeno[29],
M. Maerker[48], V. Magerl[52], N. Magini[79], J. Magro[67a,67c,r], D.J. Mahon[39], C. Maidantchik[81b],
A. Maio[139a,139b,139d], K. Maj[84a], O. Majersky[28a], S. Majewski[131], Y. Makida[82], N. Makovec[65],

B. Malaescu[135], Pa. Malecki[85], V.P. Maleev[137], F. Malek[58], D. Malito[41b,41a], U. Mallik[78],
C. Malone[32], S. Maltezos[10], S. Malyukov[80], J. Mamuzic[174], G. Mancini[51], J.P. Mandalia[93],
I. Mandić[92], L. Manhaes de Andrade Filho[81a], I.M. Maniatis[162], J. Manjarres Ramos[48],
K.H. Mankinen[97], A. Mann[114], A. Manousos[77], B. Mansoulie[144], I. Manthos[162], S. Manzoni[120],
A. Marantis[162], G. Marceca[30], L. Marchese[134], G. Marchiori[135], M. Marcisovsky[140],
L. Marcoccia[74a,74b], C. Marcon[97], M. Marjanovic[128], Z. Marshall[18], M.U.F. Martensson[172],
S. Marti-Garcia[174], C.B. Martin[127], T.A. Martin[178], V.J. Martin[50], B. Martin dit Latour[17],
L. Martinelli[75a,75b], M. Martinez[14,w], P. Martinez Agullo[174], V.I. Martinez Outschoorn[103],
S. Martin-Haugh[143], V.S. Martoiu[27b], A.C. Martyniuk[95], A. Marzin[36], S.R. Maschek[115],
L. Masetti[100], T. Mashimo[163], R. Mashinistov[111], J. Masik[101], A.L. Maslennikov[122b,122a],
L. Massa[23b,23a], P. Massarotti[70a,70b], P. Mastrandrea[72a,72b], A. Mastroberardino[41b,41a],
T. Masubuchi[163], D. Matakias[29], A. Matic[114], N. Matsuzawa[163], P. Mättig[24], J. Maurer[27b],
B. Maček[92], D.A. Maximov[122b,122a], R. Mazini[158], I. Maznas[162], S.M. Mazza[145],
J.P. Mc Gowan[104], S.P. Mc Kee[106], T.G. McCarthy[115], W.P. McCormack[18], E.F. McDonald[105],
A.E. McDougall[120], J.A. Mcfayden[18], G. Mchedlidze[159b], M.A. McKay[42], K.D. McLean[176],
S.J. McMahon[143], P.C. McNamara[105], C.J. McNicol[178], R.A. McPherson[176,aa], J.E. Mdhluli[33e],
Z.A. Meadows[103], S. Meehan[36], T. Megy[38], S. Mehlhase[114], A. Mehta[91], B. Meirose[43],
D. Melini[160], B.R. Mellado Garcia[33e], J.D. Mellenthin[53], M. Melo[28a], F. Meloni[46], A. Melzer[24],
E.D. Mendes Gouveia[139a,139e], A.M. Mendes Jacques Da Costa[21], H.Y. Meng[167], L. Meng[36],
X.T. Meng[106], S. Menke[115], E. Meoni[41b,41a], S. Mergelmeyer[19], S.A.M. Merkt[138],
C. Merlassino[134], P. Mermod[54], L. Merola[70a,70b], C. Meroni[69a], G. Merz[106], O. Meshkov[113,111],
J.K.R. Meshreki[151], J. Metcalfe[6], A.S. Mete[6], C. Meyer[66], J-P. Meyer[144], M. Michetti[19],
R.P. Middleton[143], L. Mijović[50], G. Mikenberg[180], M. Mikestikova[140], M. Mikuž[92],
H. Mildner[149], A. Milic[167], C.D. Milke[42], D.W. Miller[37], L.S. Miller[34], A. Milov[180],
D.A. Milstead[45a,45b], A.A. Minaenko[123], I.A. Minashvili[159b], L. Mince[57], A.I. Mincer[125],
B. Mindur[84a], M. Mineev[80], Y. Minegishi[163], Y. Mino[86], L.M. Mir[14], M. Mironova[134],
T. Mitani[179], J. Mitrevski[114], V.A. Mitsou[174], M. Mittal[60c], O. Miu[167], A. Miucci[20],
P.S. Miyagawa[93], A. Mizukami[82], J.U. Mjörnmark[97], T. Mkrtchyan[61a], M. Mlynarikova[121],
T. Moa[45a,45b], S. Mobius[53], K. Mochizuki[110], P. Moder[46], P. Mogg[114], S. Mohapatra[39],
R. Moles-Valls[24], K. Mönig[46], E. Monnier[102], A. Montalbano[152], J. Montejo Berlingen[36],
M. Montella[95], F. Monticelli[89], S. Monzani[69a], N. Morange[65], A.L. Moreira De Carvalho[139a],
D. Moreno[22a], M. Moreno Llácer[174], C. Moreno Martinez[14], P. Morettini[55b], M. Morgenstern[160],
S. Morgenstern[48], D. Mori[152], M. Morii[59], M. Morinaga[179], V. Morisbak[133], A.K. Morley[36],
G. Mornacchi[36], A.P. Morris[95], L. Morvaj[36], P. Moschovakos[36], B. Moser[120], M. Mosidze[159b],
T. Moskalets[144], P. Moskvitina[119], J. Moss[31,n], E.J.W. Moyse[103], S. Muanza[102], J. Mueller[138],
R.S.P. Mueller[114], D. Muenstermann[90], G.A. Mullier[97], D.P. Mungo[69a,69b],
J.L. Munoz Martinez[14], F.J. Munoz Sanchez[101], P. Murin[28b], W.J. Murray[178,143],
A. Murrone[69a,69b], J.M. Muse[128], M. Muškinja[18], C. Mwewa[33a], A.G. Myagkov[123,af],
A.A. Myers[138], G. Myers[66], J. Myers[131], M. Myska[141], B.P. Nachman[18], O. Nackenhorst[47],
A.Nag Nag[48], K. Nagai[134], K. Nagano[82], Y. Nagasaka[62], J.L. Nagle[29], E. Nagy[102], A.M. Nairz[36],
Y. Nakahama[117], K. Nakamura[82], T. Nakamura[163], H. Nanjo[132], F. Napolitano[61a],
R.F. Naranjo Garcia[46], R. Narayan[42], I. Naryshkin[137], M. Naseri[34], T. Naumann[46],
G. Navarro[22a], P.Y. Nechaeva[111], F. Nechansky[46], T.J. Neep[21], A. Negri[71a,71b], M. Negrini[23b],
C. Nellist[119], C. Nelson[104], M.E. Nelson[45a,45b], S. Nemecek[140], M. Nessi[36,f], M.S. Neubauer[173],
F. Neuhaus[100], M. Neumann[182], R. Newhouse[175], P.R. Newman[21], C.W. Ng[138], Y.S. Ng[19],
Y.W.Y. Ng[171], B. Ngair[35f], H.D.N. Nguyen[102], T. Nguyen Manh[110], E. Nibigira[38],
R.B. Nickerson[134], R. Nicolaidou[144], D.S. Nielsen[40], J. Nielsen[145], M. Niemeyer[53],
N. Nikiforou[11], V. Nikolaenko[123,af], I. Nikolic-Audit[135], K. Nikolopoulos[21], P. Nilsson[29],

H.R. Nindhito[54], A. Nisati[73a], N. Nishu[60c], R. Nisius[115], I. Nitsche[47], T. Nitta[179], T. Nobe[163],
D.L. Noel[32], Y. Noguchi[86], I. Nomidis[135], M.A. Nomura[29], M. Nordberg[36], J. Novak[92],
T. Novak[92], O. Novgorodova[48], R. Novotny[118], L. Nozka[130], K. Ntekas[171], E. Nurse[95],
F.G. Oakham[34,ak], J. Ocariz[135], A. Ochi[83], I. Ochoa[139a], J.P. Ochoa-Ricoux[146a], K. O'Connor[26],
S. Oda[88], S. Odaka[82], S. Oerdek[53], A. Ogrodnik[84a], A. Oh[101], C.C. Ohm[154], H. Oide[165],
R. Oishi[163], M.L. Ojeda[167], H. Okawa[169], Y. Okazaki[86], M.W. O'Keefe[91], Y. Okumura[163],
A. Olariu[27b], L.F. Oleiro Seabra[139a], S.A. Olivares Pino[146a], D. Oliveira Damazio[29], J.L. Oliver[1],
M.J.R. Olsson[171], A. Olszewski[85], J. Olszowska[85], Ö.O. Öncel[24], D.C. O'Neil[152], A.P. O'neill[134],
A. Onofre[139a,139e], P.U.E. Onyisi[11], H. Oppen[133], R.G. Oreamuno Madriz[121], M.J. Oreglia[37],
G.E. Orellana[89], D. Orestano[75a,75b], N. Orlando[14], R.S. Orr[167], V. O'Shea[57], R. Ospanov[60a],
G. Otero y Garzon[30], H. Otono[88], P.S. Ott[61a], G.J. Ottino[18], M. Ouchrif[35e], J. Ouellette[29],
F. Ould-Saada[133], A. Ouraou[144,*], Q. Ouyang[15a], M. Owen[57], R.E. Owen[143], V.E. Ozcan[12c],
N. Ozturk[8], J. Pacalt[130], H.A. Pacey[32], K. Pachal[49], A. Pacheco Pages[14], C. Padilla Aranda[14],
S. Pagan Griso[18], G. Palacino[66], S. Palazzo[50], S. Palestini[36], M. Palka[84b], P. Palni[84a],
C.E. Pandini[54], J.G. Panduro Vazquez[94], P. Pani[46], G. Panizzo[67a,67c], L. Paolozzi[54],
C. Papadatos[110], K. Papageorgiou[9,h], S. Parajuli[42], A. Paramonov[6], C. Paraskevopoulos[10],
D. Paredes Hernandez[63b], S.R. Paredes Saenz[134], B. Parida[180], T.H. Park[167], A.J. Parker[31],
M.A. Parker[32], F. Parodi[55b,55a], E.W. Parrish[121], J.A. Parsons[39], U. Parzefall[52],
L. Pascual Dominguez[135], V.R. Pascuzzi[18], J.M.P. Pasner[145], F. Pasquali[120], E. Pasqualucci[73a],
S. Passaggio[55b], F. Pastore[94], P. Pasuwan[45a,45b], S. Pataraia[100], J.R. Pater[101], A. Pathak[181,j],
J. Patton[91], T. Pauly[36], J. Pearkes[153], M. Pedersen[133], L. Pedraza Diaz[119], R. Pedro[139a],
T. Peiffer[53], S.V. Peleganchuk[122b,122a], O. Penc[140], C. Peng[63b], H. Peng[60a], B.S. Peralva[81a],
M.M. Perego[65], A.P. Pereira Peixoto[139a], L. Pereira Sanchez[45a,45b], D.V. Perepelitsa[29],
E. Perez Codina[168a], L. Perini[69a,69b], H. Pernegger[36], S. Perrella[36], A. Perrevoort[120],
K. Peters[46], R.F.Y. Peters[101], B.A. Petersen[36], T.C. Petersen[40], E. Petit[102], V. Petousis[141],
C. Petridou[162], F. Petrucci[75a,75b], M. Pettee[183], N.E. Pettersson[103], K. Petukhova[142],
A. Peyaud[144], R. Pezoa[146d], L. Pezzotti[71a,71b], T. Pham[105], P.W. Phillips[143], M.W. Phipps[173],
G. Piacquadio[155], E. Pianori[18], A. Picazio[103], R.H. Pickles[101], R. Piegaia[30], D. Pietreanu[27b],
J.E. Pilcher[37], A.D. Pilkington[101], M. Pinamonti[67a,67c], J.L. Pinfold[3], C. Pitman Donaldson[95],
M. Pitt[161], L. Pizzimento[74a,74b], A. Pizzini[120], M.-A. Pleier[29], V. Plesanovs[52], V. Pleskot[142],
E. Plotnikova[80], P. Podberezko[122b,122a], R. Poettgen[97], R. Poggi[54], L. Poggioli[135],
I. Pogrebnyak[107], D. Pohl[24], I. Pokharel[53], G. Polesello[71a], A. Poley[152,168a], A. Policicchio[73a,73b],
R. Polifka[142], A. Polini[23b], C.S. Pollard[46], V. Polychronakos[29], D. Ponomarenko[112],
L. Pontecorvo[36], S. Popa[27a], G.A. Popeneciu[27d], L. Portales[5], D.M. Portillo Quintero[58],
S. Pospisil[141], K. Potamianos[46], I.N. Potrap[80], C.J. Potter[32], H. Potti[11], T. Poulsen[97],
J. Poveda[174], T.D. Powell[149], G. Pownall[46], M.E. Pozo Astigarraga[36], A. Prades Ibanez[174],
P. Pralavorio[102], M.M. Prapa[44], S. Prell[79], D. Price[101], M. Primavera[68a], M.L. Proffitt[148],
N. Proklova[112], K. Prokofiev[63c], F. Prokoshin[80], S. Protopopescu[29], J. Proudfoot[6],
M. Przybycien[84a], D. Pudzha[137], A. Puri[173], P. Puzo[65], D. Pyatiizbyantseva[112], J. Qian[106],
Y. Qin[101], A. Quadt[53], M. Queitsch-Maitland[36], G. Rabanal Bolanos[59], M. Racko[28a],
F. Ragusa[69a,69b], G. Rahal[98], J.A. Raine[54], S. Rajagopalan[29], A. Ramirez Morales[93],
K. Ran[15a,15d], D.F. Rassloff[61a], D.M. Rauch[46], F. Rauscher[114], S. Rave[100], B. Ravina[57],
I. Ravinovich[180], J.H. Rawling[101], M. Raymond[36], A.L. Read[133], N.P. Readioff[149],
M. Reale[68a,68b], D.M. Rebuzzi[71a,71b], G. Redlinger[29], K. Reeves[43], D. Reikher[161], A. Reiss[100],
A. Rej[151], C. Rembser[36], A. Renardi[46], M. Renda[27b], M.B. Rendel[115], A.G. Rennie[57],
S. Resconi[69a], E.D. Resseguie[18], S. Rettie[95], B. Reynolds[127], E. Reynolds[21],
O.L. Rezanova[122b,122a], P. Reznicek[142], E. Ricci[76a,76b], R. Richter[115], S. Richter[46],
E. Richter-Was[84b], M. Ridel[135], P. Rieck[115], O. Rifki[46], M. Rijssenbeek[155], A. Rimoldi[71a,71b],

M. Rimoldi[46], L. Rinaldi[23b], T.T. Rinn[173], G. Ripellino[154], I. Riu[14], P. Rivadeneira[46],
J.C. Rivera Vergara[176], F. Rizatdinova[129], E. Rizvi[93], C. Rizzi[36], S.H. Robertson[104,aa],
M. Robin[46], D. Robinson[32], C.M. Robles Gajardo[146d], M. Robles Manzano[100], A. Robson[57],
A. Rocchi[74a,74b], C. Roda[72a,72b], S. Rodriguez Bosca[174], A. Rodriguez Rodriguez[52],
A.M. Rodríguez Vera[168b], S. Roe[36], J. Roggel[182], O. Røhne[133], R. Röhrig[115], R.A. Rojas[146d],
B. Roland[52], C.P.A. Roland[66], J. Roloff[29], A. Romaniouk[112], M. Romano[23b,23a], N. Rompotis[91],
M. Ronzani[125], L. Roos[135], S. Rosati[73a], G. Rosin[103], B.J. Rosser[136], E. Rossi[46], E. Rossi[75a,75b],
E. Rossi[70a,70b], L.P. Rossi[55b], L. Rossini[46], R. Rosten[14], M. Rotaru[27b], B. Rottler[52],
D. Rousseau[65], G. Rovelli[71a,71b], A. Roy[11], D. Roy[33e], A. Rozanov[102], Y. Rozen[160], X. Ruan[33e],
T.A. Ruggeri[1], F. Rühr[52], A. Ruiz-Martinez[174], A. Rummler[36], Z. Rurikova[52],
N.A. Rusakovich[80], H.L. Russell[104], L. Rustige[38,47], J.P. Rutherfoord[7], E.M. Rüttinger[149],
M. Rybar[142], G. Rybkin[65], E.B. Rye[133], A. Ryzhov[123], J.A. Sabater Iglesias[46], P. Sabatini[174],
L. Sabetta[73a,73b], S. Sacerdoti[65], H.F-W. Sadrozinski[145], R. Sadykov[80], F. Safai Tehrani[73a],
B. Safarzadeh Samani[156], M. Safdari[153], P. Saha[121], S. Saha[104], M. Sahinsoy[115], A. Sahu[182],
M. Saimpert[36], M. Saito[163], T. Saito[163], H. Sakamoto[163], D. Salamani[54], G. Salamanna[75a,75b],
A. Salnikov[153], J. Salt[174], A. Salvador Salas[14], D. Salvatore[41b,41a], F. Salvatore[156],
A. Salvucci[63a], A. Salzburger[36], J. Samarati[36], D. Sammel[52], D. Sampsonidis[162],
D. Sampsonidou[60d,60c], J. Sánchez[174], A. Sanchez Pineda[67a,36,67c], H. Sandaker[133],
C.O. Sander[46], I.G. Sanderswood[90], M. Sandhoff[182], C. Sandoval[22b], D.P.C. Sankey[143],
M. Sannino[55b,55a], Y. Sano[117], A. Sansoni[51], C. Santoni[38], H. Santos[139a,139b], S.N. Santpur[18],
A. Santra[174], K.A. Saoucha[149], A. Sapronov[80], J.G. Saraiva[139a,139d], O. Sasaki[82], K. Sato[169],
F. Sauerburger[52], E. Sauvan[5], P. Savard[167,ak], R. Sawada[163], C. Sawyer[143], L. Sawyer[96],
I. Sayago Galvan[174], C. Sbarra[23b], A. Sbrizzi[67a,67c], T. Scanlon[95], J. Schaarschmidt[148],
P. Schacht[115], D. Schaefer[37], L. Schaefer[136], U. Schäfer[100], A.C. Schaffer[65], D. Schaile[114],
R.D. Schamberger[155], E. Schanet[114], C. Scharf[19], N. Scharmberg[101], V.A. Schegelsky[137],
D. Scheirich[142], F. Schenck[19], M. Schernau[171], C. Schiavi[55b,55a], L.K. Schildgen[24],
Z.M. Schillaci[26], E.J. Schioppa[68a,68b], M. Schioppa[41b,41a], K.E. Schleicher[52], S. Schlenker[36],
K.R. Schmidt-Sommerfeld[115], K. Schmieden[100], C. Schmitt[100], S. Schmitt[46], L. Schoeffel[144],
A. Schoening[61b], P.G. Scholer[52], E. Schopf[134], M. Schott[100], J.F.P. Schouwenberg[119],
J. Schovancova[36], S. Schramm[54], F. Schroeder[182], A. Schulte[100], H-C. Schultz-Coulon[61a],
M. Schumacher[52], B.A. Schumm[145], Ph. Schune[144], A. Schwartzman[153], T.A. Schwarz[106],
Ph. Schwemling[144], R. Schwienhorst[107], A. Sciandra[145], G. Sciolla[26], F. Scuri[72a], F. Scutti[105],
L.M. Scyboz[115], C.D. Sebastiani[91], K. Sedlaczek[47], P. Seema[19], S.C. Seidel[118], A. Seiden[145],
B.D. Seidlitz[29], T. Seiss[37], C. Seitz[46], J.M. Seixas[81b], G. Sekhniaidze[70a], S.J. Sekula[42],
N. Semprini-Cesari[23b,23a], S. Sen[49], C. Serfon[29], L. Serin[65], L. Serkin[67a,67b], M. Sessa[60a],
H. Severini[128], S. Sevova[153], F. Sforza[55b,55a], A. Sfyrla[54], E. Shabalina[53], J.D. Shahinian[136],
N.W. Shaikh[45a,45b], D. Shaked Renous[180], L.Y. Shan[15a], M. Shapiro[18], A. Sharma[36],
A.S. Sharma[1], P.B. Shatalov[124], K. Shaw[156], S.M. Shaw[101], M. Shehade[180], Y. Shen[128],
A.D. Sherman[25], P. Sherwood[95], L. Shi[95], C.O. Shimmin[183], Y. Shimogama[179],
M. Shimojima[116], J.D. Shinner[94], I.P.J. Shipsey[134], S. Shirabe[165], M. Shiyakova[80,y],
J. Shlomi[180], A. Shmeleva[111], M.J. Shochet[37], J. Shojaii[105], D.R. Shope[154], S. Shrestha[127],
E.M. Shrif[33e], M.J. Shroff[176], E. Shulga[180], P. Sicho[140], A.M. Sickles[173], E. Sideras Haddad[33e],
O. Sidiropoulou[36], A. Sidoti[23b,23a], F. Siegert[48], Dj. Sijacki[16], M.Jr. Silva[181],
M.V. Silva Oliveira[36], S.B. Silverstein[45a], S. Simion[65], R. Simoniello[100], C.J. Simpson-allsop[21],
S. Simsek[12b], P. Sinervo[167], V. Sinetckii[113], S. Singh[152], S. Sinha[33e], M. Sioli[23b,23a], I. Siral[131],
S.Yu. Sivoklokov[113], J. Sjölin[45a,45b], A. Skaf[53], E. Skorda[97], P. Skubic[128], M. Slawinska[85],
K. Sliwa[170], V. Smakhtin[180], B.H. Smart[143], J. Smiesko[28b], N. Smirnov[112], S.Yu. Smirnov[112],
Y. Smirnov[112], L.N. Smirnova[113,s], O. Smirnova[97], E.A. Smith[37], H.A. Smith[134], M. Smizanska[90],

K. Smolek[141], A. Smykiewicz[85], A.A. Snesarev[111], H.L. Snoek[120], I.M. Snyder[131], S. Snyder[29],
R. Sobie[176,aa], A. Soffer[161], A. Søgaard[50], F. Sohns[53], C.A. Solans Sanchez[36], E.Yu. Soldatov[112],
U. Soldevila[174], A.A. Solodkov[123], A. Soloshenko[80], O.V. Solovyanov[123], V. Solovyev[137],
P. Sommer[149], H. Son[170], A. Sonay[14], W. Song[143], W.Y. Song[168b], A. Sopczak[141], A.L. Sopio[95],
F. Sopkova[28b], S. Sottocornola[71a,71b], R. Soualah[67a,67c], A.M. Soukharev[122b,122a], D. South[46],
S. Spagnolo[68a,68b], M. Spalla[115], M. Spangenberg[178], F. Spanò[94], D. Sperlich[52], T.M. Spieker[61a],
G. Spigo[36], M. Spina[156], D.P. Spiteri[57], M. Spousta[142], A. Stabile[69a,69b], B.L. Stamas[121],
R. Stamen[61a], M. Stamenkovic[120], A. Stampekis[21], E. Stanecka[85], B. Stanislaus[134],
M.M. Stanitzki[46], M. Stankaityte[134], B. Stapf[120], E.A. Starchenko[123], G.H. Stark[145], J. Stark[58],
P. Staroba[140], P. Starovoitov[61a], S. Stärz[104], R. Staszewski[85], G. Stavropoulos[44], M. Stegler[46],
P. Steinberg[29], A.L. Steinhebel[131], B. Stelzer[152,168a], H.J. Stelzer[138], O. Stelzer-Chilton[168a],
H. Stenzel[56], T.J. Stevenson[156], G.A. Stewart[36], M.C. Stockton[36], G. Stoicea[27b],
M. Stolarski[139a], S. Stonjek[115], A. Straessner[48], J. Strandberg[154], S. Strandberg[45a,45b],
M. Strauss[128], T. Strebler[102], P. Strizenec[28b], R. Ströhmer[177], D.M. Strom[131], R. Stroynowski[42],
A. Strubig[45a,45b], S.A. Stucci[29], B. Stugu[17], J. Stupak[128], N.A. Styles[46], D. Su[153],
W. Su[60d,148,60c], X. Su[60a], N.B. Suarez[138], V.V. Sulin[111], M.J. Sullivan[91], D.M.S. Sultan[54],
S. Sultansoy[4c], T. Sumida[86], S. Sun[106], X. Sun[101], C.J.E. Suster[157], M.R. Sutton[156], S. Suzuki[82],
M. Svatos[140], M. Swiatlowski[168a], S.P. Swift[2], T. Swirski[177], A. Sydorenko[100], I. Sykora[28a],
M. Sykora[142], T. Sykora[142], D. Ta[100], K. Tackmann[46,x], J. Taenzer[161], A. Taffard[171],
R. Tafirout[168a], E. Tagiev[123], R.H.M. Taibah[135], R. Takashima[87], K. Takeda[83], T. Takeshita[150],
E.P. Takeva[50], Y. Takubo[82], M. Talby[102], A.A. Talyshev[122b,122a], K.C. Tam[63b], N.M. Tamir[161],
J. Tanaka[163], R. Tanaka[65], S. Tapia Araya[173], S. Tapprogge[100],
A. Tarek Abouelfadl Mohamed[107], S. Tarem[160], K. Tariq[60b], G. Tarna[27b,e], G.F. Tartarelli[69a],
P. Tas[142], M. Tasevsky[140], E. Tassi[41b,41a], G. Tateno[163], A. Tavares Delgado[139a], Y. Tayalati[35f],
A.J. Taylor[50], G.N. Taylor[105], W. Taylor[168b], H. Teagle[91], A.S. Tee[90], R. Teixeira De Lima[153],
P. Teixeira-Dias[94], H. Ten Kate[36], J.J. Teoh[120], K. Terashi[163], J. Terron[99], S. Terzo[14],
M. Testa[51], R.J. Teuscher[167,aa], N. Themistokleous[50], T. Theveneaux-Pelzer[19], D.W. Thomas[94],
J.P. Thomas[21], E.A. Thompson[46], P.D. Thompson[21], E. Thomson[136], E.J. Thorpe[93],
V.O. Tikhomirov[111,ag], Yu.A. Tikhonov[122b,122a], S. Timoshenko[112], P. Tipton[183],
S. Tisserant[102], K. Todome[23b,23a], S. Todorova-Nova[142], S. Todt[48], J. Tojo[88], S. Tokár[28a],
K. Tokushuku[82], E. Tolley[127], R. Tombs[32], K.G. Tomiwa[33e], M. Tomoto[82,117], L. Tompkins[153],
P. Tornambe[103], E. Torrence[131], H. Torres[48], E. Torró Pastor[174], M. Toscani[30], C. Tosciri[134],
J. Toth[102,z], D.R. Tovey[149], A. Traeet[17], C.J. Treado[125], T. Trefzger[177], F. Tresoldi[156],
A. Tricoli[29], I.M. Trigger[168a], S. Trincaz-Duvoid[135], D.A. Trischuk[175], W. Trischuk[167],
B. Trocmé[58], A. Trofymov[65], C. Troncon[69a], F. Trovato[156], L. Truong[33c], M. Trzebinski[85],
A. Trzupek[85], F. Tsai[46], P.V. Tsiareshka[108,ae], A. Tsirigotis[162,v], V. Tsiskaridze[155],
E.G. Tskhadadze[159a], M. Tsopoulou[162], I.I. Tsukerman[124], V. Tsulaia[18], S. Tsuno[82],
D. Tsybychev[155], Y. Tu[63b], A. Tudorache[27b], V. Tudorache[27b], A.N. Tuna[36], S. Turchikhin[80],
D. Turgeman[180], I. Turk Cakir[4b,t], R.J. Turner[21], R. Turra[69a], P.M. Tuts[39], S. Tzamarias[162],
E. Tzovara[100], K. Uchida[163], F. Ukegawa[169], G. Unal[36], M. Unal[11], A. Undrus[29], G. Unel[171],
F.C. Ungaro[105], Y. Unno[82], K. Uno[163], J. Urban[28b], P. Urquijo[105], G. Usai[8], Z. Uysal[12d],
V. Vacek[141], B. Vachon[104], K.O.H. Vadla[133], T. Vafeiadis[36], A. Vaidya[95], C. Valderanis[114],
E. Valdes Santurio[45a,45b], M. Valente[168a], S. Valentinetti[23b,23a], A. Valero[174], L. Valéry[46],
R.A. Vallance[21], A. Vallier[36], J.A. Valls Ferrer[174], T.R. Van Daalen[14], P. Van Gemmeren[6],
S. Van Stroud[95], I. Van Vulpen[120], M. Vanadia[74a,74b], W. Vandelli[36], M. Vandenbroucke[144],
E.R. Vandewall[129], D. Vannicola[73a,73b], R. Vari[73a], E.W. Varnes[7], C. Varni[55b,55a], T. Varol[158],
D. Varouchas[65], K.E. Varvell[157], M.E. Vasile[27b], G.A. Vasquez[176], F. Vazeille[38],
D. Vazquez Furelos[14], T. Vazquez Schroeder[36], J. Veatch[53], V. Vecchio[101], M.J. Veen[120],

L.M. Veloce[167], F. Veloso[139a,139c], S. Veneziano[73a], A. Ventura[68a,68b], A. Verbytskyi[115],
V. Vercesi[71a], M. Verducci[72a,72b], C.M. Vergel Infante[79], C. Vergis[24], W. Verkerke[120],
A.T. Vermeulen[120], J.C. Vermeulen[120], C. Vernieri[153], P.J. Verschuuren[94], M.C. Vetterli[152,ak],
N. Viaux Maira[146d], T. Vickey[149], O.E. Vickey Boeriu[149], G.H.A. Viehhauser[134], L. Vigani[61b],
M. Villa[23b,23a], M. Villaplana Perez[174], E.M. Villhauer[50], E. Vilucchi[51], M.G. Vincter[34],
G.S. Virdee[21], A. Vishwakarma[50], C. Vittori[23b,23a], I. Vivarelli[156], M. Vogel[182], P. Vokac[141],
J. Von Ahnen[46], S.E. von Buddenbrock[33e], E. Von Toerne[24], V. Vorobel[142], K. Vorobev[112],
M. Vos[174], J.H. Vossebeld[91], M. Vozak[101], N. Vranjes[16], M. Vranjes Milosavljevic[16], V. Vrba[141,*],
M. Vreeswijk[120], N.K. Vu[102], R. Vuillermet[36], I. Vukotic[37], S. Wada[169], P. Wagner[24],
W. Wagner[182], J. Wagner-Kuhr[114], S. Wahdan[182], H. Wahlberg[89], R. Wakasa[169],
V.M. Walbrecht[115], J. Walder[143], R. Walker[114], S.D. Walker[94], W. Walkowiak[151],
V. Wallangen[45a,45b], A.M. Wang[59], A.Z. Wang[181], C. Wang[60a], C. Wang[60c], H. Wang[18],
H. Wang[3], J. Wang[63a], P. Wang[42], Q. Wang[128], R.-J. Wang[100], R. Wang[60a], R. Wang[6],
S.M. Wang[158], W.T. Wang[60a], W. Wang[15c], W.X. Wang[60a], Y. Wang[60a], Z. Wang[106],
C. Wanotayaroj[46], A. Warburton[104], C.P. Ward[32], R.J. Ward[21], N. Warrack[57], A.T. Watson[21],
M.F. Watson[21], G. Watts[148], B.M. Waugh[95], A.F. Webb[11], C. Weber[29], M.S. Weber[20],
S.A. Weber[34], S.M. Weber[61a], Y. Wei[134], A.R. Weidberg[134], J. Weingarten[47], M. Weirich[100],
C. Weiser[52], P.S. Wells[36], T. Wenaus[29], B. Wendland[47], T. Wengler[36], S. Wenig[36], N. Wermes[24],
M. Wessels[61a], T.D. Weston[20], K. Whalen[131], A.M. Wharton[90], A.S. White[106], A. White[8],
M.J. White[1], D. Whiteson[171], B.W. Whitmore[90], W. Wiedenmann[181], C. Wiel[48], M. Wielers[143],
N. Wieseotte[100], C. Wiglesworth[40], L.A.M. Wiik-Fuchs[52], H.G. Wilkens[36], L.J. Wilkins[94],
D.M. Williams[39], H.H. Williams[136], S. Williams[32], S. Willocq[103], P.J. Windischhofer[134],
I. Wingerter-Seez[5], E. Winkels[156], F. Winklmeier[131], B.T. Winter[52], M. Wittgen[153],
M. Wobisch[96], A. Wolf[100], R. Wölker[134], J. Wollrath[52], M.W. Wolter[85], H. Wolters[139a,139c],
V.W.S. Wong[175], A.F. Wongel[46], N.L. Woods[145], S.D. Worm[46], B.K. Wosiek[85], K.W. Woźniak[85],
K. Wraight[57], S.L. Wu[181], X. Wu[54], Y. Wu[60a], J. Wuerzinger[134], T.R. Wyatt[101], B.M. Wynne[50],
S. Xella[40], J. Xiang[63c], X. Xiao[106], X. Xie[60a], I. Xiotidis[156], D. Xu[15a], H. Xu[60a], H. Xu[60a],
L. Xu[29], R. Xu[136], T. Xu[144], W. Xu[106], Y. Xu[15b], Z. Xu[60b], Z. Xu[153], B. Yabsley[157],
S. Yacoob[33a], D.P. Yallup[95], N. Yamaguchi[88], Y. Yamaguchi[165], A. Yamamoto[82],
M. Yamatani[163], T. Yamazaki[163], Y. Yamazaki[83], J. Yan[60c], Z. Yan[25], H.J. Yang[60c,60d],
H.T. Yang[18], S. Yang[60a], T. Yang[63c], X. Yang[60a], X. Yang[60b,58], Y. Yang[163], Z. Yang[106,60a],
W-M. Yao[18], Y.C. Yap[46], H. Ye[15c], J. Ye[42], S. Ye[29], I. Yeletskikh[80], M.R. Yexley[90],
E. Yigitbasi[25], P. Yin[39], K. Yorita[179], K. Yoshihara[79], C.J.S. Young[36], C. Young[153], J. Yu[79],
R. Yuan[60b,i], X. Yue[61a], M. Zaazoua[35f], B. Zabinski[85], G. Zacharis[10], E. Zaffaroni[54],
J. Zahreddine[135], A.M. Zaitsev[123,af], T. Zakareishvili[159b], N. Zakharchuk[34], S. Zambito[36],
D. Zanzi[36], S.V. Zeißner[47], C. Zeitnitz[182], G. Zemaityte[134], J.C. Zeng[173], O. Zenin[123],
T. Ženiš[28a], D. Zerwas[65], M. Zgubič[134], B. Zhang[15c], D.F. Zhang[15b], G. Zhang[15b], J. Zhang[6],
K. Zhang[15a], L. Zhang[15c], L. Zhang[60a], M. Zhang[173], R. Zhang[181], S. Zhang[106], X. Zhang[60c],
X. Zhang[60b], Y. Zhang[15a,15d], Z. Zhang[63a], Z. Zhang[65], P. Zhao[49], Y. Zhao[145], Z. Zhao[60a],
A. Zhemchugov[80], Z. Zheng[106], D. Zhong[173], B. Zhou[106], C. Zhou[181], H. Zhou[7], M. Zhou[155],
N. Zhou[60c], Y. Zhou[7], C.G. Zhu[60b], C. Zhu[15a,15d], H.L. Zhu[60a], H. Zhu[15a], J. Zhu[106], Y. Zhu[60a],
X. Zhuang[15a], K. Zhukov[111], V. Zhulanov[122b,122a], D. Zieminska[66], N.I. Zimine[80],
S. Zimmermann[52,*], Z. Zinonos[115], M. Ziolkowski[151], L. Živković[16], G. Zobernig[181],
A. Zoccoli[23b,23a], K. Zoch[53], T.G. Zorbas[149], R. Zou[37], L. Zwalinski[36].

1   *Department of Physics, University of Adelaide, Adelaide; Australia.*

2   *Physics Department, SUNY Albany, Albany NY; United States of America.*

3   *Department of Physics, University of Alberta, Edmonton AB; Canada.*

4 (a) Department of Physics, Ankara University, Ankara;(b) Istanbul Aydin University, Application and Research Center for Advanced Studies, Istanbul;(c) Division of Physics, TOBB University of Economics and Technology, Ankara; Turkey.

5 LAPP, Université Grenoble Alpes, Université Savoie Mont Blanc, CNRS/IN2P3, Annecy; France.

6 High Energy Physics Division, Argonne National Laboratory, Argonne IL; United States of America.

7 Department of Physics, University of Arizona, Tucson AZ; United States of America.

8 Department of Physics, University of Texas at Arlington, Arlington TX; United States of America.

9 Physics Department, National and Kapodistrian University of Athens, Athens; Greece.

10 Physics Department, National Technical University of Athens, Zografou; Greece.

11 Department of Physics, University of Texas at Austin, Austin TX; United States of America.

12 (a) Bahcesehir University, Faculty of Engineering and Natural Sciences, Istanbul;(b) Istanbul Bilgi University, Faculty of Engineering and Natural Sciences, Istanbul;(c) Department of Physics, Bogazici University, Istanbul;(d) Department of Physics Engineering, Gaziantep University, Gaziantep; Turkey.

13 Institute of Physics, Azerbaijan Academy of Sciences, Baku; Azerbaijan.

14 Institut de Física d'Altes Energies (IFAE), Barcelona Institute of Science and Technology, Barcelona; Spain.

15 (a) Institute of High Energy Physics, Chinese Academy of Sciences, Beijing;(b) Physics Department, Tsinghua University, Beijing;(c) Department of Physics, Nanjing University, Nanjing;(d) University of Chinese Academy of Science (UCAS), Beijing; China.

16 Institute of Physics, University of Belgrade, Belgrade; Serbia.

17 Department for Physics and Technology, University of Bergen, Bergen; Norway.

18 Physics Division, Lawrence Berkeley National Laboratory and University of California, Berkeley CA; United States of America.

19 Institut für Physik, Humboldt Universität zu Berlin, Berlin; Germany.

20 Albert Einstein Center for Fundamental Physics and Laboratory for High Energy Physics, University of Bern, Bern; Switzerland.

21 School of Physics and Astronomy, University of Birmingham, Birmingham; United Kingdom.

22 (a) Facultad de Ciencias y Centro de Investigaciónes, Universidad Antonio Nariño, Bogotá;(b) Departamento de Física, Universidad Nacional de Colombia, Bogotá, Colombia; Colombia.

23 (a) INFN Bologna and Universita' di Bologna, Dipartimento di Fisica;(b) INFN Sezione di Bologna; Italy.

24 Physikalisches Institut, Universität Bonn, Bonn; Germany.

25 Department of Physics, Boston University, Boston MA; United States of America.

26 Department of Physics, Brandeis University, Waltham MA; United States of America.

27 (a) Transilvania University of Brasov, Brasov;(b) Horia Hulubei National Institute of Physics and Nuclear Engineering, Bucharest;(c) Department of Physics, Alexandru Ioan Cuza University of Iasi, Iasi;(d) National Institute for Research and Development of Isotopic and Molecular Technologies, Physics Department, Cluj-Napoca;(e) University Politehnica Bucharest, Bucharest;(f) West University in Timisoara, Timisoara; Romania.

28 (a) Faculty of Mathematics, Physics and Informatics, Comenius University, Bratislava;(b) Department of Subnuclear Physics, Institute of Experimental Physics of the Slovak Academy of Sciences, Kosice; Slovak Republic.

29 Physics Department, Brookhaven National Laboratory, Upton NY; United States of America.

30 Departamento de Física, Universidad de Buenos Aires, Buenos Aires; Argentina.

31 California State University, CA; United States of America.

32 Cavendish Laboratory, University of Cambridge, Cambridge; United Kingdom.

33 (a) Department of Physics, University of Cape Town, Cape Town;(b) iThemba Labs, Western Cape;(c) Department of Mechanical Engineering Science, University of Johannesburg, Johannesburg;(d) University of South Africa, Department of Physics, Pretoria;(e) School of Physics, University of the Witwatersrand, Johannesburg; South Africa.

[34] *Department of Physics, Carleton University, Ottawa ON; Canada.*

[35] *[a] Faculté des Sciences Ain Chock, Réseau Universitaire de Physique des Hautes Energies - Université Hassan II, Casablanca;[b] Faculté des Sciences, Université Ibn-Tofail, Kénitra;[c] Faculté des Sciences Semlalia, Université Cadi Ayyad, LPHEA-Marrakech;[d] Moroccan Foundation for Advanced Science Innovation and Research (MAScIR), Rabat;[e] LPMR, Faculté des Sciences, Université Mohamed Premier, Oujda;[f] Faculté des sciences, Université Mohammed V, Rabat; Morocco.*

[36] *CERN, Geneva; Switzerland.*

[37] *Enrico Fermi Institute, University of Chicago, Chicago IL; United States of America.*

[38] *LPC, Université Clermont Auvergne, CNRS/IN2P3, Clermont-Ferrand; France.*

[39] *Nevis Laboratory, Columbia University, Irvington NY; United States of America.*

[40] *Niels Bohr Institute, University of Copenhagen, Copenhagen; Denmark.*

[41] *[a] Dipartimento di Fisica, Università della Calabria, Rende;[b] INFN Gruppo Collegato di Cosenza, Laboratori Nazionali di Frascati; Italy.*

[42] *Physics Department, Southern Methodist University, Dallas TX; United States of America.*

[43] *Physics Department, University of Texas at Dallas, Richardson TX; United States of America.*

[44] *National Centre for Scientific Research "Demokritos", Agia Paraskevi; Greece.*

[45] *[a] Department of Physics, Stockholm University;[b] Oskar Klein Centre, Stockholm; Sweden.*

[46] *Deutsches Elektronen-Synchrotron DESY, Hamburg and Zeuthen; Germany.*

[47] *Lehrstuhl für Experimentelle Physik IV, Technische Universität Dortmund, Dortmund; Germany.*

[48] *Institut für Kern- und Teilchenphysik, Technische Universität Dresden, Dresden; Germany.*

[49] *Department of Physics, Duke University, Durham NC; United States of America.*

[50] *SUPA - School of Physics and Astronomy, University of Edinburgh, Edinburgh; United Kingdom.*

[51] *INFN e Laboratori Nazionali di Frascati, Frascati; Italy.*

[52] *Physikalisches Institut, Albert-Ludwigs-Universität Freiburg, Freiburg; Germany.*

[53] *II. Physikalisches Institut, Georg-August-Universität Göttingen, Göttingen; Germany.*

[54] *Département de Physique Nucléaire et Corpusculaire, Université de Genève, Genève; Switzerland.*

[55] *[a] Dipartimento di Fisica, Università di Genova, Genova;[b] INFN Sezione di Genova; Italy.*

[56] *II. Physikalisches Institut, Justus-Liebig-Universität Giessen, Giessen; Germany.*

[57] *SUPA - School of Physics and Astronomy, University of Glasgow, Glasgow; United Kingdom.*

[58] *LPSC, Université Grenoble Alpes, CNRS/IN2P3, Grenoble INP, Grenoble; France.*

[59] *Laboratory for Particle Physics and Cosmology, Harvard University, Cambridge MA; United States of America.*

[60] *[a] Department of Modern Physics and State Key Laboratory of Particle Detection and Electronics, University of Science and Technology of China, Hefei;[b] Institute of Frontier and Interdisciplinary Science and Key Laboratory of Particle Physics and Particle Irradiation (MOE), Shandong University, Qingdao;[c] School of Physics and Astronomy, Shanghai Jiao Tong University, Key Laboratory for Particle Astrophysics and Cosmology (MOE), SKLPPC, Shanghai;[d] Tsung-Dao Lee Institute, Shanghai; China.*

[61] *[a] Kirchhoff-Institut für Physik, Ruprecht-Karls-Universität Heidelberg, Heidelberg;[b] Physikalisches Institut, Ruprecht-Karls-Universität Heidelberg, Heidelberg; Germany.*

[62] *Faculty of Applied Information Science, Hiroshima Institute of Technology, Hiroshima; Japan.*

[63] *[a] Department of Physics, Chinese University of Hong Kong, Shatin, N.T., Hong Kong;[b] Department of Physics, University of Hong Kong, Hong Kong;[c] Department of Physics and Institute for Advanced Study, Hong Kong University of Science and Technology, Clear Water Bay, Kowloon, Hong Kong; China.*

[64] *Department of Physics, National Tsing Hua University, Hsinchu; Taiwan.*

[65] *IJCLab, Université Paris-Saclay, CNRS/IN2P3, 91405, Orsay; France.*

[66] *Department of Physics, Indiana University, Bloomington IN; United States of America.*

[67] *[a] INFN Gruppo Collegato di Udine, Sezione di Trieste, Udine;[b] ICTP, Trieste;[c] Dipartimento Politecnico di Ingegneria e Architettura, Università di Udine, Udine; Italy.*

68 $^{(a)}$INFN Sezione di Lecce;$^{(b)}$Dipartimento di Matematica e Fisica, Università del Salento, Lecce; Italy.

69 $^{(a)}$INFN Sezione di Milano;$^{(b)}$Dipartimento di Fisica, Università di Milano, Milano; Italy.

70 $^{(a)}$INFN Sezione di Napoli;$^{(b)}$Dipartimento di Fisica, Università di Napoli, Napoli; Italy.

71 $^{(a)}$INFN Sezione di Pavia;$^{(b)}$Dipartimento di Fisica, Università di Pavia, Pavia; Italy.

72 $^{(a)}$INFN Sezione di Pisa;$^{(b)}$Dipartimento di Fisica E. Fermi, Università di Pisa, Pisa; Italy.

73 $^{(a)}$INFN Sezione di Roma;$^{(b)}$Dipartimento di Fisica, Sapienza Università di Roma, Roma; Italy.

74 $^{(a)}$INFN Sezione di Roma Tor Vergata;$^{(b)}$Dipartimento di Fisica, Università di Roma Tor Vergata, Roma; Italy.

75 $^{(a)}$INFN Sezione di Roma Tre;$^{(b)}$Dipartimento di Matematica e Fisica, Università Roma Tre, Roma; Italy.

76 $^{(a)}$INFN-TIFPA;$^{(b)}$Università degli Studi di Trento, Trento; Italy.

77 Institut für Astro- und Teilchenphysik, Leopold-Franzens-Universität, Innsbruck; Austria.

78 University of Iowa, Iowa City IA; United States of America.

79 Department of Physics and Astronomy, Iowa State University, Ames IA; United States of America.

80 Joint Institute for Nuclear Research, Dubna; Russia.

81 $^{(a)}$Departamento de Engenharia Elétrica, Universidade Federal de Juiz de Fora (UFJF), Juiz de Fora;$^{(b)}$Universidade Federal do Rio De Janeiro COPPE/EE/IF, Rio de Janeiro;$^{(c)}$Instituto de Física, Universidade de São Paulo, São Paulo; Brazil.

82 KEK, High Energy Accelerator Research Organization, Tsukuba; Japan.

83 Graduate School of Science, Kobe University, Kobe; Japan.

84 $^{(a)}$AGH University of Science and Technology, Faculty of Physics and Applied Computer Science, Krakow;$^{(b)}$Marian Smoluchowski Institute of Physics, Jagiellonian University, Krakow; Poland.

85 Institute of Nuclear Physics Polish Academy of Sciences, Krakow; Poland.

86 Faculty of Science, Kyoto University, Kyoto; Japan.

87 Kyoto University of Education, Kyoto; Japan.

88 Research Center for Advanced Particle Physics and Department of Physics, Kyushu University, Fukuoka ; Japan.

89 Instituto de Física La Plata, Universidad Nacional de La Plata and CONICET, La Plata; Argentina.

90 Physics Department, Lancaster University, Lancaster; United Kingdom.

91 Oliver Lodge Laboratory, University of Liverpool, Liverpool; United Kingdom.

92 Department of Experimental Particle Physics, Jožef Stefan Institute and Department of Physics, University of Ljubljana, Ljubljana; Slovenia.

93 School of Physics and Astronomy, Queen Mary University of London, London; United Kingdom.

94 Department of Physics, Royal Holloway University of London, Egham; United Kingdom.

95 Department of Physics and Astronomy, University College London, London; United Kingdom.

96 Louisiana Tech University, Ruston LA; United States of America.

97 Fysiska institutionen, Lunds universitet, Lund; Sweden.

98 Centre de Calcul de l'Institut National de Physique Nucléaire et de Physique des Particules (IN2P3), Villeurbanne; France.

99 Departamento de Física Teorica C-15 and CIAFF, Universidad Autónoma de Madrid, Madrid; Spain.

100 Institut für Physik, Universität Mainz, Mainz; Germany.

101 School of Physics and Astronomy, University of Manchester, Manchester; United Kingdom.

102 CPPM, Aix-Marseille Université, CNRS/IN2P3, Marseille; France.

103 Department of Physics, University of Massachusetts, Amherst MA; United States of America.

104 Department of Physics, McGill University, Montreal QC; Canada.

105 School of Physics, University of Melbourne, Victoria; Australia.

106 Department of Physics, University of Michigan, Ann Arbor MI; United States of America.

107 Department of Physics and Astronomy, Michigan State University, East Lansing MI; United States of America.

108 *B.I. Stepanov Institute of Physics, National Academy of Sciences of Belarus, Minsk; Belarus.*

109 *Research Institute for Nuclear Problems of Byelorussian State University, Minsk; Belarus.*

110 *Group of Particle Physics, University of Montreal, Montreal QC; Canada.*

111 *P.N. Lebedev Physical Institute of the Russian Academy of Sciences, Moscow; Russia.*

112 *National Research Nuclear University MEPhI, Moscow; Russia.*

113 *D.V. Skobeltsyn Institute of Nuclear Physics, M.V. Lomonosov Moscow State University, Moscow; Russia.*

114 *Fakultät für Physik, Ludwig-Maximilians-Universität München, München; Germany.*

115 *Max-Planck-Institut für Physik (Werner-Heisenberg-Institut), München; Germany.*

116 *Nagasaki Institute of Applied Science, Nagasaki; Japan.*

117 *Graduate School of Science and Kobayashi-Maskawa Institute, Nagoya University, Nagoya; Japan.*

118 *Department of Physics and Astronomy, University of New Mexico, Albuquerque NM; United States of America.*

119 *Institute for Mathematics, Astrophysics and Particle Physics, Radboud University/Nikhef, Nijmegen; Netherlands.*

120 *Nikhef National Institute for Subatomic Physics and University of Amsterdam, Amsterdam; Netherlands.*

121 *Department of Physics, Northern Illinois University, DeKalb IL; United States of America.*

122 [a]*Budker Institute of Nuclear Physics and NSU, SB RAS, Novosibirsk;*[b]*Novosibirsk State University Novosibirsk; Russia.*

123 *Institute for High Energy Physics of the National Research Centre Kurchatov Institute, Protvino; Russia.*

124 *Institute for Theoretical and Experimental Physics named by A.I. Alikhanov of National Research Centre "Kurchatov Institute", Moscow; Russia.*

125 *Department of Physics, New York University, New York NY; United States of America.*

126 *Ochanomizu University, Otsuka, Bunkyo-ku, Tokyo; Japan.*

127 *Ohio State University, Columbus OH; United States of America.*

128 *Homer L. Dodge Department of Physics and Astronomy, University of Oklahoma, Norman OK; United States of America.*

129 *Department of Physics, Oklahoma State University, Stillwater OK; United States of America.*

130 *Palacký University, RCPTM, Joint Laboratory of Optics, Olomouc; Czech Republic.*

131 *Institute for Fundamental Science, University of Oregon, Eugene, OR; United States of America.*

132 *Graduate School of Science, Osaka University, Osaka; Japan.*

133 *Department of Physics, University of Oslo, Oslo; Norway.*

134 *Department of Physics, Oxford University, Oxford; United Kingdom.*

135 *LPNHE, Sorbonne Université, Université de Paris, CNRS/IN2P3, Paris; France.*

136 *Department of Physics, University of Pennsylvania, Philadelphia PA; United States of America.*

137 *Konstantinov Nuclear Physics Institute of National Research Centre "Kurchatov Institute", PNPI, St. Petersburg; Russia.*

138 *Department of Physics and Astronomy, University of Pittsburgh, Pittsburgh PA; United States of America.*

139 [a]*Laboratório de Instrumentação e Física Experimental de Partículas - LIP, Lisboa;*[b]*Departamento de Física, Faculdade de Ciências, Universidade de Lisboa, Lisboa;*[c]*Departamento de Física, Universidade de Coimbra, Coimbra;*[d]*Centro de Física Nuclear da Universidade de Lisboa, Lisboa;*[e]*Departamento de Física, Universidade do Minho, Braga;*[f]*Departamento de Física Teórica y del Cosmos, Universidad de Granada, Granada (Spain);*[g]*Dep Física and CEFITEC of Faculdade de Ciências e Tecnologia, Universidade Nova de Lisboa, Caparica;*[h]*Instituto Superior Técnico, Universidade de Lisboa, Lisboa; Portugal.*

140 *Institute of Physics of the Czech Academy of Sciences, Prague; Czech Republic.*

141 *Czech Technical University in Prague, Prague; Czech Republic.*

142 *Charles University, Faculty of Mathematics and Physics, Prague; Czech Republic.*

143 *Particle Physics Department, Rutherford Appleton Laboratory, Didcot; United Kingdom.*

[144] IRFU, CEA, Université Paris-Saclay, Gif-sur-Yvette; France.

[145] Santa Cruz Institute for Particle Physics, University of California Santa Cruz, Santa Cruz CA; United States of America.

[146] [a] Departamento de Física, Pontificia Universidad Católica de Chile, Santiago; [b] Universidad Andres Bello, Department of Physics, Santiago; [c] Instituto de Alta Investigación, Universidad de Tarapacá; [d] Departamento de Física, Universidad Técnica Federico Santa María, Valparaíso; Chile.

[147] Universidade Federal de São João del Rei (UFSJ), São João del Rei; Brazil.

[148] Department of Physics, University of Washington, Seattle WA; United States of America.

[149] Department of Physics and Astronomy, University of Sheffield, Sheffield; United Kingdom.

[150] Department of Physics, Shinshu University, Nagano; Japan.

[151] Department Physik, Universität Siegen, Siegen; Germany.

[152] Department of Physics, Simon Fraser University, Burnaby BC; Canada.

[153] SLAC National Accelerator Laboratory, Stanford CA; United States of America.

[154] Physics Department, Royal Institute of Technology, Stockholm; Sweden.

[155] Departments of Physics and Astronomy, Stony Brook University, Stony Brook NY; United States of America.

[156] Department of Physics and Astronomy, University of Sussex, Brighton; United Kingdom.

[157] School of Physics, University of Sydney, Sydney; Australia.

[158] Institute of Physics, Academia Sinica, Taipei; Taiwan.

[159] [a] E. Andronikashvili Institute of Physics, Iv. Javakhishvili Tbilisi State University, Tbilisi; [b] High Energy Physics Institute, Tbilisi State University, Tbilisi; Georgia.

[160] Department of Physics, Technion, Israel Institute of Technology, Haifa; Israel.

[161] Raymond and Beverly Sackler School of Physics and Astronomy, Tel Aviv University, Tel Aviv; Israel.

[162] Department of Physics, Aristotle University of Thessaloniki, Thessaloniki; Greece.

[163] International Center for Elementary Particle Physics and Department of Physics, University of Tokyo, Tokyo; Japan.

[164] Graduate School of Science and Technology, Tokyo Metropolitan University, Tokyo; Japan.

[165] Department of Physics, Tokyo Institute of Technology, Tokyo; Japan.

[166] Tomsk State University, Tomsk; Russia.

[167] Department of Physics, University of Toronto, Toronto ON; Canada.

[168] [a] TRIUMF, Vancouver BC; [b] Department of Physics and Astronomy, York University, Toronto ON; Canada.

[169] Division of Physics and Tomonaga Center for the History of the Universe, Faculty of Pure and Applied Sciences, University of Tsukuba, Tsukuba; Japan.

[170] Department of Physics and Astronomy, Tufts University, Medford MA; United States of America.

[171] Department of Physics and Astronomy, University of California Irvine, Irvine CA; United States of America.

[172] Department of Physics and Astronomy, University of Uppsala, Uppsala; Sweden.

[173] Department of Physics, University of Illinois, Urbana IL; United States of America.

[174] Instituto de Física Corpuscular (IFIC), Centro Mixto Universidad de Valencia - CSIC, Valencia; Spain.

[175] Department of Physics, University of British Columbia, Vancouver BC; Canada.

[176] Department of Physics and Astronomy, University of Victoria, Victoria BC; Canada.

[177] Fakultät für Physik und Astronomie, Julius-Maximilians-Universität Würzburg, Würzburg; Germany.

[178] Department of Physics, University of Warwick, Coventry; United Kingdom.

[179] Waseda University, Tokyo; Japan.

[180] Department of Particle Physics and Astrophysics, Weizmann Institute of Science, Rehovot; Israel.

[181] Department of Physics, University of Wisconsin, Madison WI; United States of America.

[182] Fakultät für Mathematik und Naturwissenschaften, Fachgruppe Physik, Bergische Universität Wuppertal, Wuppertal; Germany.

[183] *Department of Physics, Yale University, New Haven CT; United States of America.*

[a] *Also at Borough of Manhattan Community College, City University of New York, New York NY; United States of America.*

[b] *Also at Center for High Energy Physics, Peking University; China.*

[c] *Also at Centro Studi e Ricerche Enrico Fermi; Italy.*

[d] *Also at CERN, Geneva; Switzerland.*

[e] *Also at CPPM, Aix-Marseille Université, CNRS/IN2P3, Marseille; France.*

[f] *Also at Département de Physique Nucléaire et Corpusculaire, Université de Genève, Genève; Switzerland.*

[g] *Also at Departament de Fisica de la Universitat Autonoma de Barcelona, Barcelona; Spain.*

[h] *Also at Department of Financial and Management Engineering, University of the Aegean, Chios; Greece.*

[i] *Also at Department of Physics and Astronomy, Michigan State University, East Lansing MI; United States of America.*

[j] *Also at Department of Physics and Astronomy, University of Louisville, Louisville, KY; United States of America.*

[k] *Also at Department of Physics, Ben Gurion University of the Negev, Beer Sheva; Israel.*

[l] *Also at Department of Physics, California State University, East Bay; United States of America.*

[m] *Also at Department of Physics, California State University, Fresno; United States of America.*

[n] *Also at Department of Physics, California State University, Sacramento; United States of America.*

[o] *Also at Department of Physics, King's College London, London; United Kingdom.*

[p] *Also at Department of Physics, St. Petersburg State Polytechnical University, St. Petersburg; Russia.*

[q] *Also at Department of Physics, University of Fribourg, Fribourg; Switzerland.*

[r] *Also at Dipartimento di Matematica, Informatica e Fisica, Università di Udine, Udine; Italy.*

[s] *Also at Faculty of Physics, M.V. Lomonosov Moscow State University, Moscow; Russia.*

[t] *Also at Giresun University, Faculty of Engineering, Giresun; Turkey.*

[u] *Also at Graduate School of Science, Osaka University, Osaka; Japan.*

[v] *Also at Hellenic Open University, Patras; Greece.*

[w] *Also at Institucio Catalana de Recerca i Estudis Avancats, ICREA, Barcelona; Spain.*

[x] *Also at Institut für Experimentalphysik, Universität Hamburg, Hamburg; Germany.*

[y] *Also at Institute for Nuclear Research and Nuclear Energy (INRNE) of the Bulgarian Academy of Sciences, Sofia; Bulgaria.*

[z] *Also at Institute for Particle and Nuclear Physics, Wigner Research Centre for Physics, Budapest; Hungary.*

[aa] *Also at Institute of Particle Physics (IPP); Canada.*

[ab] *Also at Institute of Physics, Azerbaijan Academy of Sciences, Baku; Azerbaijan.*

[ac] *Also at Instituto de Fisica Teorica, IFT-UAM/CSIC, Madrid; Spain.*

[ad] *Also at Istanbul University, Dept. of Physics, Istanbul; Turkey.*

[ae] *Also at Joint Institute for Nuclear Research, Dubna; Russia.*

[af] *Also at Moscow Institute of Physics and Technology State University, Dolgoprudny; Russia.*

[ag] *Also at National Research Nuclear University MEPhI, Moscow; Russia.*

[ah] *Also at Physics Department, An-Najah National University, Nablus; Palestine.*

[ai] *Also at Physikalisches Institut, Albert-Ludwigs-Universität Freiburg, Freiburg; Germany.*

[aj] *Also at The City College of New York, New York NY; United States of America.*

[ak] *Also at TRIUMF, Vancouver BC; Canada.*

[al] *Also at Universita di Napoli Parthenope, Napoli; Italy.*

[am] *Also at University of Chinese Academy of Sciences (UCAS), Beijing; China.*

[*] *Deceased*